# Three-Dimensional, Time-Dependent, Compressible, Turbulent, Integral Boundary-Layer Equations in General Curvilinear Coordinates and Their Numerical Solution

Timothy Wade Swafford
Sverdrup Technology, Inc.

September 1983

Final Report for Period August 1982 — August 1983

**ARNOLD ENGINEERING DEVELOPMENT CENTER**
**ARNOLD AIR FORCE STATION, TENNESSEE**
**AIR FORCE SYSTEMS COMMAND**
**UNITED STATES AIR FORCE**

## NOTICES

This report has been reviewed by the Office of Public Affairs (PA) and is releasable to the National Technical Information Service (NTIS). At NTIS, it will be available to the general public, including foreign nations.
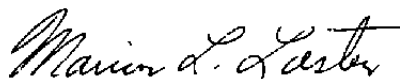
### APPROVAL STATEMENT

This report has been reviewed and approved.

KEITH L. KUSHMAN
Directorate of Technology
Deputy for Operations

Approved for publication:

FOR THE COMMANDER

MARION L. LASTER
Director of Technology
Deputy for Operations

| REPORT DOCUMENTATION PAGE | | READ INSTRUCTIONS BEFORE COMPLETING FORM |
|---|---|---|
| 1 REPORT NUMBER<br>AEDC-TR-83-37 | 2 GOVT ACCESSION NO | 3 RECIPIENT'S CATALOG NUMBER |
| 4 TITLE *(and Subtitle)*<br>THREE-DIMENSIONAL, TIME-DEPENDENT, COMPRESSIBLE, TURBULENT, INTEGRAL BOUNDARY-LAYER EQUATIONS IN GENERAL CURVILINEAR COORDINATES AND THEIR NUMERICAL SOLUTION | | 5 TYPE OF REPORT & PERIOD COVERED<br>Final Report – August 1982 – August 1983 |
| | | 6 PERFORMING ORG REPORT NUMBER |
| 7 AUTHOR*(s)*<br>Timothy Wade Swafford,<br>Sverdrup Technology, Inc./AEDC Group | | 8 CONTRACT OR GRANT NUMBER*(s)* |
| 9 PERFORMING ORGANIZATION NAME AND ADDRESS<br>Arnold Engineering Development Center/DOT<br>Air Force Systems Command<br>Arnold Air Force Station, TN 37389 | | 10 PROGRAM ELEMENT PROJECT, TASK AREA & WORK UNIT NUMBERS<br>Program Element 65807F |
| 11 CONTROLLING OFFICE NAME AND ADDRESS<br>Arnold Engineering Development Center/DOS<br>Air Force Systems Command<br>Arnold Air Force Station, TN 37389 | | 12 REPORT DATE<br>September 1983 |
| | | 13 NUMBER OF PAGES<br>134 |
| 14 MONITORING AGENCY NAME & ADDRESS*(if different from Controlling Office)* | | 15 SECURITY CLASS *(of this report)*<br>UNCLASSIFIED |
| | | 15a DECLASSIFICATION/DOWNGRADING SCHEDULE<br>N/A |

16 DISTRIBUTION STATEMENT *(of this Report)*

Approved for public release; distribution unlimited.

17 DISTRIBUTION STATEMENT *(of the abstract entered in Block 20, if different from Report)*

18 SUPPLEMENTARY NOTES

Available in Defense Technical Information Center (DTIC).

19 KEY WORDS *(Continue on reverse side if necessary and identify by block number)*

turbulent boundary layer
mathematical analysis
three dimensional flow
time dependence

20 ABSTRACT *(Continue on reverse side if necessary and identify by block number)*
A method is presented for computing three-dimensional, time-dependent, compressible, turbulent boundary layers in nonorthogonal curvilinear coordinates. An integral method is employed in the interest of computational speed and because the three-dimensional method is an extension of an existing two-dimensional method. After presenting a detailed derivation of the integral form of the boundary-layer equations, the necessary auxiliary relations are given along with the relationships between integral lengths

20. ABSTRACT, Concluded.

expressed in streamline and nonorthogonal coordinates. A time-dependent approach is used to account for time accuracy (if desired) and to provide a method that is compatible with the surface grid used by an inviscid solver for use in viscous-inviscid interaction calculations. The equations are solved using a Runge-Kutta scheme with local time stepping to accelerate convergence. Stability and convergence of the numerical scheme are examined for various space difference approximations. Finally, computed steady-state results are compared with measurements and with computations of previous investigators.

# PREFACE

The work reported herein was sponsored by the Arnold Engineering Development Center (AEDC), Air Force Systems Command (AFSC), under Contract No. F40600-81-C-0007. The results were obtained by Sverdrup Technology, Inc./AEDC Group, operating contractor of the propulsion test facilities at AEDC, under Project Number D173EW.

This work is a dissertation submitted by the author in partial fulfillment of the requirements for a Doctor of Philosophy degree from the Department of Aerospace Engineering, Mississippi State University. The reproducibles used in the reproduction of this report were primarily those used for the dissertation.

Acknowledgment is given Dr. David L. Whitfield, Mississippi State University, Mr. Fran C. Loper, Sverdrup Technology, Inc./AEDC Group, and the members of the author's graduate committee.

CONTENTS

## LIST OF FIGURES

Chapter I

INTRODUCTION

One of the most significant contributions to viscous flow theory came in 1904 when Prandtl [1][1] published his boundary-layer theory. Since that time, the theoretical analysis of two-dimensional boundary layers has been advanced to the point where accurate solutions can be obtained rather routinely, even for turbulent flow. However, most flows of practical interest are markedly turbulent and three-dimensional; hence, the advancement of three-dimensional viscous flow calculation methods becomes important.

An effective method to obtain turbulent, viscous flow solutions about typically encountered aerodynamic configurations is to numerically solve the full Navier-Stokes equations (using some means to model the turbulent Reynolds stresses). However, this approach is time-consuming and expensive (sometimes to the point of being prohibitive) due to the large amount of computational resources required for fully three-dimensional geometries.

------

[1]Numbers in brackets refer to similarly numbered references in the Bibliography.

As an alternative, the coupling of an inviscid flow solver
with a viscous flow (boundary-layer) solver has proved to
be a useful method for the computation of viscous-inviscid
interactive flow, particularly two-dimensional steady flow
(e.g., see [2-4]). The coupling approach has also been
applied successfully to three-dimensional flow [5]. The
last several years have seen significant advances in the
development of three-dimensional Euler equation calcu-
lation methods [6-9], and as a consequence the advancement
of three-dimensional boundary-layer solution methods
becomes important such that practical three-dimensional
problems can be addressed using the viscous-inviscid
interaction approach. Therefore, it is the purpose of the
present study to develop a three-dimensional, compressible,
turbulent boundary-layer calculation method that can be
used for transonic flow over adiabatic surfaces. It is
emphasized that although three-dimensional, viscous-
inviscid interaction is the ultimate goal, only the viscous
(boundary-layer) portion of a coupling approach is con-
sidered here.

The computation of three-dimensional boundary
layers over commonly encountered configurations has
received considerable attention in the past several years
(e.g., see [10-20]). Typically, a computational method is
created to cater to a particular need and/or application.

The following discussion addresses the reasoning which led to the present approach.

The methods described in [10-20] can be classed as either integral or differential. As discussed by East [10], and Smith [21], among others, integral methods are computationally faster than differential methods because the former have one less space dimension to contend with and also because more empiricism is "built into" integral methods. Although generally less flexible than differential methods, integral methods have proved to be as accurate (and in some cases, more accurate) as differential methods for two-dimensional steady flow [22,23]. Therefore, an integral approach is taken here in the interest of speed, and also because the three-dimensional method is an extension of an accurate two-dimensional method [24]. However, the question of accuracy between integral and differential methods for three-dimensional flow has been investigated to a much lesser degree than two-dimensional methods [10,25,26].

When using a coupled approach, it is desirable that the viscous and inviscid surface grids (which could be nonorthogonal) be interchangeable such that information generated by one method can easily be conveyed back to the other. For example, surface velocities obtained from the inviscid solution must be used as input to the boundary-

layer equations. The steady form of the three-dimensional boundary-layer equations must be solved on a grid which is dictated by domain-of-dependence principles [13,27] implying that interpolation is required on each viscous/inviscid iteration. However, if the time-dependent boundary-layer equations are used, the condition of interchangeable grids can be achieved, because for a fixed grid system an appropriate time step can be chosen to maintain computational stability. Thus, a time-dependent approach in nonorthogonal coordinates is adopted in order to: (1) provide a method that can use the same surface grid as an inviscid solver, and (2) account for time accuracy, if desired. To the author's knowledge, all previous three-dimensional, compressible, turbulent boundary-layer calculation methods have been for steady flow.

The system of equations used herein is the three-dimensional, time-dependent, compressible momentum and mean-flow kinetic energy integral equations in nonorthogonal curvilinear coordinates. To take advantage of the previous work in two-dimensional flow, the nonorthogonal coordinates are related to streamline coordinates as suggested by Smith [14]. The streamwise velocity profile used is that of Whitfield et al. [28], which can be expressed analytically over the entire domain $0 \leq x_3 < \infty$.

4

The cross-flow velocity profile used is the triangular model of Johnston [29].

In this study, a detailed derivation of the boundary-layer integral equations is given. The necessary empirical relationships in streamline coordinates are listed in addition to the relations between streamwise and nonorthogonal quantities for the Johnston [29] cross-flow velocity profile. The numerical scheme used and stability and convergence for various spatial difference approximations are discussed. Finally, computed steady-state results are compared with measurements and with computations of previous investigators.

## Chapter II

## DERIVATION OF EQUATIONS

The derivation of the boundary-layer integral equations to be solved is given in this chapter. It is important to include the derivation of these equations because they apparently do not exist in the literature for the general case of three-dimensional, time-dependent, compressible flow in nonorthogonal curvilinear coordinates. An abbreviated version is given in [30], but attention here is focused on the details of the development.

### 2.1. Differential to Integral Form

The differential form of the continuity and momentum boundary-layer equations for steady flow is given by Cebeci et al. [17]. These equations with the time-dependent terms are given below in a compact form:

Continuity:

$$h_1 h_2 \sin\lambda \frac{\partial \rho}{\partial t} + \frac{\partial}{\partial x_1}(\rho u_1 h_2 \sin\lambda) + \frac{\partial}{\partial x_2}(\rho u_2 h_1 \sin\lambda)$$

$$+ \frac{\partial}{\partial x_3}(\rho u_3 h_1 h_2 \sin\lambda) = 0 \qquad (2.1)$$

6

Momentum:

$$\rho h_1 h_2 \frac{\partial u_i}{\partial t} + \rho u_1 h_2 \frac{\partial u_i}{\partial x_1} + \rho u_2 h_1 \frac{\partial u_i}{\partial x_2} + \rho u_3 h_1 h_2 \frac{\partial u_i}{\partial x_3}$$

$$- \rho h_1 h_2 \cot\lambda \, K_i u_i^2 + \rho h_1 h_2 \csc\lambda \, K_{i+1} \, u_{i+1}^2$$

$$+ \rho h_1 h_2 \, K_{i,i+1} \, u_1 u_2$$

$$= -h_{i+1} \csc^2\lambda \frac{\partial p}{\partial x_i} + h_i \cot\lambda \csc\lambda \frac{\partial p}{\partial x_{i+1}}$$

$$+ h_1 h_2 \frac{\partial \tau_{x_i}}{\partial x_3} \qquad (2.2)$$

$$\frac{\partial p}{\partial x_3} = 0 \qquad (2.3)$$

where

$$i = 1 \text{ or } 2$$

$$i + 1 \equiv 1 \text{ when } i = 2$$

For example,

$$K_{i,i+1} = K_{12} \text{ when } i = 1$$

$$K_{i,i+1} = K_{21} \text{ when } i = 2$$

That is, when $i = 1$, Eq. (2.2) is the $x_1$-momentum equation, and when $i = 2$, Eq. (2.2) is the $x_2$-momentum equation. Equations (2.1) and (2.2) are written for a general non-orthogonal curvilinear coordinate system (fixed in time) like that depicted in Figure 1 (see Nomenclature for definition of terms). It should be noted that $h_3 \equiv 1$ in

7
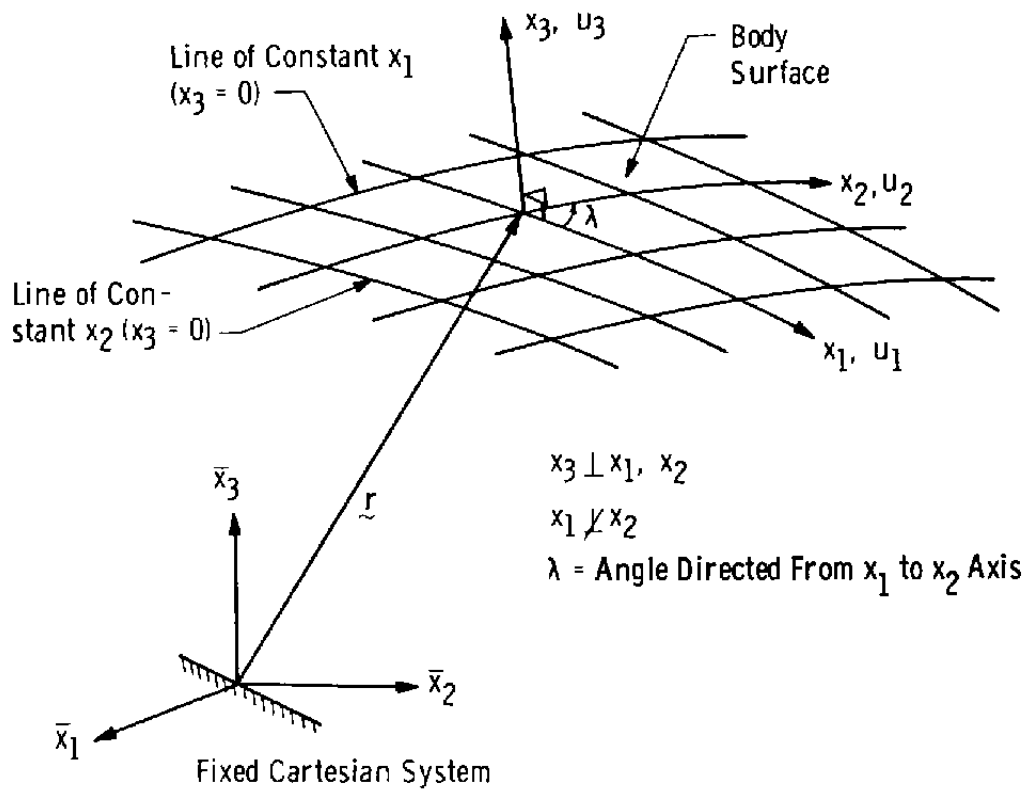
Figure 1.   General Nonorthogonal Curvilinear Coordinate System on the Body Surface.

8

Eqs. (2.1) and (2.2) such that $x_3$ is the actual distance measured normal from the surface. Also, density, pressure, and velocity appearing in Eqs. (2.1) and (2.2) are time-averaged turbulent quantities, and $\tau_{x_i}$ is the total shear stress (molecular plus turbulent) in the $x_i$-direction.

## 2.1.1. Momentum Integral Equations

Various methods can be used to arrive at the integral form of the equations. The approach taken here is to first eliminate the pressure gradient terms from Eq. (2.2) as follows: (1) multiply Eq. (2.2) by $\sin\lambda$, (2) write this result at the edge of the layer, and then (3) subtract this result from that of Step (1), which yields

$$\bar{\rho}h_1 h_2 \sin\lambda \frac{\partial \bar{u}_i}{\partial t} + \bar{\rho}\bar{u}_1 h_2 \sin\lambda \frac{\partial \bar{u}_i}{\partial x_1} + \bar{\rho}\bar{u}_2 h_1 \sin\lambda \frac{\partial \bar{u}_i}{\partial x_2}$$

$$+ \bar{\rho}\bar{u}_3 h_1 h_2 \sin\lambda \frac{\partial \bar{u}_i}{\partial x_3} + \bar{\rho}h_1 h_2 K_{i+1} \bar{u}_{i+1}^2$$

$$+ \bar{\rho}h_1 h_2 \sin\lambda K_{i,i+1} \bar{u}_1 \bar{u}_2 - \bar{\rho}h_1 h_2 \cos\lambda K_i \bar{u}_i^2$$

$$- \rho h_1 h_2 \sin\lambda \frac{\partial u_i}{\partial t} - \rho u_1 h_2 \sin\lambda \frac{\partial u_i}{\partial x_1} - \rho u_2 h_1 \sin\lambda \frac{\partial u_i}{\partial x_2}$$

$$- \rho u_3 h_1 h_2 \sin\lambda \frac{\partial u_i}{\partial x_3} + \rho h_1 h_2 \cos\lambda K_i u_i^2$$

$$- \rho h_1 h_2 K_{i+1} u_{i+1}^2 - \rho h_1 h_2 \sin\lambda K_{i,i+1} u_1 u_2$$

$$+ h_1 h_2 \sin\lambda \frac{\partial \tau_{x_i}}{\partial x_3} = 0 \tag{2.4}$$

where overbars denote boundary layer edge values and the assumption of $[\tau_{x_i}]_{edge} = 0$ has been made.

Note that the negative of the eighth through the eleventh terms of Eq. (2.4) can be written as

$$\rho h_1 h_2 \sin\lambda \frac{\partial u_i}{\partial t} + \rho u_1 h_2 \sin\lambda \frac{\partial u_i}{\partial x_1} + \rho u_2 h_1 \sin\lambda \frac{\partial u_i}{\partial x_2}$$

$$+ \rho u_3 h_1 h_2 \sin\lambda \frac{\partial u_i}{\partial x_3}$$

$$= \frac{\partial}{\partial t} (\rho u_i h_1 h_2 \sin\lambda) + \frac{\partial}{\partial x_1} (\rho u_1 u_i h_2 \sin\lambda)$$

$$+ \frac{\partial}{\partial x_2} (\rho u_2 u_i h_1 \sin\lambda) + \frac{\partial}{\partial x_3} (\rho u_3 u_i h_1 h_2 \sin\lambda)$$

$$- u_i \left[ \frac{\partial}{\partial t} (\rho h_1 h_2 \sin\lambda) + \frac{\partial}{\partial x_1} (\rho u_1 h_2 \sin\lambda) \right.$$

$$\left. + \frac{\partial}{\partial x_2} (\rho u_2 h_1 \sin\lambda) + \frac{\partial}{\partial x_3} (\rho u_3 h_1 h_2 \sin\lambda) \right] \qquad (2.5)$$

and from Eq. (2.1), the term in brackets in Eq. (2.5) is zero (metric coefficients are assumed to be invariant with time). Using Eq. (2.5) in (2.4) and rearranging, the result is

$$
\left[\bar{\rho}\, h_1 h_2\, \sin\lambda\, \frac{\partial \bar{u}_i}{\partial t} + \bar{\rho} h_2\, \sin\lambda\, \bar{u}_1\, \frac{\partial \bar{u}_i}{\partial x_1} + \bar{\rho} h_1\, \sin\lambda\, \bar{u}_2\, \frac{\partial \bar{u}_i}{\partial x_2}\right.
$$

$$
\left. + \bar{\rho}\bar{u}_3 h_1 h_2\, \sin\lambda\, \frac{\partial \bar{u}_i}{\partial x_3}\right] - \left[\frac{\partial}{\partial t}\,(\rho u_i h_1 h_2\, \sin\lambda)\right.
$$

①

$$
+ \frac{\partial}{\partial x_1}\,(\rho u_i u_1 h_2\, \sin\lambda) + \frac{\partial}{\partial x_2}\,(\rho u_2 u_i h_1\, \sin\lambda)
$$

$$
\left. + \frac{\partial}{\partial x_3}\,(\rho u_3 u_i h_1 h_2\, \sin\lambda)\right] - \left[h_1 h_2\, \cos\lambda\, K_i\,(\bar{\rho}\bar{u}_i^2 - \rho u_i^2)\right.
$$

②

$$
- h_1 h_2\, K_{i+1}\,(\bar{\rho}\bar{u}_{i+1}^2 - \rho u_{i+1}^2)
$$

$$
\left. - h_1 h_2\, \sin\lambda\, K_{i,i+1}\,(\bar{\rho}\bar{u}_1 \bar{u}_2 - \rho u_1 u_2)\right]
$$

③

$$
+ \left[h_1 h_2\, \sin\lambda\, \frac{\partial \tau_{x_i}}{\partial x_3}\right] = 0 \qquad\qquad (2.6)
$$

④

(The numbered brackets appearing in Eq. (2.6) will be used later on). By assuming $\partial \bar{u}_i/\partial x_3 = 0$, adding and subtracting the term

$$
\frac{\partial}{\partial t}\,(\rho \bar{u}_i h_1 h_2\, \sin\lambda) + \frac{\partial}{\partial x_1}\,(\rho u_1 \bar{u}_i h_2\, \sin\lambda)
$$

$$
+ \frac{\partial}{\partial x_2}(\rho u_2 \bar{u}_i h_1\, \sin\lambda) + \frac{\partial}{\partial x_3}\,(\rho u_3 \bar{u}_i h_1 h_2\, \sin\lambda)
$$

in Eq. (2.6), and using Eq. (2.1) in a similar fashion as in Eq. (2.5), some algebraic manipulation yields

$$\frac{\partial}{\partial t} [h_1 h_2 \sin\lambda \, \rho(\bar{u}_i - u_i)] + h_1 h_2 \sin\lambda(\bar{\rho}-\rho) \frac{\partial \bar{u}_i}{\partial t}$$

$$+ \frac{\partial}{\partial x_1}[h_2 \sin\lambda \, \rho u_1(\bar{u}_i - u_i)] + \frac{\partial}{\partial x_2} [h_1 \sin\lambda \, \rho u_2(\bar{u}_i - u_i)]$$

$$+ h_2 \sin\lambda(\overline{\rho\,u}_1 - \rho u_1) \frac{\partial \bar{u}_i}{\partial x_1} + h_1 \sin\lambda(\overline{\rho\,u}_2 - \rho u_2) \frac{\partial \bar{u}_i}{\partial x_2}$$

$$- h_1 h_2 \cos\lambda \, K_i(\overline{\rho}\,\bar{u}_i^2 - \rho u_i^2) + h_1 h_2 \, K_{i+1}(\overline{\rho}\,\bar{u}_{i+1}^2 - \rho u_{i+1}^2)$$

$$+ h_1 h_2 \sin\lambda \, K_{i,i+1}(\overline{\rho}\,\bar{u}_1\bar{u}_2 - \rho u_1 u_2)$$

$$+ \frac{\partial}{\partial x_3} [h_1 h_2 \sin\lambda \, \rho u_3(\bar{u}_i - u_i)]$$

$$+ h_1 h_2 \sin\lambda \frac{\partial \tau_{x_i}}{\partial x_3} = 0 \qquad\qquad (2.7)$$

Rearranging the first line of Eq. (2.7) and using the identities

$$\overline{\rho}\,\bar{u}_i^2 - \rho u_i^2 = \bar{u}_i(\overline{\rho}\,\bar{u}_i - \rho u_i) + \rho u_i(\bar{u}_i - u_i) \qquad (2.8a)$$

$$\overline{\rho}\,\bar{u}_1\bar{u}_2 - \rho u_1 u_2 = \bar{u}_i(\overline{\rho}\,\bar{u}_j - \rho u_j) + \rho u_j(\bar{u}_i - u_i) \, , \ i \neq j \qquad (2.8b)$$

results in

$$h_1 h_2 \sin\lambda \left[ \frac{\partial}{\partial t} (\overline{\rho}\,\overline{u}_i - \rho u_i) - \overline{u}_i \frac{\partial}{\partial t} (\overline{\rho} - \rho) \right]$$

$$+ h_2 \sin\lambda (\overline{\rho}\,\overline{u}_1 - \rho u_1) \frac{\partial \overline{u}_i}{\partial x_1} + h_1 \sin\lambda (\overline{\rho}\,\overline{u}_2 - \rho u_2) \frac{\partial \overline{u}_i}{\partial x_2}$$

$$+ \frac{\partial}{\partial x_1} [\rho u_1 h_2 \sin\lambda (\overline{u}_i - u_i)] + \frac{\partial}{\partial x_2} [\rho u_2 h_1 \sin\lambda (\overline{u}_i - u_i)]$$

$$+ \frac{\partial}{\partial x_3} [\rho u_3 h_1 h_2 \sin\lambda (\overline{u}_i - u_i)] - h_1 h_2 \cos\lambda \, K_i [\overline{u}_i (\overline{\rho}\,\overline{u}_i - \rho u_i)$$

$$+ \rho u_i (\overline{u}_i - u_i)] + h_1 h_2 \, K_{i+1} [\overline{u}_{i+1} (\overline{\rho}\,\overline{u}_{i+1} - \rho u_{i+1})$$

$$+ \rho u_{i+1} (\overline{u}_{i+1} - u_{i+1})]$$

$$+ h_1 h_2 \sin\lambda \, K_{i,i+1} [\overline{u}_i (\overline{\rho}\,\overline{u}_{i+1} - \rho u_{i+1}) + \rho u_{i+1} (\overline{u}_i - u_i)]$$

$$+ h_1 h_2 \sin\lambda \frac{\partial \tau_{x_i}}{\partial x_3} = 0 \qquad\qquad (2.9)$$

The $x_1$- and $x_2$-momentum integral equations are obtained by integrating Eq. (2.9) over $0 \leq x_3 < \infty$. Using the assumption that surface metrics are independent of $x_3$ [31], defining the following integral thicknesses as

$$\overline{\rho}\,\overline{q}\,\delta_i^* = \int_0^\infty (\overline{\rho}\,\overline{u}_i - \rho u_i) dx_3 \qquad\qquad (2.10a)$$

$$\overline{\rho}\,\overline{q}^2 \theta_{ij} = \int_0^\infty \rho u_j (\overline{u}_i - u_i) dx_3 \qquad\qquad (2.10b)$$

13

$$\overline{\rho}\,\overline{q}^3 \epsilon_{ij} = \int_0^\infty \rho u_j (\overline{u}_i^2 - u_i^2) dx_3 \qquad (2.10c)$$

$$\overline{q}\delta_{u_i}^* = \int_0^\infty (\overline{u}_i - u_i) dx_3 \qquad (2.10d)$$

$$\overline{\rho}\theta_\rho = \int_0^\infty (\overline{\rho} - \rho) dx_3 \qquad (2.10e)$$

and considering only an impermeable wall; i.e., $(\rho u_3)_{wall} = 0$, Eq. (2.9) becomes

$$\frac{1}{\overline{\rho}\,\overline{q}^2}\left[\frac{\partial}{\partial t}(\overline{\rho}\,\overline{q}\,\delta_i^*) - \overline{u}_i\,\frac{\partial}{\partial t}(\overline{\rho}\theta_\rho)\right]$$

$$+ \frac{1}{\overline{\rho}\,\overline{q}^2\, h_1 h_2\, \sin\lambda}\left[\frac{\partial}{\partial x_1}(\overline{\rho}\,\overline{q}^2\, h_2\, \sin\lambda\, \theta_{i1})\right.$$

$$+ \frac{\partial}{\partial x_2}(\overline{\rho}\,\overline{q}^2\, h_1\, \sin\lambda\, \theta_{i2})\bigg]$$

$$+ \frac{\delta_1^*}{h_1\overline{q}}\,\frac{\partial\overline{u}_i}{\partial x_1} + \frac{\delta_2^*}{h_2\overline{q}}\,\frac{\partial\overline{u}_i}{\partial x_2} - K_i\, \cot\lambda\left(\frac{\overline{u}_i}{\overline{q}}\,\delta_i^* + \theta_{ii}\right)$$

$$+ K_{i+1}\, \csc\lambda\left(\frac{\overline{u}_{i+1}}{\overline{q}}\,\delta_{i+1}^* + \theta_{i+1,i+1}\right)$$

$$+ K_{i,i+1}\left(\frac{\overline{u}_i}{\overline{q}}\,\delta_{i+1}^* + \theta_{i,i+1}\right) - \frac{1}{2}\,c_{f_{x_i}} = 0 \qquad (2.11)$$

where $\overline{q}$ is the resultant boundary-layer edge velocity and $c_{f_{x_i}}$ is the local skin friction coefficient defined as

$$c_{f_{x_i}} \equiv \frac{2\tau_{x_{i_w}}}{\bar{\rho}\bar{q}^2} \tag{2.12}$$

The $x_1$- and $x_2$-momentum integral equations result from Eq. (2.11) by setting $i = 1$ or $i = 2$, respectively. Again note that a subscript 3 resulting from $i + 1$ when $i = 2$ is taken as subscript 1. Also, a comma between subscripts such as $\theta_{i,i+1}$ is taken as $\theta_{12}$ for $i = 1$ and $\theta_{21}$ for $i = 2$.

### 2.1.2. Mean-Flow Kinetic Energy Integral Equation

To obtain the mean-flow kinetic energy integral equation, the approach is to multiply Eq. (2.6) by $u_i$, integrate both over $0 \leq x_3 < \infty$, and then sum the two resulting integral equations. One can begin this program by multiplying Eq. (2.6) by $u_i$ and writing the result as

$$u_i(L_1^i + L_2^i + L_3^i + L_4^i) = 0 \tag{2.13}$$

where subscripts 1 to 4 in Eq. (2.13) denote the terms included within the similarly numbered brackets of Eq. (2.6), and subscript i on $u_i$ and superscript i on $L^i$ are one or two. Note the $u_i L_2^i$ term of the above can be written as

$$u_i L_2^i = -u_i\left[\frac{\partial}{\partial t}(\rho u_i\ h_1 h_2\ \sin\lambda) + \frac{\partial}{\partial x_1}(\rho u_1 u_i\ h_2\ \sin\lambda)\right.$$

$$\left. + \frac{\partial}{\partial x_2}(\rho u_2 u_i\ h_1\ \sin\lambda) + \frac{\partial}{\partial x_3}(\rho u_3 u_i\ h_1 h_2\ \sin\lambda)\right]$$

15

or, using the continuity equation,

$$u_i L_2^i = -\frac{1}{2}\left[\frac{\partial}{\partial t}(\rho u_i^2 h_1 h_2 \sin\lambda) + \frac{\partial}{\partial x_1}(\rho u_1 u_i^2 h_2 \sin\lambda)\right.$$

$$\left. + \frac{\partial}{\partial x_2}(\rho u_2 u_i^2 h_1 \sin\lambda) + \frac{\partial}{\partial x_3}(\rho u_3 u_i^2 h_1 h_2 \sin\lambda)\right](2.14)$$

Using Eq. (2.14) in Eq. (2.13) results in

$$\bar{\rho} u_i h_1 h_2 \sin\lambda \frac{\partial \bar{u}_i}{\partial t} + \bar{\rho}\bar{u}_1 u_i h_2 \sin\lambda \frac{\partial \bar{u}_i}{\partial x_1} + \bar{\rho}\bar{u}_2 u_i h_1 \sin\lambda \frac{\partial \bar{u}_i}{\partial x_2}$$

$$+ \bar{\rho}\bar{u}_3 u_i h_1 h_2 \sin\lambda \frac{\partial \bar{u}_i}{\partial x_3} - \frac{1}{2}\left[\frac{\partial}{\partial t}(\rho u_i^2 h_1 h_2 \sin\lambda)\right.$$

$$+ \frac{\partial}{\partial x_1}(\rho u_1 u_i^2 h_2 \sin\lambda) + \frac{\partial}{\partial x_2}(\rho u_2 u_i^2 h_1 \sin\lambda)$$

$$\left. + \frac{\partial}{\partial x_3}(\rho u_3 u_i^2 h_1 h_2 \sin\lambda)\right] - h_1 h_2 \cos\lambda \, K_i u_i (\bar{\rho}\bar{u}_i^2 - \rho u_i^2)$$

$$+ h_1 h_2 \, K_{i+1} \, u_i (\bar{\rho}\bar{u}_{i+1}^2 - \rho u_{i+1}^2)$$

$$+ h_1 h_2 \sin\lambda \, K_{i,i+1} \, u_i (\bar{\rho}\bar{u}_1 \bar{u}_2 - \rho u_1 u_2)$$

$$+ h_1 h_2 \sin\lambda \, u_i \frac{\partial \tau_{x_i}}{\partial x_3} = 0 \qquad\qquad (2.15)$$

Adding and subtracting the term

$$\frac{1}{2}\left[\frac{\partial}{\partial t}(\rho\bar{u}_i^2 h_1 h_2 \sin\lambda) + \frac{\partial}{\partial x_1}(\rho u_1 \bar{u}_i^2 h_2 \sin\lambda)\right.$$

$$\left. + \frac{\partial}{\partial x_2}(\rho u_2 \bar{u}_i^2 h_1 \sin\lambda) + \frac{\partial}{\partial x_3}(\rho u_3 \bar{u}_i^2 h_1 h_2 \sin\lambda)\right]$$

to Eq. (2.15) results in

$$\bar{\rho}u_i h_1 h_2 \sin\lambda \frac{\partial \bar{u}_i}{\partial t} - \frac{1}{2} \frac{\partial}{\partial t}(\rho\bar{u}_i^2 h_1 h_2 \sin\lambda) + \bar{\rho}\bar{u}_1 u_i h_2 \sin\lambda \frac{\partial \bar{u}_i}{\partial x_1}$$

$$- \frac{1}{2} \frac{\partial}{\partial x_1}(\rho u_1 \bar{u}_i^2 h_2 \sin\lambda) + \bar{\rho}\bar{u}_2 u_i h_1 \sin\lambda \frac{\partial \bar{u}_i}{\partial x_2}$$

$$- \frac{1}{2} \frac{\partial}{\partial x_2}(\rho u_2 \bar{u}_i^2 h_1 \sin\lambda) + \bar{\rho}\bar{u}_3 u_i h_1 h_2 \sin\lambda \frac{\partial \bar{u}_i}{\partial x_3}$$

$$- \frac{1}{2} \frac{\partial}{\partial x_3}(\rho u_3 \bar{u}_i^2 h_1 h_2 \sin\lambda) + \frac{1}{2}\left\{ \frac{\partial}{\partial t}[h_1 h_2 \sin\lambda \ \rho(\bar{u}_i^2 - u_i^2)] \right.$$

$$+ \frac{\partial}{\partial x_1}[h_2 \sin\lambda \ \rho u_1(\bar{u}_i^2 - u_i^2)] + \frac{\partial}{\partial x_2}[h_1 \sin\lambda \ \rho u_2(\bar{u}_i^2 - u_i^2)]$$

$$+ \frac{\partial}{\partial x_3}[h_1 h_2 \sin\lambda \ \rho u_3(\bar{u}_i^2 - u_i^2)]\Big\}$$

$$- h_1 h_2 \cos\lambda \ K_i u_i(\bar{\rho}\bar{u}_i^2 - \rho u_i^2)$$

$$+ h_1 h_2 \ K_{i+1} \ u_i(\bar{\rho}\bar{u}_{i+1}^2 - \rho u_{i+1}^2)$$

$$+ h_1 h_2 \sin\lambda \ K_{i,i+1} \ u_i(\bar{\rho}\bar{u}_1\bar{u}_2 - \rho u_1 u_2)$$

$$+ h_1 h_2 \sin\lambda \ u_i \frac{\partial \tau_{x_i}}{\partial x_3} = 0 \tag{2.16}$$

One can use the continuity equation and rewrite the first eight terms of Eq. (2.16) to give

$$h_1 h_2 \sin\lambda(\overline{\rho}\,\overline{u}_i - \rho\overline{u}_i)\frac{\partial \overline{u}_i}{\partial t} + h_2 \sin\lambda(\overline{\rho}\,\overline{u}_1 u_i - \rho u_1 \overline{u}_i)\frac{\partial \overline{u}_i}{\partial x_1}$$

$$+ h_1 \sin\lambda(\overline{\rho}\,\overline{u}_2 u_i - \rho u_2 \overline{u}_i)\frac{\partial \overline{u}_i}{\partial x_2}$$

$$+ h_1 h_2 \sin\lambda(\overline{\rho}\,\overline{u}_3 u_i - \rho u_3 \overline{u}_i)\frac{\partial \overline{u}_i}{\partial x_3}$$

$$+ \frac{1}{2}\left\{\frac{\partial}{\partial t}[h_1 h_2 \sin\lambda\rho(\overline{u}_i^2 - u_i^2)] + \frac{\partial}{\partial x_1}[h_2 \sin\lambda\rho u_1(\overline{u}_i^2 - u_i^2)]\right.$$

$$\left. + \frac{\partial}{\partial x_2}[h_1 \sin\lambda\rho u_2(\overline{u}_i^2 - u_i^2)] + \frac{\partial}{\partial x_3}[h_1 h_2 \sin\lambda\rho u_3(\overline{u}_i^2 - u_i^2)]\right\}$$

$$- h_1 h_2 \cos\lambda\, K_i u_i(\overline{\rho}\,\overline{u}_i^2 - \rho u_i^2) + h_1 h_2\, K_{i+1}\, u_i(\overline{\rho}\,\overline{u}_{i+1}^2 - \rho u_{i+1}^2)$$

$$+ h_1 h_2 \sin\lambda\, K_{i,i+1}\, u_i(\overline{\rho}\,\overline{u}_1\overline{u}_2 - \rho u_1 u_2)$$

$$+ h_1 h_2 \sin\lambda\, u_i \frac{\partial \tau_{x_i}}{\partial x_3} = 0 \tag{2.17}$$

Using the identities,

$$\overline{\rho u_i} - \rho\overline{u}_i = \overline{u}_i(\overline{\rho} - \rho) - \overline{\rho}(\overline{u}_i - u_i) \tag{2.18a}$$

$$\rho(\overline{u}_i^2 - u_i^2) = \rho u_i(\overline{u}_i - u_i) + \overline{u}_i(\overline{\rho u_i} - \rho u_i) - \overline{u}_i^2(\overline{\rho} - \rho) \tag{2.18b}$$

$$\overline{\rho}\,\overline{u}_j u_i - \rho u_j \overline{u}_i = \overline{u}_i(\overline{\rho}\,\overline{u}_j - \rho u_j) - \overline{\rho}\,\overline{u}_j(\overline{u}_i - u_i) \tag{2.18c}$$

$$u_i(\overline{\rho}\,\overline{u}_i^2 - \rho u_i^2) = \rho u_i(\overline{u}_i^2 - u_i^2) + \overline{u}_i^2(\overline{\rho}\,\overline{u}_i - \rho u_i) - \overline{\rho}\,\overline{u}_i^2(\overline{u}_i - u_i) \tag{2.18d}$$

$$u_i(\overline{\rho}\,\overline{u}_{i+1}^2 - \overline{\rho u_{i+1}^2}) = \rho u_i(\overline{u}_{i+1}^2 - \overline{u_{i+1}^2}) + \overline{u}_{i+1}^2(\overline{\rho}\,\overline{u}_i - \overline{\rho u_i})$$

$$- \overline{\rho}\,\overline{u}_{i+1}^2(\overline{u}_i - u_i) \qquad (2.18e)$$

$$u_i(\overline{\rho}\,\overline{u}_i\overline{u}_j - \overline{\rho u_i u_j}) = \rho u_j(\overline{u}_i^2 - \overline{u_i^2}) + \overline{u}_i^2(\overline{\rho}\,\overline{u}_j - \overline{\rho u_j})$$

$$- \overline{\rho}\,\overline{u}_i\overline{u}_j(\overline{u}_i - u_i) \; , \; i \neq j \qquad (2.18f)$$

integrating over $0 \leq x_3 < \infty$ using the integral thickness
definitions given in Eq. (2.10), and again taking
$\partial\overline{u}_i/\partial x_3 = (\rho u_3)_{wall} = 0$, results in

$$\left(\frac{\overline{u}_i}{\overline{q}^3}\theta_\rho - \frac{\delta_{u_i}^*}{\overline{q}^2}\right)\frac{\partial\overline{u}_i}{\partial t} + \frac{1}{2\overline{\rho}\,\overline{q}^3}\frac{\partial}{\partial t}\left(\overline{\rho}\,\overline{q}^2\,\theta_{ii} + \overline{\rho}\,\overline{u}_i\overline{q}\delta_i^* - \overline{\rho}\,\overline{u}_i^2\,\theta_\rho\right)$$

$$+\left(\frac{\overline{u}_i\delta_1^*}{h_1\overline{q}^2} - \frac{\overline{u}_1\delta_{u_i}^*}{h_1\overline{q}^2}\right)\frac{\partial\overline{u}_i}{\partial x_1} + \left(\frac{\overline{u}_i\delta_2^*}{h_2\overline{q}^2} - \frac{\overline{u}_2\delta_{u_i}^*}{h_2\overline{q}^2}\right)\frac{\partial\overline{u}_i}{\partial x_2}$$

$$+ \frac{1}{2h_1h_2\sin\lambda\,\overline{\rho}\,\overline{q}^3}\left[\frac{\partial}{\partial x_1}(h_2\,\sin\lambda\,\overline{\rho}\,\overline{q}^3\varepsilon_{i1})\right.$$

$$+ \frac{\partial}{\partial x_2}(h_1\,\sin\lambda\,\overline{\rho}\,\overline{q}^3\,\varepsilon_{i2})\Bigg] - \cot\lambda\,K_i\left(\varepsilon_{ii} + \frac{\overline{u}_i^2}{\overline{q}^2}\delta_i^* - \frac{\overline{u}_i^2}{\overline{q}^2}\,\delta_{u_i}^*\right)$$

$$+ \csc\lambda\,K_{i+1}\left(\varepsilon_{i+1,i} + \frac{\overline{u}_{i+1}^2}{\overline{q}^2}\delta_i^* - \frac{\overline{u}_{i+1}^2}{\overline{q}^2}\delta_{u_i}^*\right)$$

$$+ K_{i,i+1}\left(\varepsilon_{i,i+1} + \frac{\overline{u}_i^2}{\overline{q}^2}\delta_{i+1}^* - \frac{\overline{u}_i\overline{u}_{i+1}}{\overline{q}^2}\delta_{u_i}^*\right)$$

$$+ \frac{1}{\overline{\rho}\,\overline{q}^3}\int_0^\infty u_i\,\frac{\partial\tau_{x_i}}{\partial x_3}\,dx_3 = 0 \qquad (2.19)$$

19

The mean flow kinetic energy integral equation is obtained by summing Eq. (2.19) for i = 1 and i = 2, yielding the following clean but formidable equation:

$$\frac{1}{2\bar{\rho}\bar{q}^3} \frac{\partial}{\partial t}\left[\bar{\rho}\,\bar{q}^2\left(\theta_{11} + \theta_{22}\right) + \bar{\rho}\,\bar{q}\left(\bar{u}_1\delta_1^* + \bar{u}_2\delta_2^*\right) - \bar{\rho}\theta_\rho\left(\bar{u}_1^2 + \bar{u}_2^2\right)\right]$$

$$+ \frac{1}{\bar{q}^2}\left(\frac{\bar{u}_1}{\bar{q}}\,\theta_\rho - \delta_{u_1}^*\right)\frac{\partial\bar{u}_1}{\partial t} + \frac{1}{\bar{q}^2}\left(\frac{\bar{u}_2}{\bar{q}}\,\theta_\rho - \delta_{u_2}^*\right)\frac{\partial\bar{u}_2}{\partial t}$$

$$+ \frac{1}{2h_1 h_2\,\sin\lambda\,\bar{\rho}\,\bar{q}^3}\left\{\frac{\partial}{\partial x_1}\left[h_2\,\sin\lambda\,\bar{\rho}\,\bar{q}^3\left(\epsilon_{11} + \epsilon_{21}\right)\right]\right.$$

$$\left.+ \frac{\partial}{\partial x_2}\left[h_1\,\sin\lambda\,\bar{\rho}\,\bar{q}^3\left(\epsilon_{12} + \epsilon_{22}\right)\right]\right\} + \frac{\bar{u}_1}{h_1\bar{q}^2}\left(\delta_1^* - \delta_{u_1}^*\right)\frac{\partial\bar{u}_1}{\partial x_1}$$

$$+ \frac{1}{h_1\bar{q}^2}\left(\bar{u}_2\delta_1^* - \bar{u}_1\delta_{u_2}^*\right)\frac{\partial\bar{u}_2}{\partial x_1} + \frac{1}{h_2\bar{q}^2}\left(\bar{u}_1\delta_2^* - \bar{u}_2\delta_{u_1}^*\right)\frac{\partial\bar{u}_1}{\partial x_2}$$

$$+ \frac{\bar{u}_2}{h_2\bar{q}^2}\left(\delta_2^* - \delta_{u_2}^*\right)\frac{\partial\bar{u}_2}{\partial x_2}$$

$$- K_1\,\cot\lambda\left[\epsilon_{11} + \frac{\bar{u}_1^2}{\bar{q}^2}\left(\delta_1^* - \delta_{u_1}^*\right)\right] + K_2\,\csc\lambda\left[\epsilon_{21} + \frac{\bar{u}_2^2}{\bar{q}^2}\left(\delta_1^* - \delta_{u_1}^*\right)\right]$$

$$- K_2\,\cot\lambda\left[\epsilon_{22} + \frac{\bar{u}_2^2}{\bar{q}^2}\left(\delta_2^* - \delta_{u_2}^*\right)\right] + K_1\,\csc\lambda\left[\epsilon_{12} + \frac{\bar{u}_1^2}{\bar{q}^2}\left(\delta_2^* - \delta_{u_2}^*\right)\right]$$

$$+ K_{21}\left[\epsilon_{21} + \frac{\bar{u}_2}{\bar{q}^2}\left(\bar{u}_2\delta_1^* - \bar{u}_1\delta_{u_2}^*\right)\right] + K_{12}\left[\epsilon_{12} + \frac{\bar{u}_1}{\bar{q}^2}\left(\bar{u}_1\delta_2^* - \bar{u}_2\delta_{u_1}^*\right)\right]$$

$$+ \frac{1}{\bar{\rho}\,\bar{q}^3}\int_0^\infty\left(u_1\,\frac{\partial\tau_{x_1}}{\partial x_3} + u_2\,\frac{\partial\tau_{x_2}}{\partial x_3}\right)dx_3 = 0 \qquad\qquad (2.20)$$

Therefore, in summary: (1) the momentum integral equations are given by Eq. (2.11) for $i = 1$ and $i = 2$, (2) the mean-flow kinetic energy integral equation is given by Eq. (2.20), and (3) the integral lengths are given by Eq. (2.10). All metric coefficients are listed in Appendix A.

It is worth noting that the validity of the derivation just presented was checked for some special cases by comparing Eqs. (2.11) and (2.20) to corresponding equations in the literature. For example, Eq. (2.11) for $i = 1$ and Eq. (2.20) reduce to those obtained by McDonald et al. [32] for the case of two-dimensional, time-dependent, compressible flow. Also, Eqs. (2.11) and (2.20) reduce to those given by Nash et al. [31, Eqs. (3.39), (3.40), and (3.44), pp. 43 and 45] for the case of three-dimensional, steady, incompressible flow using orthogonal curvilinear coordinates (i.e., $\lambda = \pi/2$). However, the careful reader will note that a sign discrepancy exists in one term between the $x_1$-momentum integral equation as given by Mager [33, Eq. (5.1), p. 298] and Eq. (2.11) for $i = 1$ for the case of three-dimensional, time-dependent, compressible flow in orthogonal curvilinear coordinates; whereas, Eq. (2.11) for $i = 2$ and Eq. (5.2) in [33, p. 298] are identical for these conditions. After careful scrutiny, the present author is convinced that Eqs. (2.11) and (2.20)

are correct and that the sign of the "curl$_3$Q" term in Mager's Eq. (5.1) [33, p. 298] should be negative. The interested reader is invited to assert himself concerning the origin of this discrepancy.

## 2.1.3. Restrictions Pertaining to Steady Edge Conditions

Equations (2.11) and (2.20) can be written

$$\frac{1}{\overline{\rho}\,\overline{q}^2}\left[\frac{\partial}{\partial t}\left(\overline{\rho}\,\overline{q}\delta_i^*\right) - \overline{u}_i\frac{\partial}{\partial t}\left(\overline{\rho}\,\theta_\rho\right)\right] = \ell_i \;,\; i = 1 \text{ or } 2 \quad (2.21)$$

$$\frac{1}{2\overline{\rho}\,\overline{q}^3}\frac{\partial}{\partial t}\left[\overline{\rho}\,\overline{q}^2\left(\theta_{11} + \theta_{22}\right) + \overline{\rho}\,\overline{q}\left(\overline{u}_1\delta_1^* + \overline{u}_2\delta_2^*\right) - \overline{\rho}\theta_\rho\left(\overline{u}_1^2 + \overline{u}_2^2\right)\right]$$
$$+ \frac{1}{\overline{q}^2}\left[\left(\frac{\overline{u}_1}{\overline{q}}\,\theta_\rho - \delta_{u_1}^*\right)\frac{\partial\overline{u}_1}{\partial t} + \left(\frac{\overline{u}_2}{\overline{q}}\,\theta_\rho - \delta_{u_2}^*\right)\frac{\partial\overline{u}_2}{\partial t}\right] = L \quad (2.22)$$

where $\ell_i$ and L are defined by referring to Eqs. (2.11) and (2.20). Expanding the derivatives with respect to time results in (for i = 1 and i = 2)

$$\frac{\partial\delta_1^*}{\partial t} - \frac{\overline{u}_1}{\overline{q}}\frac{\partial\theta_\rho}{\partial t} = \overline{q}\ell_1 - T_{\ell_1} \quad (2.23a)$$

$$\frac{\partial}{\partial t}(\theta_{11} + \theta_{22}) = 2\overline{q}L - T_L - \frac{\overline{u}_1}{\overline{q}}(\overline{q}\ell_1 - T_{\ell_1}) - \frac{\overline{u}_2}{\overline{q}}(\overline{q}\ell_2 - T_{\ell_2}) \quad (2.23b)$$

$$\frac{\partial\delta_2^*}{\partial t} - \frac{\overline{u}_2}{\overline{q}}\frac{\partial\theta_\rho}{\partial t} = \overline{q}\ell_2 - T_{\ell_2} \quad (2.23c)$$

where

$$T_{\ell_1} = \frac{\delta_1^*}{\overline{\rho}\,\overline{q}} \frac{\partial}{\partial t}(\overline{\rho}\,\overline{q}) - \frac{\theta_{\rho}\overline{u}_1}{\overline{\rho}\,\overline{q}} \frac{\partial\overline{\rho}}{\partial t} \qquad (2.24a)$$

$$T_{\ell_2} = \frac{\delta_2^*}{\overline{\rho}\,\overline{q}} \frac{\partial}{\partial t}(\overline{\rho}\,\overline{q}) - \frac{\theta_{\rho}\overline{u}_2}{\overline{\rho}\,\overline{q}} \frac{\partial\overline{\rho}}{\partial t} \qquad (2.24b)$$

$$T_L = \frac{1}{\overline{\rho}\,\overline{q}^2}\left\{ (\theta_{11} + \theta_{22}) \frac{\partial}{\partial t}(\overline{\rho}\,\overline{q}^2) + \delta_1^* \frac{\partial}{\partial t}(\overline{\rho}\,\overline{q}\,\overline{u}_1) \right.$$

$$+ \delta_2^* \frac{\partial}{\partial t}(\overline{\rho}\,\overline{q}\,\overline{u}_2) - \theta_{\rho}\frac{\partial}{\partial t}[\overline{\rho}\,(\overline{u}_1^2 + \overline{u}_2^2)]\Big\}$$

$$+ \frac{2}{\overline{q}}\left[\left(\frac{\overline{u}_1}{\overline{q}}\theta_{\rho} - \delta_{u_1}^*\right)\frac{\partial\overline{u}_1}{\partial t} + \left(\frac{\overline{u}_2}{\overline{q}}\theta_{\rho} - \delta_{u_2}^*\right)\frac{\partial\overline{u}_2}{\partial t}\right] \qquad (2.24c)$$

Up to this point, Eqs. (2.23a,b,c) are valid for time-varying edge conditions. The analysis hereafter is restricted to the case of steady edge conditions; that is,

$$\frac{\partial\overline{\rho}}{\partial t} = \frac{\partial\overline{q}}{\partial t} = \frac{\partial\overline{u}_1}{\partial t} = \frac{\partial\overline{u}_2}{\partial t} = \frac{\partial M_e}{\partial t} = 0$$

and therefore,

$$T_{\ell_1} = T_{\ell_2} = T_L = 0$$

This is a physically unrealistic situation in that the boundary-layer edge conditions are steady but the boundary-layer is unsteady developing from arbitrary initial conditions that do not correspond to reality. However, the solutions were found to be insensitive to initial conditions as discussed in Chapter 3, Section 3.3. With these

23

restrictions, Eqs. (2.23a,b,c) reduce to

$$\frac{\partial \delta_1^*}{\partial t} - \frac{\overline{u}_1}{\overline{q}} \frac{\partial \theta_\rho}{\partial t} = \overline{q} \ell_1 \qquad (2.25a)$$

$$\frac{\partial}{\partial t}(\theta_{11} + \theta_{22}) = 2\overline{q}L - \overline{u}_1 \ell_1 - \overline{u}_2 \ell_2 \qquad (2.25b)$$

$$\frac{\partial \delta_2^*}{\partial t} - \frac{\overline{u}_2}{\overline{q}} \frac{\partial \theta_\rho}{\partial t} = \overline{q} \ell_2 \qquad (2.25c)$$

Equations (2.25a,b,c) contain the 13 integral lengths $\delta_i^*$, $\theta_{ij}$, $\varepsilon_{ij}$, $\delta_{u_i}^*$, and $\theta_\rho$ where $i = 1$ or $2$, and $j = 1$ or $2$. In the present analysis, the fundamental step which permits the construction of a determinant system of equations is the resolution of the three-dimensional, turbulent boundary-layer velocity profile into a streamline coordinate system with "streamwise" and "cross-flow" components as illustrated in Figure 2. The streamline coordinate system is formed by the projection onto the body surface of the external streamlines with local normals constructed to them; the direction of the external streamline is called the "streamwise" direction and the "cross-flow" direction is normal to it. This allows each velocity component to be modeled separately, which is important because it has been observed (see, e.g., [34]) that flow in the streamwise direction is remarkably similar to a
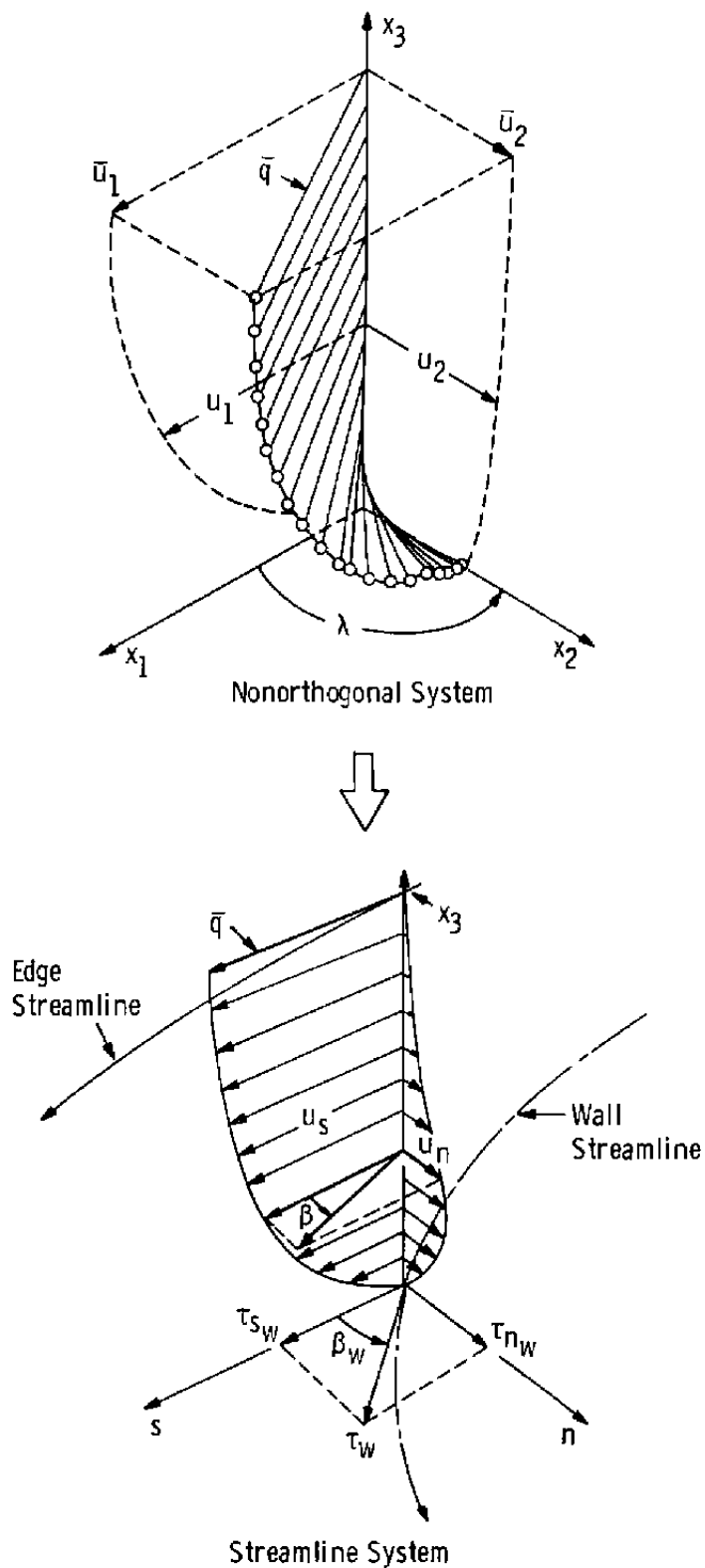
Figure 2.  Resolution of Three-Dimensional Boundary-Layer
Velocity Profile Into Streamwise Components.

corresponding two-dimensional boundary layer, and empirical relations derived for two-dimensional flow (e.g., skin friction and shape factor correlations and velocity profile families) provide good approximations to the streamwise components of velocity, skin friction, and so forth, in a fully three-dimensional boundary layer.

Once the resolution of the boundary-layer velocity components into streamline coordinates has been accomplished, the reduction of the number of unknowns appearing in Eq. (2.25) is hinged upon several auxiliary relations: (1) empirical relationships in streamline coordinates, (2) relations between streamwise integral lengths using Johnston's cross-flow profile, and (3) relationships between streamwise and nonorthogonal integral lengths. The following sections address the manner in which these tasks are resolved such that the number of unknowns appearing in Eq. (2.25) is reduced to three. In the following discussion, integral lengths written with upper-case Greek letters represent those in the streamline coordinates; whereas lower-case letters denote integral lengths resolved in the nonorthogonal system (unfortunately, this is opposite to the nomenclature used by Smith [14]).

## 2.2. Empirical Relationships in Streamline Coordinates

The degree of success of an integral boundary-layer computational procedure is ultimately related to how well the auxiliary relations represent reality. The present analysis requires models for (1) the streamwise velocity profile, (2) the cross-flow velocity profile, (3) skin friction correlations, and (4) shape factor correlations.

### 2.2.1. Streamwise Velocity Profile and Shape Factor Correlations

The present work relies heavily upon the velocity profile originally postulated by Whitfield [35] for steady, two-dimensional, incompressible or compressible adiabatic, turbulent boundary layers, which was later extended to include profiles with reversed flow [28,36]. It should be pointed out that the analytical representations of the streamwise and cross-flow velocity profiles do not appear explicitly in the analysis; rather, shape factor correlations and relationships between the streamwise integral lengths which are based upon the velocity profiles are used.

The streamwise velocity profile [28,36] is a function of "incompressible" values of shape factor, $\bar{H}$, and momentum thickness Reynolds number, $\overline{Re}_{\Theta_{11}}$, that is,

$$\frac{u_s}{\overline{q}} = \frac{u_s}{\overline{q}}\left(\overline{H}, \ \overline{Re}_{\theta_{11}}\right) \tag{2.26}$$

where

$$\overline{H} = \frac{\Delta_u^*}{\Theta_u} = \frac{\displaystyle\int_0^\infty \left(1 - \frac{u_s}{\overline{q}}\right)dx_3}{\displaystyle\int_0^\infty \frac{u_s}{\overline{q}}\left(1 - \frac{u_s}{\overline{q}}\right)dx_3} \tag{2.27a}$$

(As seen in Eq. (2.27a), "incompressible" here means simply that integral lengths are defined to be independent of density.) In addition, the following shape factors can be defined in streamline coordinates as

$$H = \frac{\Delta_1^*}{\Theta_{11}} \tag{2.27b}$$

$$H_{\theta_\rho} = \frac{\Theta_\rho}{\Theta_{11}} \tag{2.27c}$$

$$H_{\theta^*} = \frac{E_{11}}{\Theta_{11}} \tag{2.27d}$$

and

$$\frac{\Theta_{11}}{\Theta_u} \tag{2.27e}$$

where the above streamwise lengths are defined in Appendix B. Using Eq. (2.26), it was shown in [24] that $H$, $\Theta_{11}/\Theta_u$, and $H_{\theta^*}$ can be correlated with $\overline{H}$ and edge Mach

number, $M_e$, with only a weak dependence upon $Re_{\theta_{11}}$. The $H_{\theta}*$ correlation actually used herein is based upon a streamwise velocity profile valid for attached and separated flow [36]. All shape factor correlations used are listed in Appendix C, including the $H_{\theta\rho}$ correlation originally derived by Donegan [37] which was reported in [30].

## 2.2.2. Cross-Flow Velocity Profile

The choice of cross-flow velocity profile representation can have a significant influence on the results of the calculations, as shown by the results of Smith's integral method [14] reported by East [10]. Because the main objective of the present study was to obtain solutions of the three-dimensional, turbulent, integral boundary-layer equations, it was decided that the relatively uncomplicated triangular model of Johnston [29] would suffice, with the understanding that an improved model could be used later. Smith [14] also used this model and obtained reasonable results for a fairly large class of three-dimensional, turbulent boundary-layer test cases [14,10,25,26]. However, it was concluded by Johnston himself [38], that "there can be no general, universal cross-flow model" (for example, consider a "crossover" or "s-shaped" profile where the cross-flow velocity is both positive and negative over the boundary-layer

29

thickness [38]). This is undoubtedly one of the weakest areas concerning the use of integral methods for the calculation of three-dimensional turbulent boundary layers.

Johnston's cross-flow model [29] is given as

$$\frac{u_n}{u_s} = \tan(\beta_w) \qquad (2.31a)$$

in the thin layer adjacent to the wall, and

$$\frac{u_n}{q} = A\left(1 - \frac{u_s}{q}\right) \qquad (2.31b)$$

over the remaining portion of the boundary layer, where A is a parameter which must be related to the limiting wall streamline angle, $\beta_w$. In the present case, the relationship originally given by Johnston [29] and later modified by Smith [14] as

$$\tan(\beta_w) = A \left\{ \frac{0.1}{\left[c_f \, \cos\left(\beta_w\right)\left(1 + 0.18 \, M_e^2\right)\right]^{1/2}} - 1 \right\} \qquad (2.32)$$

is used, where $c_f$ in the above is the local skin friction coefficient resolved along the external streamline flow direction (in the present case, $\beta_w$ is solved for iteratively by knowing A, $c_f$, and $M_e$).

## 2.2.3. Skin Friction

The skin friction correlation used is that given by Whitfield et al. [28], as

$$\bar{c}_f = \frac{0.3e^{-1.33\bar{H}}}{\left(\log_{10}\overline{Re}_{\theta_{11}}\right)^{1.74+0.31\bar{H}}}$$
$$+ (1.1 \times 10^{-4}) \left[\tanh\left(4 - \frac{\bar{H}}{0.875}\right) - 1\right] \qquad (2.33)$$

where $\bar{c}_f$, $\bar{H}$, and $\overline{Re}_{\theta_{11}}$ denote "incompressible" values. The first term on the right-hand side of Eq. (2.33) was derived by White [23] (Eq. 6-179, p. 518) from curve fits of the Law-of-the-Wall/Law-of-the-Wake using Coles' constants in the Law-of-the-Wall [23]. The second term of Eq. (2.33) was originally reported in [39] and later in [28] and [36] and was appended to White's relation to allow $c_f$ to become negative. Although separated flows are not addressed in this work, Eq. (2.33) is used because of its behavior at high shape factors (for low shape factors, the contribution of this term is negligible).

The relations used to interrelate compressible and incompressible variables in Eq. (2.33) are Coles' "Law of Corresponding Stations" [40] given as

$$Re_{\theta_{11}} c_f = \overline{Re}_{\theta_{11}} \bar{c}_f \qquad (2.34a)$$

and the correlation of Winter and Gaudet [41], which relates $c_f$ to $\bar{c}_f$ by the relation

$$\frac{\overline{c}_f}{c_f} = F_c \qquad (2.34b)$$

or, in effect

$$\frac{c_f}{\overline{c}_f} = \frac{\overline{Re_\theta}_{11}}{Re_{\theta_{11}}} = \frac{1}{F_c} \qquad (2.34c)$$

where

$$F_c^2 = 1 + \frac{\gamma - 1}{2} M_e^2 \qquad (2.34d)$$

Finally, the equations used to resolve $c_f$ in streamwise coordinates into nonorthogonal components (which Eqs. (2.25a,b,c) contain) are those used by Myring [13] and Smith [14],

$$c_{f_{x_1}} = c_f \left[ \frac{\sin(\xi) - \cos(\xi) \tan(\beta_w)}{\sin(\lambda)} \right] \qquad (2.35a)$$

$$c_{f_{x_2}} = c_f \left[ \frac{\sin(\alpha) + \cos(\alpha) \tan(\beta_w)}{\sin(\lambda)} \right] \qquad (2.35b)$$

where $c_{f_{x_i}}$ is the value of skin friction resolved in the $x_i$-direction, $\alpha$ is the angle between the local resultant edge velocity vector and the $x_1$-axis, $\lambda$ is the angle between the $x_1$- and $x_2$-axes, and $\xi \equiv \lambda - \alpha$.

## 2.2.4. Dissipation Integrals

As shown in Appendix D, the dissipation integrals appearing in Eq. (2.20) can be written in terms of stream-wise and cross-flow velocities and then integrated by parts using Johnston's cross-flow profile [29], yielding

$$
\frac{1}{\rho q^3} \int_0^\infty \left( u_1 \frac{\partial \tau_{x_1}}{\partial x_3} + u_2 \frac{\partial \tau_{x_2}}{\partial x_3} \right) dx_3
$$

$$
= -\frac{1}{\sin^2\lambda} \frac{c_f D_u^S}{2} \left( t_1 + t_2 \frac{D_u^n}{D_u^S} \right) \tag{2.36}
$$

where $D_u^S$, $D_u^n$, $t_1$, and $t_2$ are defined in Appendix D. The "streamwise" dissipation $D_u^S$ is evaluated in this study using the correlation developed by Donegan [42] and later improved by Thomas [43]. Actually, the product $c_f D_u^S/2$ was correlated as

$$
\frac{c_f D_u^S}{2} = \frac{c_f D_u^S}{2} \left( \overline{H}, \overline{Re}_{\Theta 11}, M_e \right) \tag{2.37}
$$

This correlation was derived by numerically evaluating $D_u^S$ using a constant laminar plus turbulent shear stress in the region very near the wall, the Cebeci-Smith eddy viscosity model [44] in the inner and outer regions, and the derivative of the velocity profile used in [28]. In the present study, the contribution of $D_u^n$ has been

33

neglected in comparison to $D_u^S$ with the understanding that significant error could be introduced in flows with large crossflow (see Appendix D).

### 2.3. Relationships Between Streamwise Integral Lengths Using Johnston's Cross-Flow Profile

As defined by Eq. (B.8) in Appendix B, the stream-wise integral length $\Delta_2^*$ is given by

$$\bar{\rho}\bar{q}\Delta_2^* = - \int_0^\infty \rho u_n \, dx_3 \tag{2.38}$$

Using Eq. (2.31b) in Eq. (2.38) (according to Smith [14], only the outer part of Johnston's model is needed to evaluate streamwise integral lengths) results in

$$\bar{\rho}\,\bar{q}\,\Delta_2^* = -A \int_0^\infty (\rho\bar{u}_s - \rho u_s) \, dx_3$$

$$= -A \int_0^\infty [(\bar{\rho}\,\bar{u}_s - \rho u_s) - \bar{u}_s(\bar{\rho} - \rho)] \, dx_3$$

$$= -A [\bar{\rho}\,\bar{q}\Delta_1^* - \bar{\rho}\,\bar{u}_s \theta_\rho]$$

Thus,

$$\Delta_2^* = -A(\Delta_1^* - \theta_\rho) \tag{2.39}$$

It is shown in Appendix E that the remaining integral lengths in streamline coordinates $(\Theta_{12}, \Theta_{21},$ etc.) can also be related to A, $\Delta_l^*$, $\Delta_u^*$, $\Theta_{11}$, $E_{11}$, $\Theta_u$, and $\theta_\rho$.

## 2.4. Relationships Between Streamwise and Nonorthogonal Integral Lengths

As pointed out by Smith [14], all integral quantities in one axis system are uniquely related to those in the other and these relations are independent of the choice of cross-flow profile. For example, Smith [14] shows that the momentum thickness $\theta_{11}$ in the nonorthogonal system is related to those in the streamline system as

$$\theta_{11} = \frac{1}{\sin^2\lambda}[\Theta_{11} \sin^2\xi - (\Theta_{12}+\Theta_{21})\sin\xi \cos\xi + \Theta_{22} \cos^2\xi] \quad (2.40)$$

Stock [15] has listed all of these relationships using different nomenclature than that used herein; whereas Myring [13] and Smith [14] give the relationships between streamline and nonorthogonal displacement and momentum thicknesses. The complete list using the present nomenclature is given in Appendix F.

## 2.5. Reduction of the Number of Unknowns--Summary

The number of parameters in the system can now be related to the three unknowns $\Theta_{11}$, $\overline{H}$, and A. This process can be summarized as follows. If the values of $\Theta_{11}$, $\overline{H}$,

and A are known at all points on the surface and at a
particular time, and given the edge conditions $\bar{\rho}$, $\bar{u}_1$, $\bar{u}_2$,
$M_e$, and geometric parameters $\alpha$, $\lambda$, and $\xi$, the following
sequence of calculations produces all remaining unknowns
in the system (Eq. (2.25)):

1.  Compute shape factor correlations

$$H = H(\bar{H}, M_e)$$

$$H_{\theta*} = H_{\theta*}(\bar{H}, M_e)$$

$$H_{\theta_\rho} = H_{\theta_\rho}(\bar{H}, M_e)$$

$$\frac{\Theta_u}{\Theta_{11}} = \frac{\Theta_u}{\Theta_{11}}(\bar{H}, M_e)$$

(see Appendix C)

$$\Delta_1^* = H\,\Theta_{11}$$

$$E_{11} = H_{\theta*}\,\Theta_{11}$$

2.  Compute streamwise integral quantities $\Delta_2^*$,
    $\Theta_{21}$, $\Theta_{12}$, etc. (see Appendix E).

3.  Compute streamwise skin friction (Eq. (2.33)),
    $\beta_w$ (Eq. (2.32)), $c_f D_u^S/2$ (see Appendix C),
    $c_{f_{x_1}}$ and $c_{f_{x_2}}$ (Eq. (2.35)).

4.  Compute nonorthogonal integral quantities $\delta_1^*$,
    $\delta_2^*$, $\theta_{11}$, etc. (see Appendix F).

## 2.6. Formulation for Solution

Using the relations between streamwise and non-orthogonal integral lengths given in Appendix F, the aforementioned empirical correlations, and assuming steady edge conditions, it is shown in Appendix G that Eqs. (2.25a,b,c) can be recast into matrix form as

$$\hat{A} \frac{\partial}{\partial t} (\underset{\sim}{U}) = \underset{\sim}{b} \qquad (2.41)$$

where

$\hat{A}$ = 3x3 coefficient matrix

$\underset{\sim}{U}$ = vector of unknowns

$\quad = (\theta_{11}, \bar{H}, A)^{T}$

$\underset{\sim}{b}$ = RHS vector containing spatial derivatives and edge conditions

The elements of the matrix $\hat{A}$ and vector $\underset{\sim}{b}$ are also given in Appendix G. Equation (2.41) represents a system of three first-order, nonlinear, coupled partial differential equations for the three unknowns, $\theta_{11}$, $\bar{H}$, and A. The numerical approach taken here is to first reduce the above system of partial differential equations (PDE) to a system of ordinary differential equations (ODE) and then use a standard integrator for ordinary differential equations. Particular aspects of the numerical method used herein are discussed in Chapter III.

37

Chapter III

NUMERICAL METHOD

The aforementioned numerical approach is commonly referred to as the Method of Lines, which, as discussed by Ames [45, pp. 302-304], is primarily Russian in origin (see, e.g., Liskovets [46]). This numerical method was chosen for the present study because of the success demonstrated by Jameson et al. [47] who used this approach to solve the unsteady Euler equations in transonic flow, and in addition, showed that when using a Runge-Kutta scheme, convergence to a steady-state solution could be accelerated by using a local time-step as dictated by the local CFL number (Courant-Friedrichs-Lewy stability criterion). The approach taken here is also a Runge-Kutta scheme using a variable time-step to accelerate convergence (transient results were not considered important for the cases presented).

### 3.1. Implementing Four-Stage Runge-Kutta for a System of PDE's

Consider the single linear model equation

$$\frac{\partial u}{\partial t} + a \frac{\partial u}{\partial x} = 0, \ a = \text{constant} > 0 \qquad (3.1)$$

applied in the x-t plane. By discretizing the continuous x-t space as depicted in Figure 3a, Eq. (3.1) can be converted to an ordinary differential equation by expressing the spatial derivative with an appropriate finite-difference approximation, or

$$\frac{du_i}{dt} = - aD_x(u_i^n) \equiv f(t,u_i^n) \tag{3.2}$$

where $D_x(u_i^n)$ is a finite-difference operator and i and n denote the $i^{th}$ value of u at a time level n. Writing Eq. (3.2) at each i mesh point at the $n^{th}$ time-level results in a system of ordinary differential equations which can be integrated using any standard ODE integration scheme.

As mentioned above, a Runge-Kutta (R-K) scheme was chosen for the present study. The particular scheme is what is usually referred to as the "classical" R-K scheme (Eq. (20), p. 120 of Lambert [48]) is given here as

$$u_i^{n+1} = u_i^n + \frac{\Delta t}{6}(k_1 + 2k_2 + 2k_3 + k_4) \tag{3.3a}$$

where

$$k_1 = f(t,u_i^n) \tag{3.3b}$$

$$k_2 = f(t + \frac{\Delta t}{2}, u_i^n + \frac{\Delta t}{2}k_1) \tag{3.3c}$$
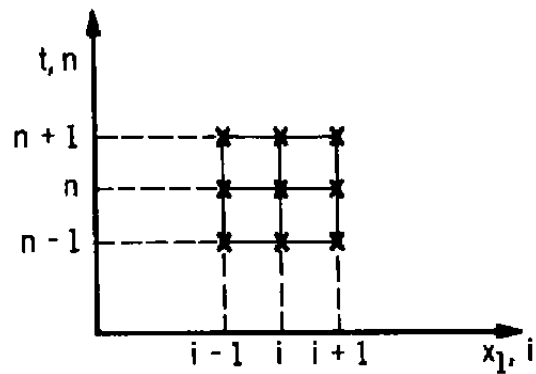
a.  One-Space Dimension



b.  Two-Space Dimensions

Figure 3.  Space Discretization.

$$k_3 = f( \ t + \frac{\Delta t}{2} \ , \ u_i^n + \frac{\Delta t}{2} \ k_2 \ ) \qquad (3.3d)$$

$$k_4 = f( \ t + \Delta t \ , \ u_i^n + \Delta t \ k_3 \ ) \qquad (3.3e)$$

which advances the solution at each i mesh point at time-level n to time-level n+1 with a local truncation error of $O(\Delta t^5)$.

For a model equation containing two space dimensions, Eq. (3.1) becomes

$$\frac{\partial u}{\partial t} + a \ \frac{\partial u}{\partial x_1} + b \ \frac{\partial u}{\partial x_2} = 0 \qquad (3.4)$$
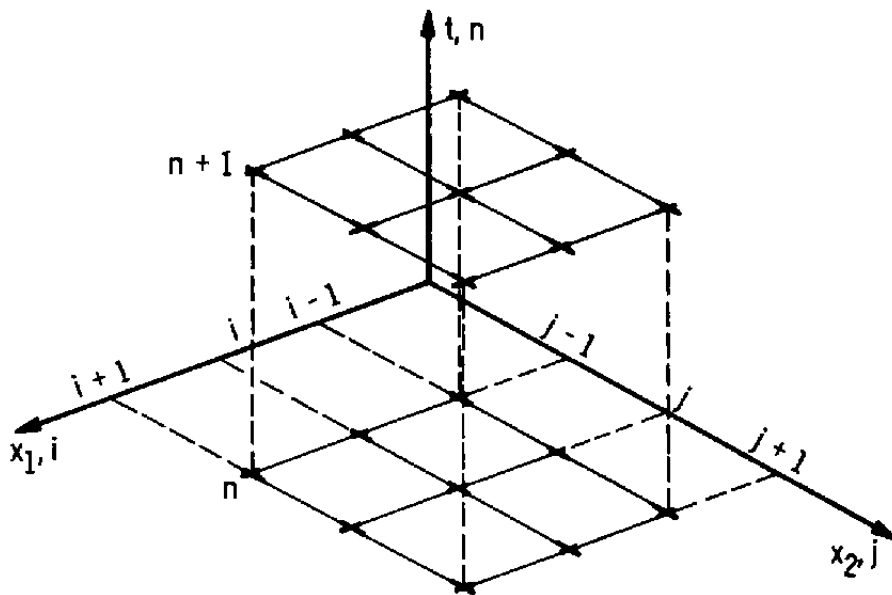
where a and b are positive constants. Using a space-time discretization as depicted in Figure 3b, the corresponding ODE is

$$\frac{du_{ij}}{dt} = - \ aD_{x_1}( \ u_{ij}^n \ ) - bD_{x_2}( \ u_{ij}^n \ ) \qquad (3.5)$$

$$\equiv g( \ t, u_{ij}^n \ )$$

Applying the R-K scheme at each (i,j) surface grid point results in

$$u_{ij}^{n+1} = u_{ij}^n + \frac{\Delta t}{6} \ (k_1 + 2k_2 + 2k_3 + k_4) \qquad (3.6a)$$

where now,

$$k_1 = g( t, u_{ij}^n ) \tag{3.6b}$$

$$k_2 = g( t + \frac{\Delta t}{2} , u_{ij}^n + \frac{\Delta t}{2} k_1 ) \tag{3.6c}$$

$$k_3 = g( t + \frac{\Delta t}{2} , u_{ij}^n + \frac{\Delta t}{2} k_2 ) \tag{3.6d}$$

$$k_4 = g( t + \Delta t, u_{ij}^n + \Delta t k_3 ) \tag{3.6e}$$

The present set of equations (Eq. (2.41)) can be written in vector form as

$$\frac{\partial \underset{\sim}{U}}{\partial t} + M \frac{\partial \underset{\sim}{U}}{\partial x_1} + N \frac{\partial \underset{\sim}{U}}{\partial x_2} = \underset{\sim}{c} \tag{3.7}$$

where $\underset{\sim}{U}$ is the vector of unknowns

$$\underset{\sim}{U} = (\Theta_{11} , \bar{H} , A)^T \tag{3.8}$$

M and N are 3x3 matrices, and $\underset{\sim}{c}$ is a vector. Thus, replacing the $u_{ij}$ in Eq. (3.5) with $\underset{\sim}{U}_{ij}$ results in

$$\frac{d\underset{\sim}{U}_{ij}}{dt} = - M_{ij} D_{x_1} ( \underset{\sim}{U}_{ij}^n ) - N_{ij} D_{x_2} ( \underset{\sim}{U}_{ij}^n ) + \underset{\sim}{c} \tag{3.9}$$

and the solution for $\underset{\sim}{U}_{ij}$ can be advanced from n to n+1 using Eq. (3.6) for each unknown (i.e., $\Theta_{11}$, $\bar{H}$, and A).

Although a system of equations is involved, the numerical method described above is explicit (i.e., all quantities on the right-hand side of Eq. (3.6a) are known). For stability, explicit methods are typically restricted to CFL numbers less than one. However, as discussed in the next section, the R-K scheme used herein permits the solution process to advance using CFL numbers greater than one, depending upon the type of space differences used.

## 3.2. Stability and Convergence

### 3.2.1. General

As pointed out by Mitchell and Griffiths [49, pp. 181-182], "a stability analysis of a hyperbolic system in two-space dimensions is extremely difficult, even with A and B constant" (where in this case, A and B correspond to $M_{ij}$ and $N_{ij}$). For example, see [50] and [51]. It follows that stability requirements used in the present study do not stem from an analysis on the complete system of equations in two-space dimensions, but rather from a Fourier analysis based upon a linearized version of Eq. (3.9) which has been "split" into two, one-dimensional (in space) problems. That is, stability requirements are based upon the "worst case" stemming from a separate analysis of each of the "split" equations

$$\frac{dU_{ij}}{dt} = - M_{ij} D_{x_1} ( U_{ij}^n )$$ (3.10a)

and

$$\frac{dU_{ij}}{dt} = - N_{ij} D_{x_2} ( U_{ij}^n )$$ (3.10b)

Actually, the requirements for stability come from analyzing the single linearized two-dimensional model equation, Eq. (3.5), where a and b are interpreted as eigenvalues of the $M_{ij}$ and $N_{ij}$ matrices, respectively (see Lambert [48], p. 227). Therefore, the equations from which the stability criterion is derived reduce to

$$\frac{du_{ij}}{dt} = -\rho_{ij}(M) D_{x_1} (u_{ij}^n)$$ (3.11a)

and

$$\frac{du_{ij}}{dt} = -\rho_{ij}(N) D_{x_2} (u_{ij}^n)$$ (3.11b)

where $\rho_{ij}(M)$ and $\rho_{ij}(N)$ are the spectral radii of the $M_{ij}$ and $N_{ij}$ matrices, respectively, at each surface grid point. A stable time-step is chosen as follows: at the beginning of each time-step and for each mesh point:

1.  Compute the elements of the M and N matrices.

2.  Compute all eigenvalues of both M and N matrices and determine the spectral radius of each; that is, find $\rho_{ij}(M)$ and $\rho_{ij}(N)$.

As will be shown presently, a local CFL stability criterion for the four-stage R-K scheme is given by

$$\left[ \rho(M) \text{ or } \rho(N) \cdot \frac{\Delta t}{\Delta x} \right]_{ij} < CFL$$

where CFL is determined from a stability analysis of the R-K scheme, and $\Delta x$ is either $\Delta x_1$ or $\Delta x_2$. Thus,

3. Compute each local time-step as

$$(\Delta t_{x_1})_{ij} = \left[ \frac{CFL \cdot \Delta x_1}{\rho(M)} \right]_{ij}$$

$$(\Delta t_{x_2})_{ij} = \left[ \frac{CFL \cdot \Delta x_2}{\rho(N)} \right]_{ij}$$

4. Compute $\Delta t_{ij} = \min[ (\Delta t_{x_1})_{ij} , (\Delta t_{x_2})_{ij} ]$.

Although not mathematically rigorous, this analysis for determining a locally stable time-step has proved to be somewhat conservative, at least for the cases considered. For example, numerical experiments revealed that the van den Berg and Elsenaar test case (Section 5.4) could be computed successfully using backward space differences and a local time-step which would require a CFL of 1.55 (it will be seen that linear stability analysis gives a maximum stable CFL of approximately 1.3). It seems plausible, however, that just the opposite could occur

when considering the liberties taken during the course of
the analysis; i.e., the "splitting" of the complete problem
into two, one-dimensional problems, and, of course, using
a CFL number derived from a locally linearized equation.
Therefore, time-steps as determined from the above analysis
should be used with care.

### 3.2.2.   Stability and Convergence Using Various Space Difference Approximations

The stability characteristics of the R-K scheme
used herein depend explicitly upon the type of difference
used to approximate the spatial derivative ($D_{x_1}$ and $D_{x_2}$)
in Eqs. (3.11a,b).  Stability of the model problem
Eq. (3.2) is investigated in the present study using a
Fourier analysis [45, pp. 47-48] with three different
representations of $D_x(u_i^n)$ ((1) first-order backward,
(2) second-order central, and (3) second-order backward).[1]
Using this method, the propagation of a single row of
errors represented by a Fourier series along some initial
time line is examined to investigate the growth of the
error for large values of time.

---

[1]In the present work, the "order" of a difference
approximation is to be interpreted as the order of the
local truncation error.  For example, a second-order
difference has a local truncation error of $O(\Delta x^2)$.

Using a first-order backward difference for $\partial u/\partial x$ in Eq. (3.1) results in

$$D_x(u_i^n) \doteq \frac{1}{\Delta x} ( u_i^n - u_{i-1}^n ) \qquad (3.12)$$

Thus, Eq. (3.2) becomes

$$\frac{du_i}{dt} = - \frac{a}{\Delta x} \nabla(u_i^n) = f(t, u_i^n) \qquad (3.13a)$$

where

$$\nabla(u_i^n) \equiv u_i^n - u_{i-1}^n \qquad (3.13b)$$

Similar relations are obtained for second-order central

$$D_x(u_i^n) \doteq \frac{1}{2\Delta x} ( u_{i+1}^n - u_{i-1}^n ) \qquad (3.14)$$

and second-order backward differences:

$$D_x(u_i^n) \doteq \frac{1}{2\Delta x} ( 3u_i^n - 4u_{i-1}^n + u_{i-2}^n ) \qquad (3.15)$$

As given in Appendix H, the amplification factor $|G|$ for the R-K scheme Eq. (3.3a) using Eqs. (3.12), (3.14), or (3.15) is

$$|G| = \left| \frac{u_i^{n+1}}{u_i^n} \right| = | R(CFL, \phi) + \kappa I(CFL, \phi) | \qquad (3.16)$$

where

$$CFL = a \frac{\Delta t}{\Delta x} \qquad (3.17)$$

$\phi$ = wave number (linear function of $\Delta x$)

$\kappa = \sqrt{-1}$

and $R(CFL,\phi)$ and $I(CFL,\phi)$ are the real and imaginary contributions of $|G|$, respectively, and are somewhat complicated functions of CFL and $\phi$. The R's and I's resulting from the different difference representations are given in Appendix H.

For the solution to remain bounded for large time, the condition

$$|G| < 1 \qquad (3.18)$$

must prevail. The behavior of $|G|$ for the three space-difference approximations used is shown in Figures 4a, b, and c for second-order central, first-order backward, and second-order backward differences, respectively. Figure 4a illustrates the desirable feature of using second-order central differences in that a CFL of $2\sqrt{2}$ (approximately 2.8) can be used (this result was reported earlier by Jameson et al. [47]); whereas, using first- and
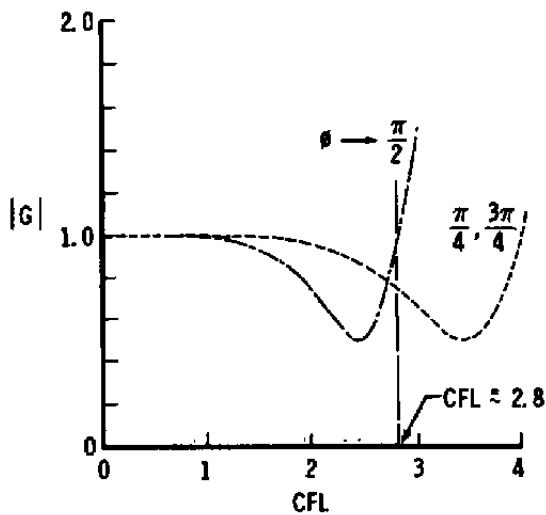
a.   Second-Order Central
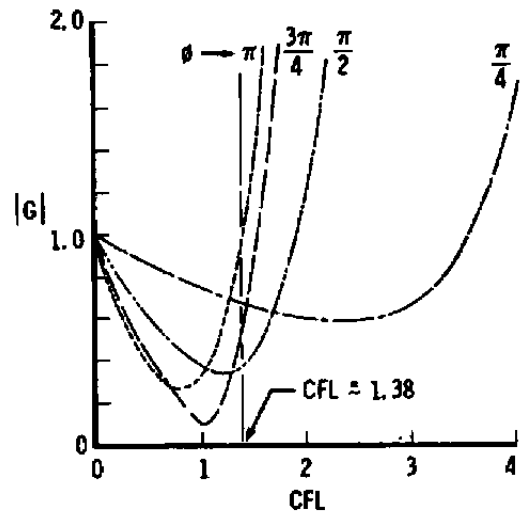
b.   First-Order Backward



c.   Second-Order Backward

Figure 4.   Stability Characteristics for Model Problem
Using Four-Stage Runge-Kutta.

second-order backward differences require using CFL numbers of approximately 1.3 and 0.6, respectively, to maintain stability (Figure 4b and c). It should be noted that the R-K scheme using central differences is stable regardless of the sign of a [45].

Initially, the present system of equations (Eq. (2.41)) was solved using central space differences with a CFL = 2.8. Smoothi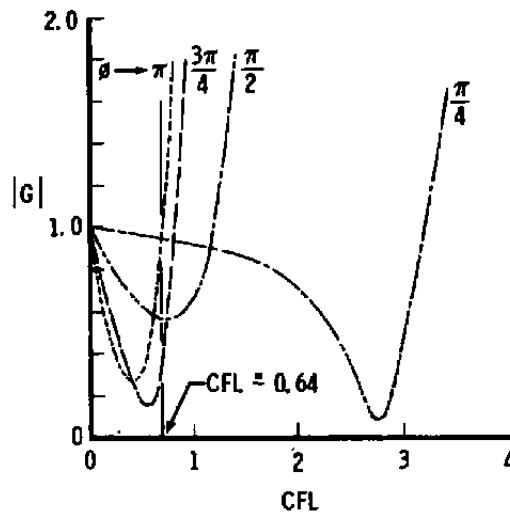ng was required and although reasonable answers were obtained, convergence was not good and the amount of smoothing needed was problem-dependent (smoothing here means that a simple weighted averaging was performed after each time cycle). After examining the eigenvalues of the $M_{ij}$ and $N_{ij}$ matrices in Eq. (3.9), it was found that, for most cases considered, eigenvalues at each grid point for both coefficient matrices were positive. As shown by Steger et al. [52], a stable scheme for the model problem (with a > 0) can be constructed using backward space differences which has better dissipative and dispersion properties than that of a centered scheme. Figure 5 illustrates the convergence obtained for the dummy infinite swept-wing case of Cumpsty and Head [16] by solving the system of equations (Eq. (2.41)) using second-order central, first-order backward, and second-order backward spatial differences. Here, as in all cases
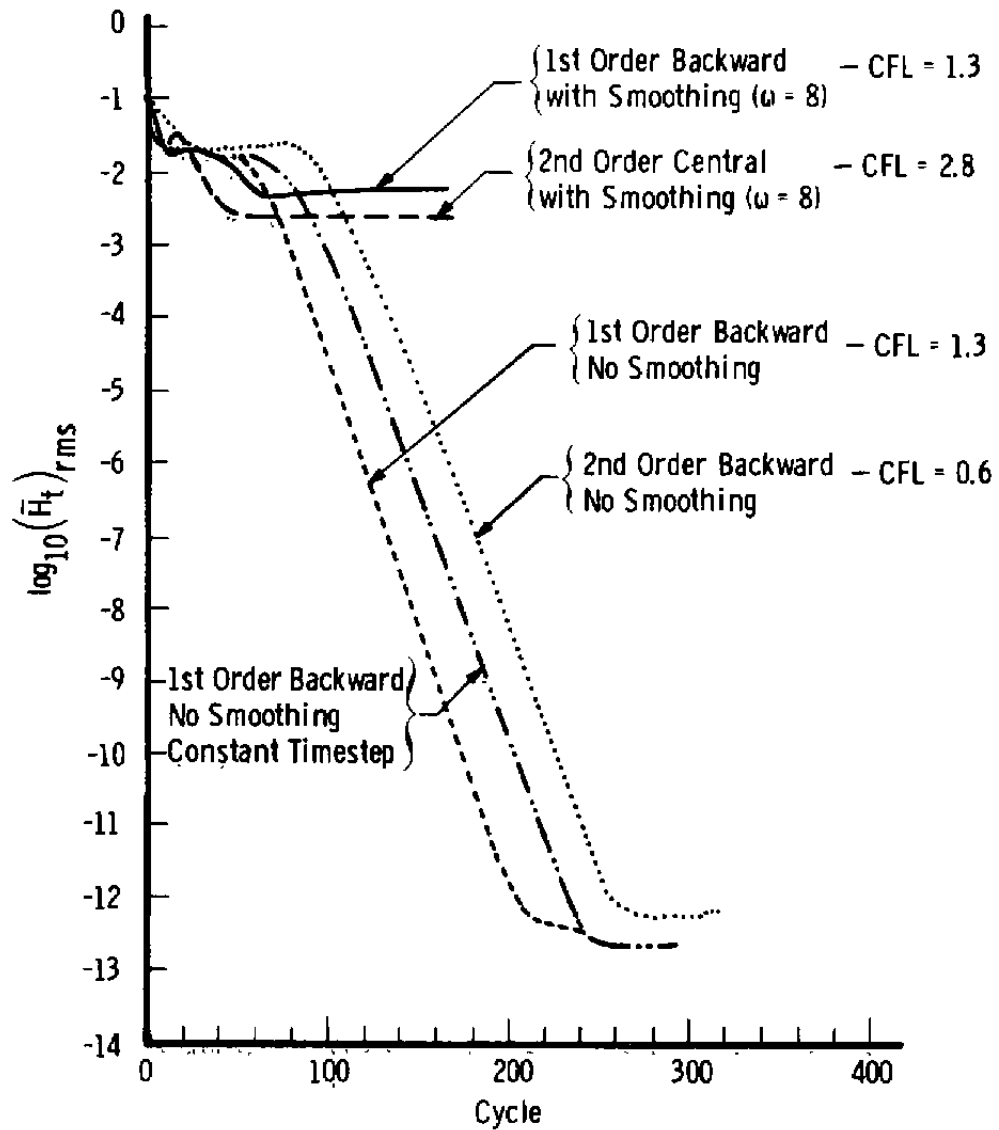
Figure 5. Convergence Histories for the Cumpsty and Head
Infinite Swept-Wing Dummy Test Case.

computed, convergence is measured by the root-mean-square of the $\partial \overline{H}/\partial t$ derivative, that is,

$$\left[\overline{H}_t\right]_{rms} \equiv \left[\frac{\sum\limits_{i,j}^{NI,NJ}\left(\frac{\partial \overline{H}}{\partial t}\right)^2_{i,j}}{NI \cdot NJ}\right]^{1/2} \tag{3.19}$$

For the solution obtained using central differences, the following simple smoothing scheme was used for the solution vector $\underset{\sim}{U}_{ij} = (\theta_{11}, \overline{H}, A)^T$ after each time-cycle:

$$\left[\underset{\sim}{U}_{ij}\right]_{smoothed} = \frac{\underset{\sim}{U}_{i+1,j}+\underset{\sim}{U}_{i-1,j}+\underset{\sim}{U}_{i,j+1}+\underset{\sim}{U}_{i,j-1}+\omega\underset{\sim}{U}_{i,j}}{\omega + 4} \tag{3.20}$$

with $\omega = 8$.

From Figure 5, it can be seen that convergence for the backward schemes using no smoothing is much better than that obtained using central differences with smoothing. The convergence obtained using the backward schemes with no smoothing is essentially limited by the machine truncation error (in this case, approximately 14 significant digits). Also shown in Figure 5 is the convergence history of the first-order backward scheme with smoothing, which illustrates that convergence is limited when smoothing is applied.

As mentioned earlier, Jameson et al. [47] showed that convergence could be accelerated by using local

time-steps (recall transient results were not considered important here). Figure 5 also illustrates how convergence is accelerated for the present system of equations by using spatially variable time-steps as opposed to using a constant time-step (i.e., maximum allowable over the field). Therefore, almost all of the solutions presented herein were computed using first-order backward differencing with spatially variable time-stepping and no artificial smoothing; however, as discussed in the next section, central differences were required for one test case, but only for the $x_2$ spatial derivative.

### 3.3.  Boundary and Initial Conditions

Depicted in Figure 6 is a general computational mesh as used in the present method. The boundary conditions used to compute all solutions presented here were to fix or "clamp" the three dependent variables ($\Theta_{11}$, $\overline{H}$, and A) along the initial start line (say, along the leading edge of a wing) and let the conditions at all other boundaries "float." That is, the dependent variables along all boundaries except the initial start line were computed in the same fashion as those in the interior of the mesh using appropriately modified spatial differencing near each boundary. This essentially amounts to extrapolating
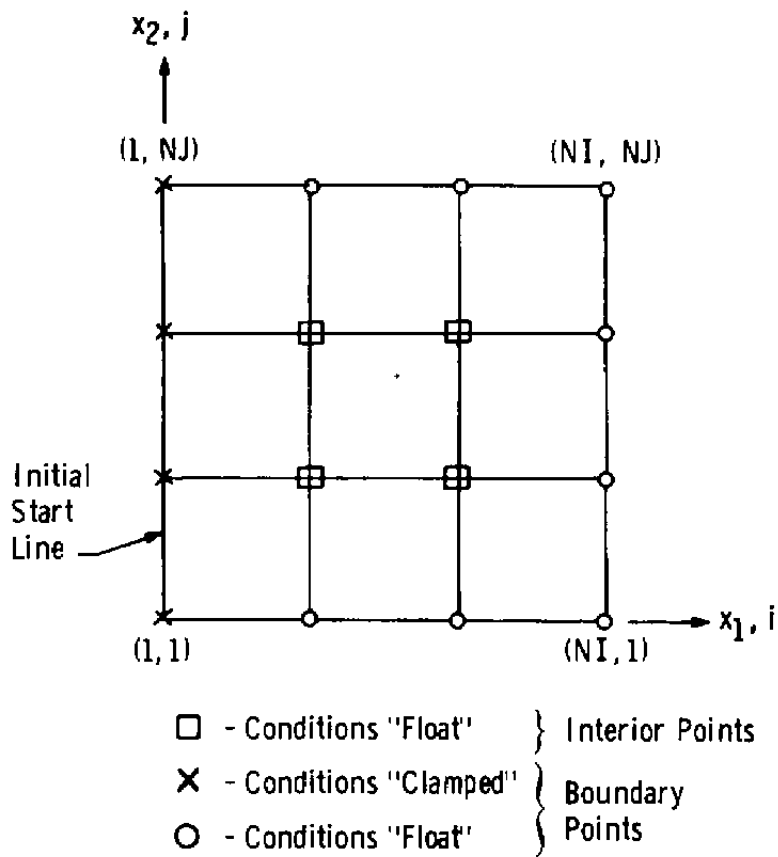
Figure 6.  General Computational Domain.

the conditions at the boundaries from the interior of the computational domain.

As previously mentioned, all eigenvalues of both the $M_{ij}$ and $N_{ij}$ matrices in Eq. (3.9) for most flow cases are positive at each mesh point. Therefore, specification of boundary conditions along the initial start line ($i = 1$, $j = 1 \rightarrow NJ$) and extrapolation along the "outflow" boundary ($i = NI$, $j = 1 \rightarrow NJ$) is compatible with the sign of the characteristics (eigenvalues). However, the signs of the eigenvalues of the $N_{ij}$ matrix were mixed at some mesh points for one test case (to be presented) and central differences were used to approximate the $D_{x_2}(u_{ij}^n)$ derivative while using a CFL of 1.3 (see Chapter V, Section 5.7). For this test case, extrapolation of boundary conditions along the ($i = 1 \rightarrow NI$, $j = 1$) line and ($i = 1 \rightarrow NI$, $j = NJ$) line is not correct if one adheres strictly to the information obtained from the sign of the eigenvalues. However, based upon the results to be presented, it seems that this erroneous treatment of conditions along the upper and lower boundaries does not significantly affect the outcome of the computations, at least for the cases considered.

Solutions generated by the present method were found to be insensitive to initial conditions. This was determined by comparing steady-state solutions obtained using identical edge conditions but different initial

conditions. Therefore, the initial conditions used for all computations presented herein were to set the values of the dependent variables at each mesh point to those given along the initial start line (see Figure 6).

## Chapter IV

## COMPUTATION OF SURFACE METRICS

The primary objective of the present work was to develop a three-dimensional, time-dependent, turbulent integral boundary-layer computational capability that can be used for compressible adiabatic flow in nonorthogonal curvilinear coordinates. However, before any boundary-layer computations can take place, the surface metrics, i.e., $h_1$ and $h_2$ (scale factors), and $K_1$, $K_2$ $K_{12}$, and $K_{21}$ (curvature terms) must be known. Most of the cases which have been computed thus far were such that specification of the surface metrics was trivial (i.e., $h_1 = h_2 = 1$ and $K_1 = K_2 = K_{12} = K_{21} = 0$). Therefore, the effects of these parameters on the boundary-layer calculations in a general sense are not included in the present study. However, two test cases have been calculated which use surface metrics other than those for the trivial case: (1) an axisymmetric flow where the metrics are determined analytically, and (2) a finite swept wing case using a skewed mesh where the surface metrics are computed from the given Cartesian coordinates.

As shown in Appendix A, all metrics depend explicitly upon derivatives of the given Cartesian

coordinates with respect to the chosen curvilinear coordinates, e.g., $\partial \bar{x}_1 / \partial x_2$. For the axisymmetric case, these derivatives are evaluated analytically; whereas, for the finite swept wing case, the surface derivatives were evaluated using simple central differences except near the boundaries where extrapolation was used; for example, $(h_1)_{i,NJ} = (h_1)_{i,NJ-1}$. This is a rather crude approximation compared to, for example, the method described by Smith and Gaffney [53] who approximate the metric tensor using bicubic splines. However, computed results indicate that the approximations used here were adequate for the case considered, which was a flat surface.

Chapter V

RESULTS OF COMPUTATIONS

Computations using the present method are compared with the results of seven experimental/analytical test cases in steady, turbulent flow. These data sets include: (1) the two-dimensional (planar) supercritical RAE airfoil flow of Cook, McDonald, and Firmin [54]; (2) the two-dimensional (axisymmetric) experiment reported by Winter, Rotta, and Smith [55] concerning the flow about a body-of-revolution; the infinite swept-wing cases of (3) Cumpsty and Head [16], (4) van den Berg and Elsenaar [56], and (5) Bradshaw and Terrell [57]; and the fully three-dimensional cases of (6) East and Hoxey [58], and (7) Humphreys [25]. The first two cases were run to investigate whether the results of the present three-dimensional, time-dependent method duplicate the results of its steady, two-dimensional predecessor [24]; whereas, the remaining cases test the three-dimensional computational capabilities of the code. In addition, results using the present method are compared with results of other calculations when available.

## 5.1. RAE Airfoil--Two-Dimensional Planar

The experiment of Cook et al. [54] involved the measurement of turbulent boundary-layer quantities over a planar, supercritical airfoil in adiabatic, high Reynolds number, transonic flow at various angles of attack. The particular flow conditions at which comparisons will be made are

$$M_\infty = 0.600$$
$$Re_{\infty,c} = 6.3 \times 10^6$$

and

2.57 deg angle of attack

which is denoted as Case 3 in [54].

Comparisons between experiment and results computed by the present method are shown in Figure 7 for displacement and momentum thicknesses, shape factor, and skin friction. Also given in Figure 7 are the results of the calculation method described in [24]. Comparing the results of the present method with those of [24] reveals that the curves are virtually indistinguishable, except for shape factor near the airfoil trailing edge, where the present results are slightly lower. In addition, the agreement between measured and calculated results is considered good.
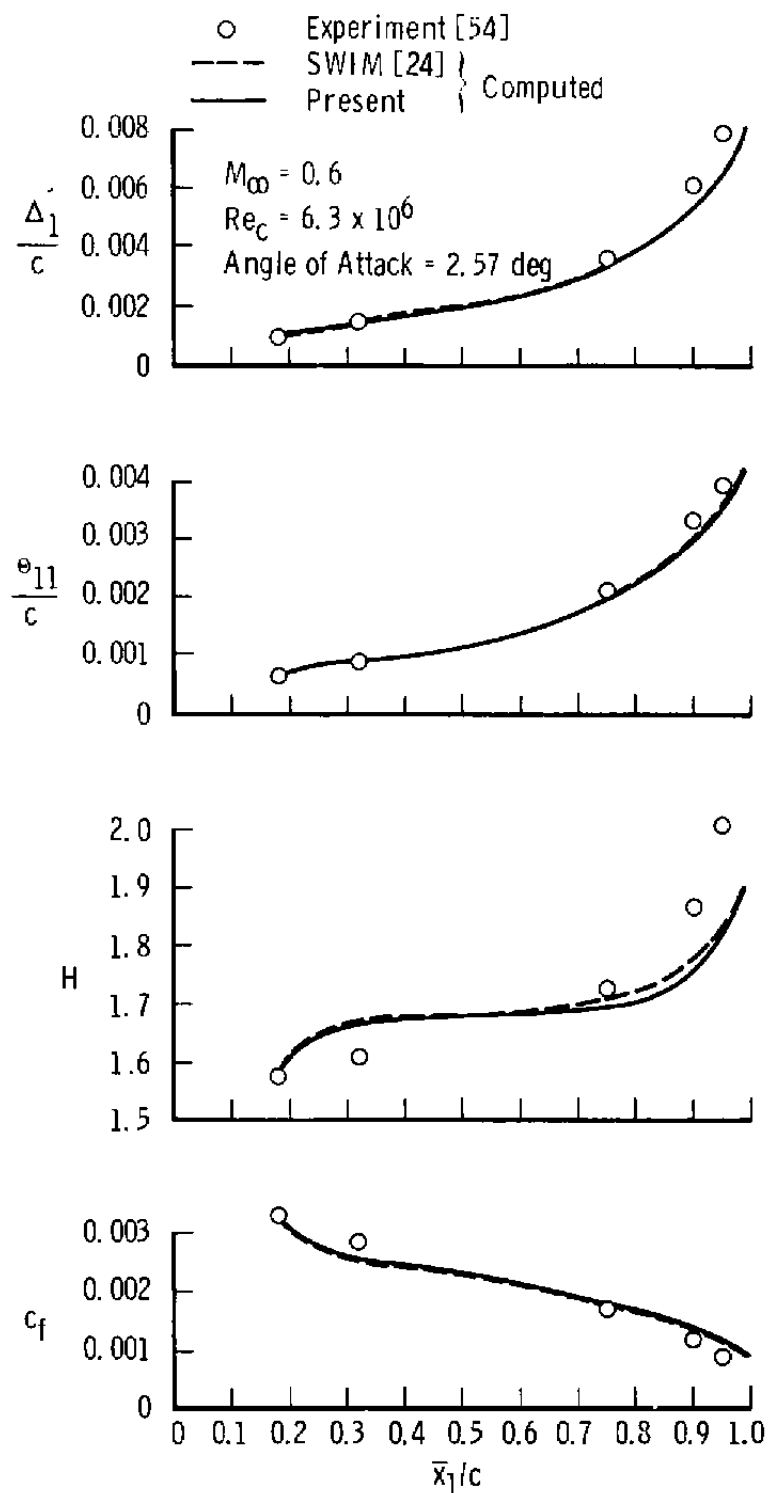
Figure 7.  Computed and Measured Boundary-Layer Quantities for the RAE Airfoil [54].

## 5.2. Waisted Body of Revolution--
## Two-Dimensional Axisymmetric

The objective of the investigation reported by Winter et al. [55] was to produce an axisymmetric, converging flow with an adverse pressure gradient to determine the effects of Mach number, pressure gradient, and streamline convergence and divergence on adiabatic, turbulent boundary-layer development. Comparisons between results computed by the present method and by the method in [24] with experiment are made at the following freestream conditions:

$$M_\infty = 0.597$$

$$Re_{\infty,L} = 9.98 \times 10^6$$

The present computations were made using the following metric coefficients:

$$h_1 = 1$$
$$h_2 = r_w = \text{local body radius}$$
$$K_1 = 0$$
$$K_2 = -\frac{1}{r_w} \frac{dr_w}{d\bar{x}_1} \left[ 1 + \left( \frac{dr_w}{d\bar{x}_1} \right)^2 \right]^{-1/2}$$
$$K_{12} = 0$$
$$K_{21} = -K_2$$

Figure 8a illustrates measured and computed distributions of skin friction, displacement and momentum thickness, and shape factor, and the agreement is considered good. Differences between the present computations and those of [24] are seen to be rather small. In addition, Figure 8b gives comparisons between measured and computed boundary-layer velocity profiles at five axial locations down the body; the agreement is considered excellent.

The results presented in Figures 7 and 8 for these special cases (i.e., two-dimensional-planar and axisymmetric) lend credence to the present method in that results generated by a previous method were essentially duplicated. The remaining cases were chosen such that the three-dimensional capabilities of the present method could be investigated.

### 5.3. Cumpsty and Head--Infinite Swept Wing

The Cumpsty and Head [16] "dummy" test case is that of an infinite swept wing in an incompressible flow with a constant linear gradient of chordwise velocity and a constant spanwise velocity, given by

$M_\infty = 0.597$
$Re_{\infty, L} = 9.98 \times 10^6$
○ Measured [55]
—— Present    } Computed
----SWIM [24]
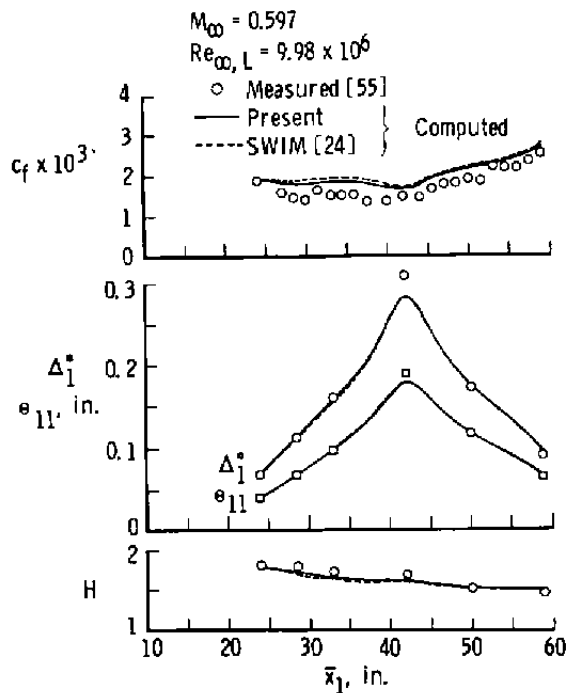


a.   Skin Friction, Momentum and Displacement
     Thicknesses, and Shape Factor
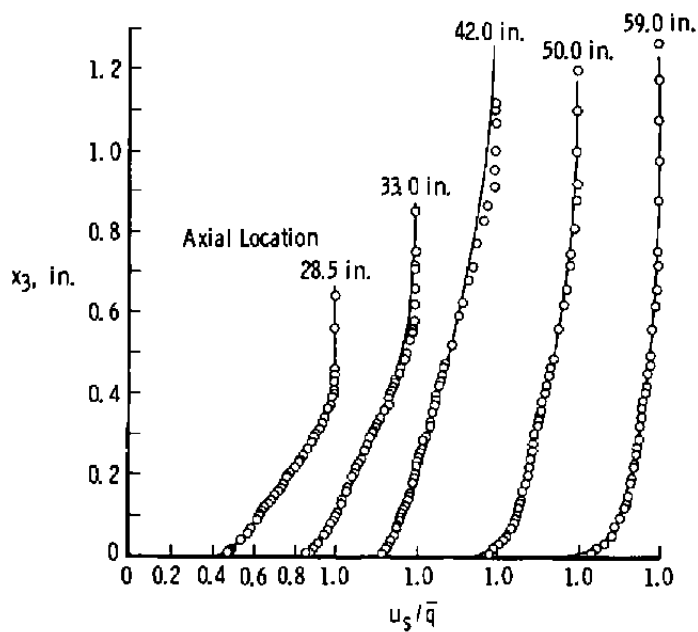


b.   Velocity Profiles

Figure 8.   Computed and Measured Boundary-Layer Quantities
            for the Waisted Body of Revolution [55].

64

$$u_{e_c} = \begin{cases} q_\infty \cos \alpha_o \, , \, x_c < 0 \\ \\ q_\infty \cos \alpha_o \, (1 - kx_c) \, , \, x_c > 0 \end{cases}$$

$$u_{e_s} = q_\infty \sin \alpha_o$$

where $u_{e_c}$ and $u_{e_s}$ are chordwise and spanwise edge veloci-
ties, respectively, $\alpha_o$ is the sweep angle, and k is the
velocity gradient. The cases considered here are for
$\alpha_o$ = 35 deg, k = 0.250, and k = 0.267. All calculations
were begun at $x_c$ = 0.

Comparisons of results between the present method
and the calculations of Cumpsty and Head [16] for momentum
thickness, shape factor, wall streamline angle, and chord-
wise skin friction are shown in Figure 9 for the case of
k = 0.267. The agreement between the two calculation
methods is considered good. It should be noted that the
computations of Cumpsty and Head shown in Figure 9 are
those resulting from using all the terms in their equations
with overall iteration (curves labeled "7(a)" in [16]).
Figure 10 compares the present calculations of chordwise
skin friction with those of Cumpsty and Head [16],
Cebeci [59], and Bradshaw [60] for the k = 0.250 case.
Although the present computations are slightly lower than

a.  Momentum Thickness



b.  Shape Factor



c.  Wall Streamline Angle
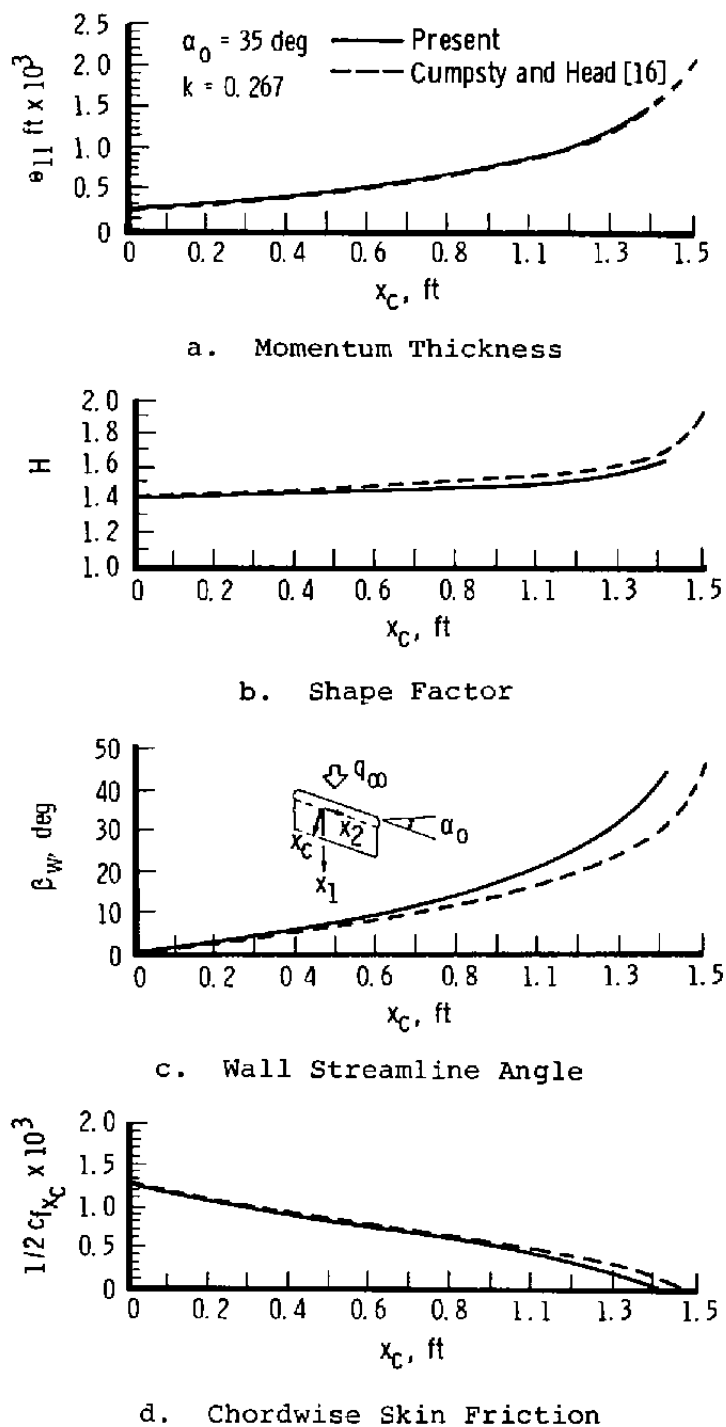


d.  Chordwise Skin Friction

Figure 9.  Calculated Results for the Dummy Test Case of
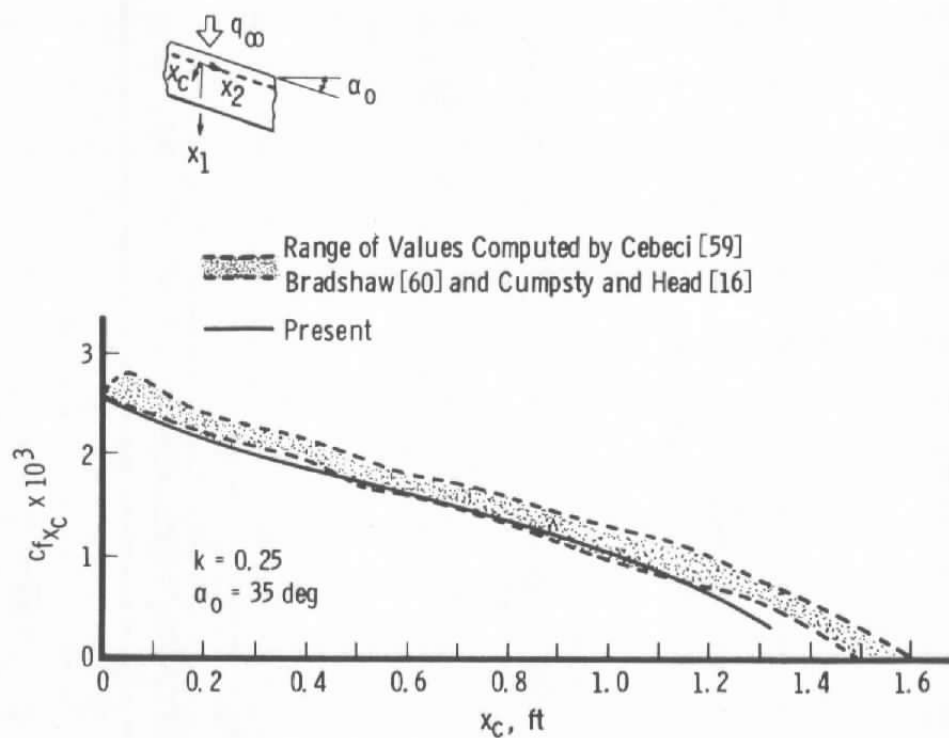Cumpsty and Head [16].

Figure 10.   Calculated Skin Friction Distribution for the
Dummy Test Case of Cumpsty and Head [16].

those of the other investigators, correct trends are
indicated.

### 5.4. van den Berg and Elsenaar--Infinite Swept Wing

The low speed flow of van den Berg and Elsenaar
[56] involved probing the three-dimensional boundary layer
on a flat surface swept at 35 deg with an external pres-
sure distribution induced by an appropriately shaped body
such that infinite swept-wing conditions were approxi-
mately simulated (this experiment was performed specifi-
cally for comparison to computational methods). Figure 11
illustrates the measured flow angle and surface pressure
distributions. Also shown in Figure 11 are the analytic
representations of measured flow angles and pressures. As
suggested in [56], the analytical representations of the
external flow conditions were used as input in the present
computations. It is seen that measured pressures are
represented well over the entire axial distance, whereas
the expression for flow angle falls below those measured
for $x_1 > 1.05$ m. Comparisons between measured and computed
boundary-layer quantities are shown in Figure 12. Agree-
ment between the computations and measurements upstream of
$x_1 = 1$ meter is considered good; whereas, past this point,
considerable discrepancies exist, particularly with the
streamwise integral thicknesses. Similar results were

a. External Flow Angle



Symbols Represent Measured Data

Solid Lines Are Analytical Representations Used in the Computations
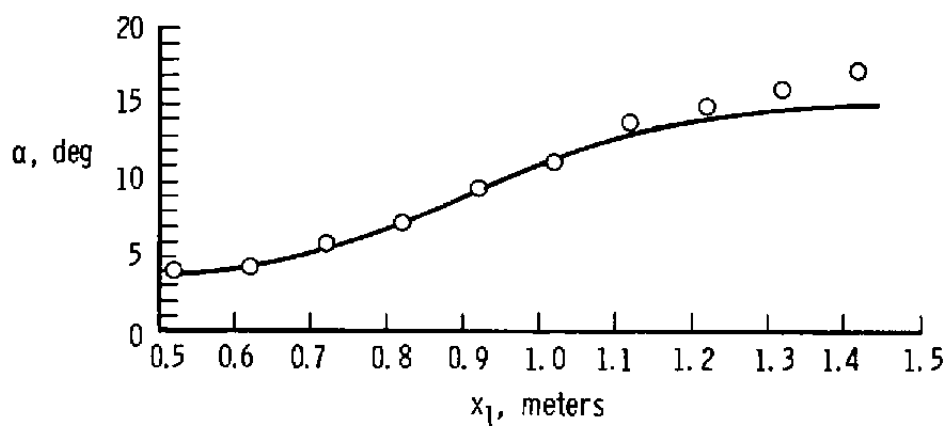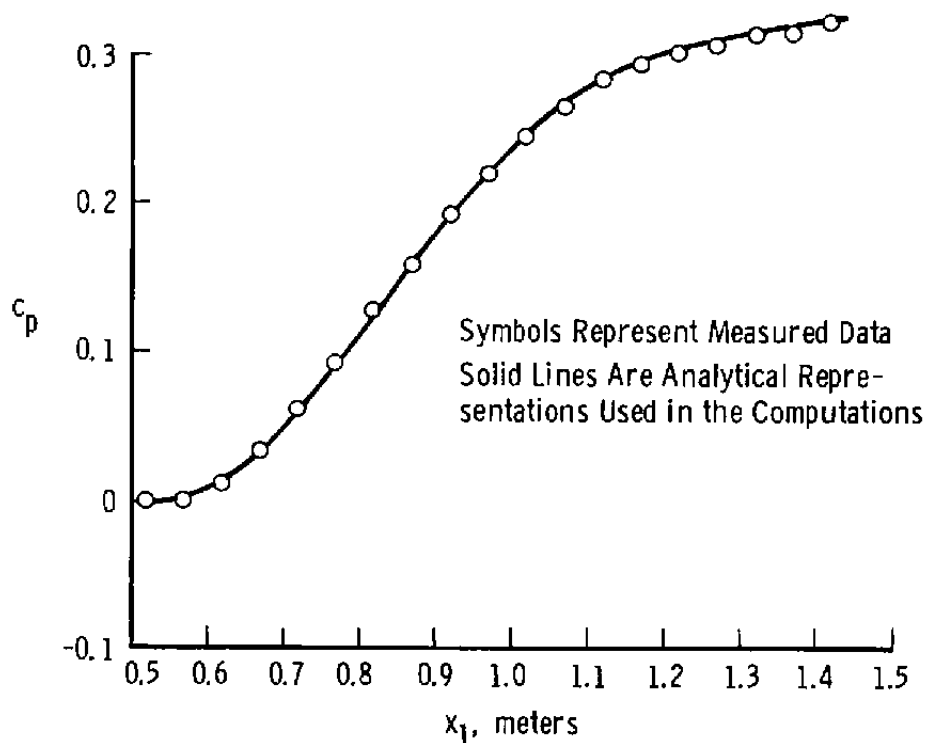
b. Surface Pressures

Figure 11. Inputs for van den Berg and Elsenaar [56] Infinite Swept-Wing Case.

69

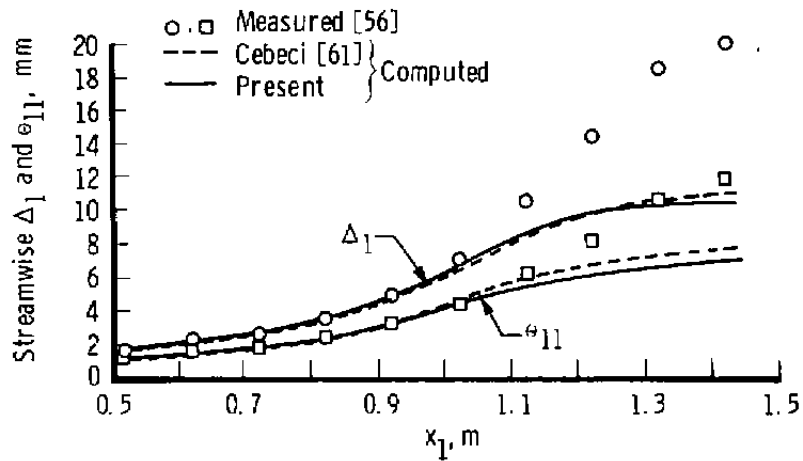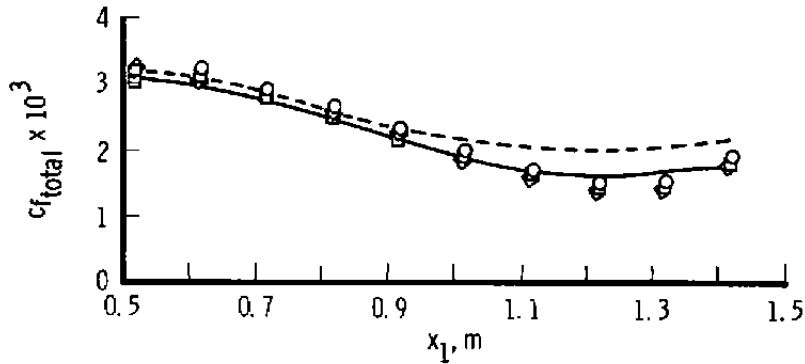a.  Displacement and Momentum Thickness



b.  Total Skin Friction
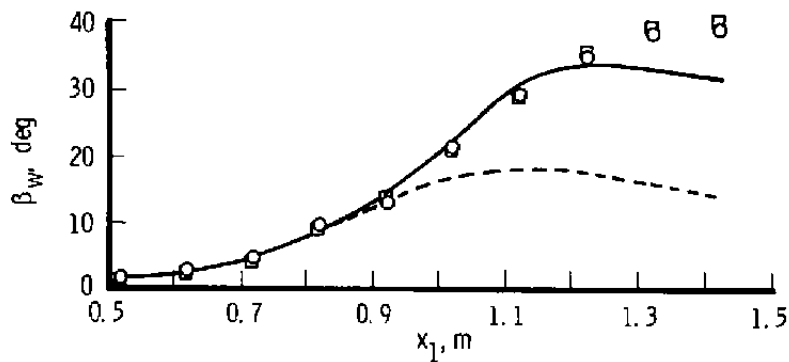


c.  Wall Streamline Angle

Figure 12.  Computed and Measured Boundary-Layer Quantities
for the van den Berg and Elsenaar [56]
Infinite Swept-Wing Case.

obtained by Cebeci and Chang [61] using a finite-difference method. However, as shown in Figure 11a, the measured flow angles downstream of $x_1 = 1$ meter deviated from those which were used as input for the computations (the analytical representation was that for an infinite swept-wing [56]). Illustrated in Figure 13 is a comparison between computed wall streamlines and a surface oil flow photograph which indicates reasonable qualitative agreement between the experiment and the computations.

An unsuccessful attempt was made to compute this flow using the measured flow angles as given by the symbols in Figure 11a. According to the experiment [56], the flow was separated near the trailing edge and it is suspected that this phenomenon is responsible for an instability in the code which leads to program failure. (In fact, Delery and Formery [62] use this experiment to test their inverse method which also indicates that the flow was separated.)

## 5.5. Bradshaw and Terrell--Infinite Swept Wing

The experiment of Bradshaw and Terrell [57] was set up to test the outer-layer assumptions in extending Bradshaw's et al., calculation method [63] from two to three dimensions. This was an infinite swept wing in a low-speed flow where boundary-layer measurements were obtained over the rear, flat portion of the wing. The axial pressure gradient was nominally zero with a decaying

a. Oil Flow Photograph

b. Computed Wall
   Streamlines

—— Inviscid Streamlines
----- Wall Streamlines
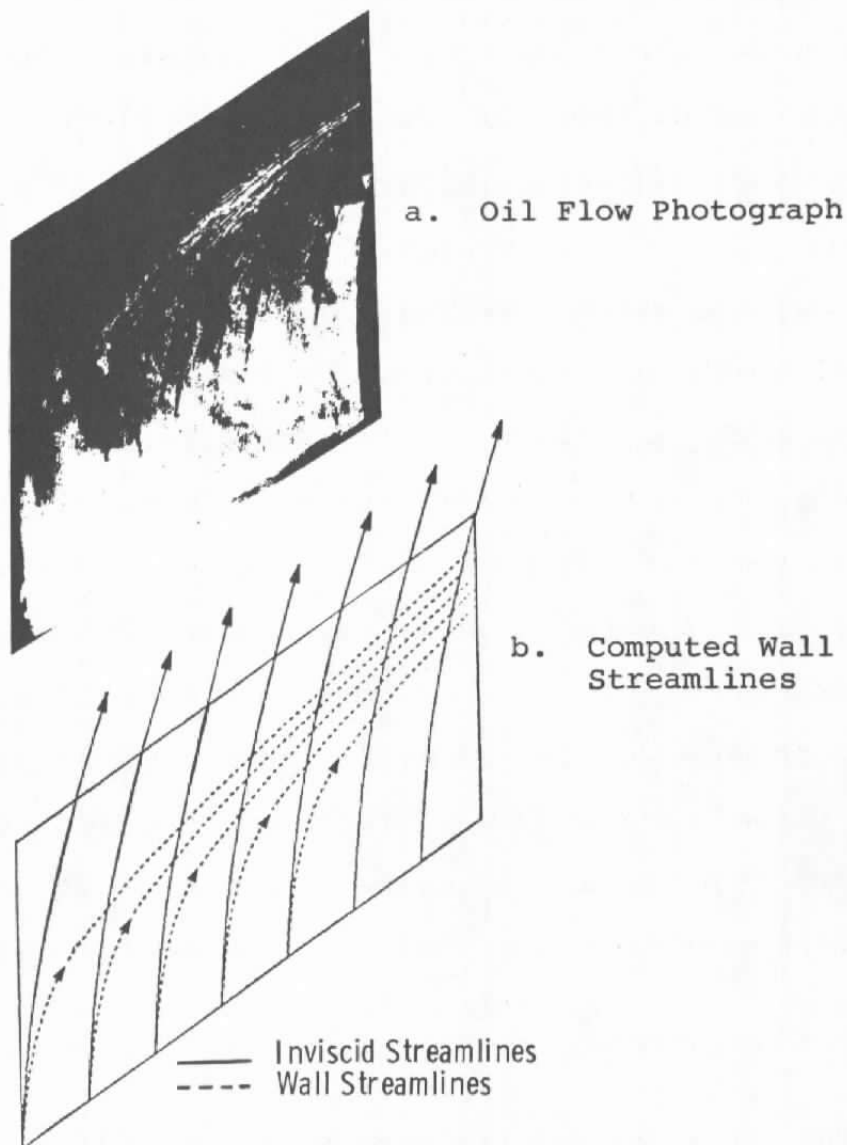
Figure 13.   Computed and Measured Wall Streamlines for the
             van den Berg and Elsenaar [56] Test Case.

crossflow. Comparisons of computed and measured boundary-layer quantities are given in Figure 14. Agreement among measured and calculated skin friction, cross-flow angle distribution, and wall streamline angle is not as good as the computations of Cebeci [59] and Bradshaw [60] (which are differential methods). For this flow, East [10] reported similar findings regarding the relative performance of integral and differential methods, and blamed the poor performance of integral methods on the use of Johnston's [29] cross-flow profile which is not representative of a decaying three-dimensional flow, particularly in the wall region. East [10] points out that this flow demonstrates how differential methods are generally more flexible than integral methods when applied to a variety of different types of flows. However, as shown in Figure 14c, the present computations of streamwise velocity agree very well with experiment.

## 5.6. East and Hoxey--Fully Three-Dimensional

The experiment of East and Hoxey [58] consisted of an obstruction placed in a thick two-dimensional boundary layer on the floor of a low-speed wind tunnel. Pressure gradients caused by the obstruction induced three-dimensionality and separation. Boundary-layer quantities
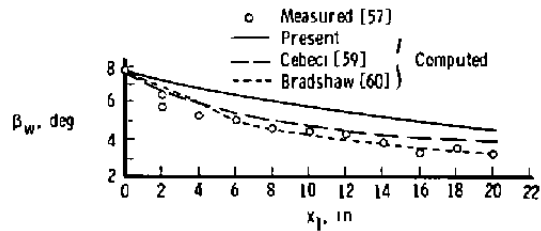
a. Wall Streamline Angle
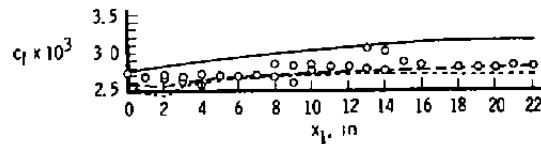


b. Streamwise Skin Friction
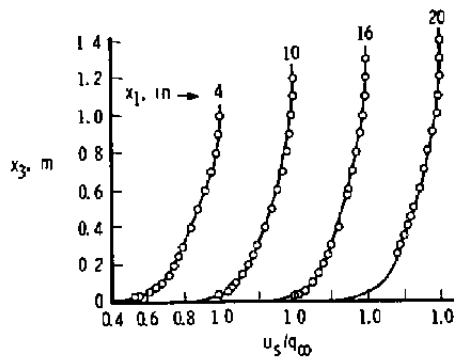


c. Streamwise Velocity
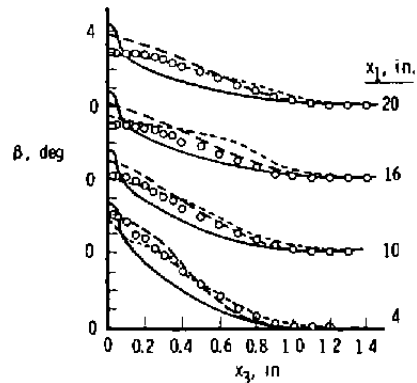


d. Crossflow Angle Distribution

Figure 14. Computed and Measured Boundary-Layer Quantities
for the Bradshaw and Terrell [57]
Infinite Swept-Wing Case.

were measured upstream of the obstruction in a region off the plane of symmetry. Measured wall pressures and edge flow angles were used as inputs to the computations. Figure 15 gives comparisons of measured and computed boundary-layer parameters 6 inches from the plane of symmetry. Also shown are the results of Myring's integral method [13]. Good qualitative trends are obtained with the present method, although values of momentum thickness, shape factor, and wall streamline angle are generally underpredicted for $x_1 < 25$ inches. Agreement between measured and calculated streamwise velocity profiles is considered satisfactory.

Illustrated in Figure 16 are computed streamline patterns at the wall (those at the edge are input) along with those as deduced from the flow field measurements. Reasonable qualitative trends are indicated by the computations except near the separation line (indicated in Figure 16b), which is not surprising because the present computations did not predict separation.

### 5.7.  1978 Stockholm Test Case--Finite Swept Wing

The 1978 Stockholm Test Case [25] was based upon the flow about a swept wing of modern configuration in high subsonic flow ($M_\infty = 0.5$, $Re_\infty = 7 \times 10^6$/unit length).
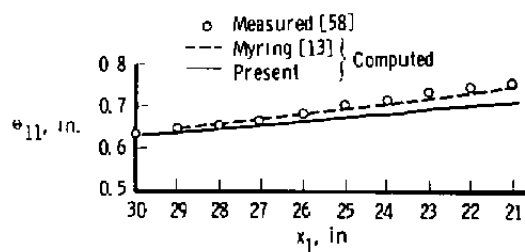
a. Momentum Thickness
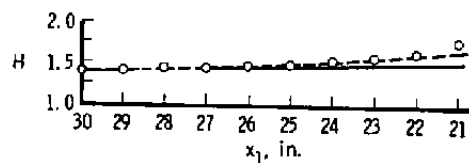


b. Shape Factor
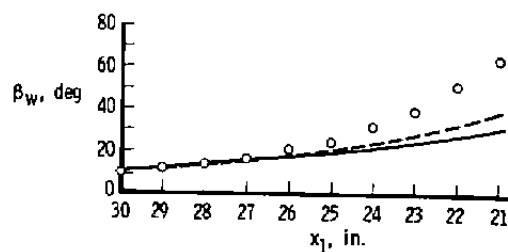


c. Wall Streamline Angle
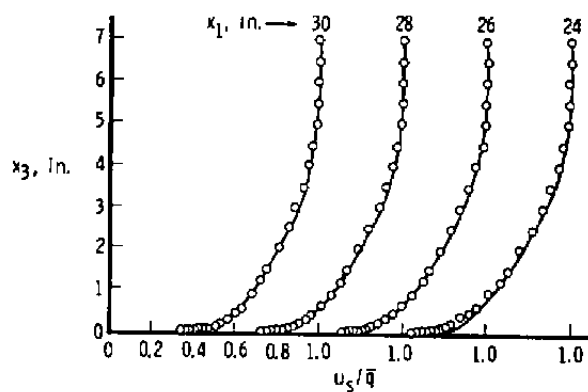


d. Streamwise Velocity

Figure 15. Computed and Measured Boundary-Layer Quantities for the Experiment of East and Hoxey [58].
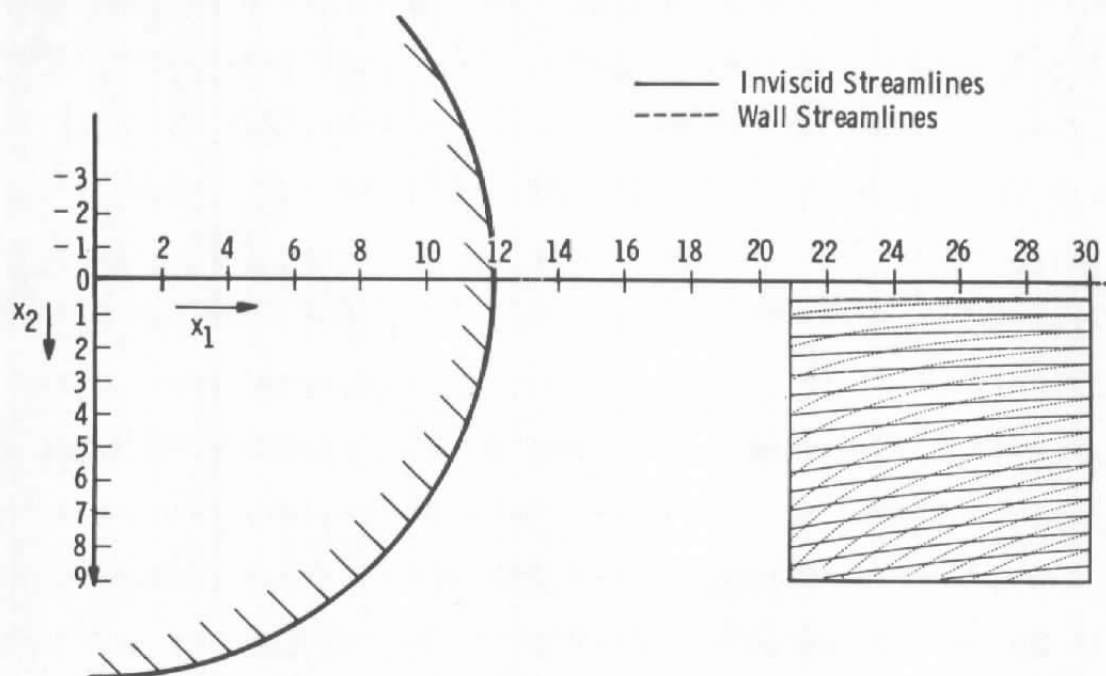
a. Computed Wall Streamlines
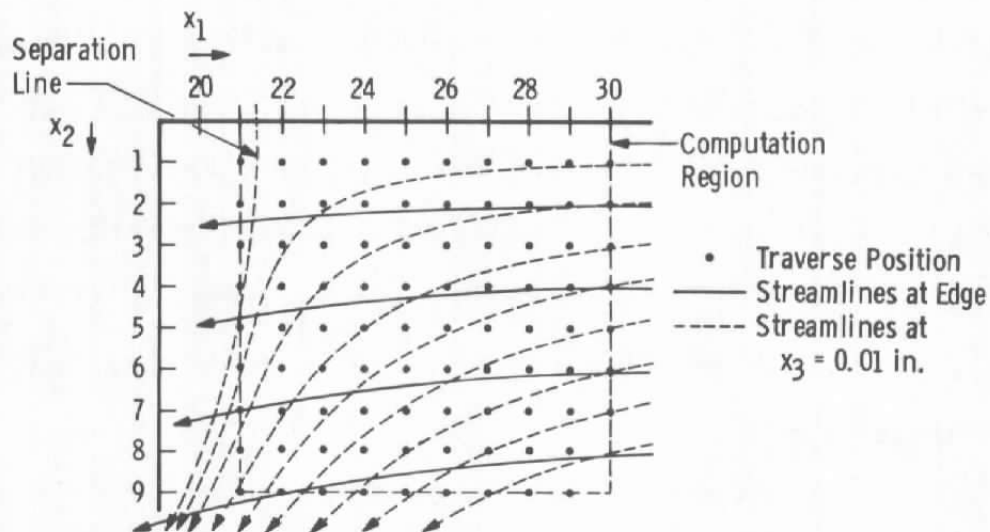


b. Streamline Patterns Deduced from Flow Measurements

Figure 16.  Computed and Measured Wall Streamlines for the
East and Hoxey Test Case [58].

77

Effects of three-dimensionality and compressibility were small but non-negligible. Because the test case was designed to test three-dimensional boundary-layer calculation methods, the inviscid velocity distribution was provided by a higher order panel method. The only experimental data provided for comparison were oil flow photographs of the wing surface. Boundary values at the initial start line are given in [25]. Figure 17 gives the results at span stations 2, 4, and 6 as computed by the present method along with the range of all eight calculation methods which were compared in [25] for the case of zero angle of attack. Favorable agreement is seen to exist when comparing momentum thickness, shape factor, and skin friction; whereas, the present computations for $\beta_w$ indicate a more rapid increase for $x/c > 0.4$ at all span stations than do the other calculations. Figure 18 gives the wall streamline patterns as computed by the present method and as measured using oil flow visualization; good qualitative agreement is seen to exist between the computations and the measurements.

Similar to the van den Berg and Elsenaar infinite swept-wing case [56] discussed in Section 5.4, another program failure was encountered when an attempt was made to compute the 8-deg angle-of-attack case reported in [25].
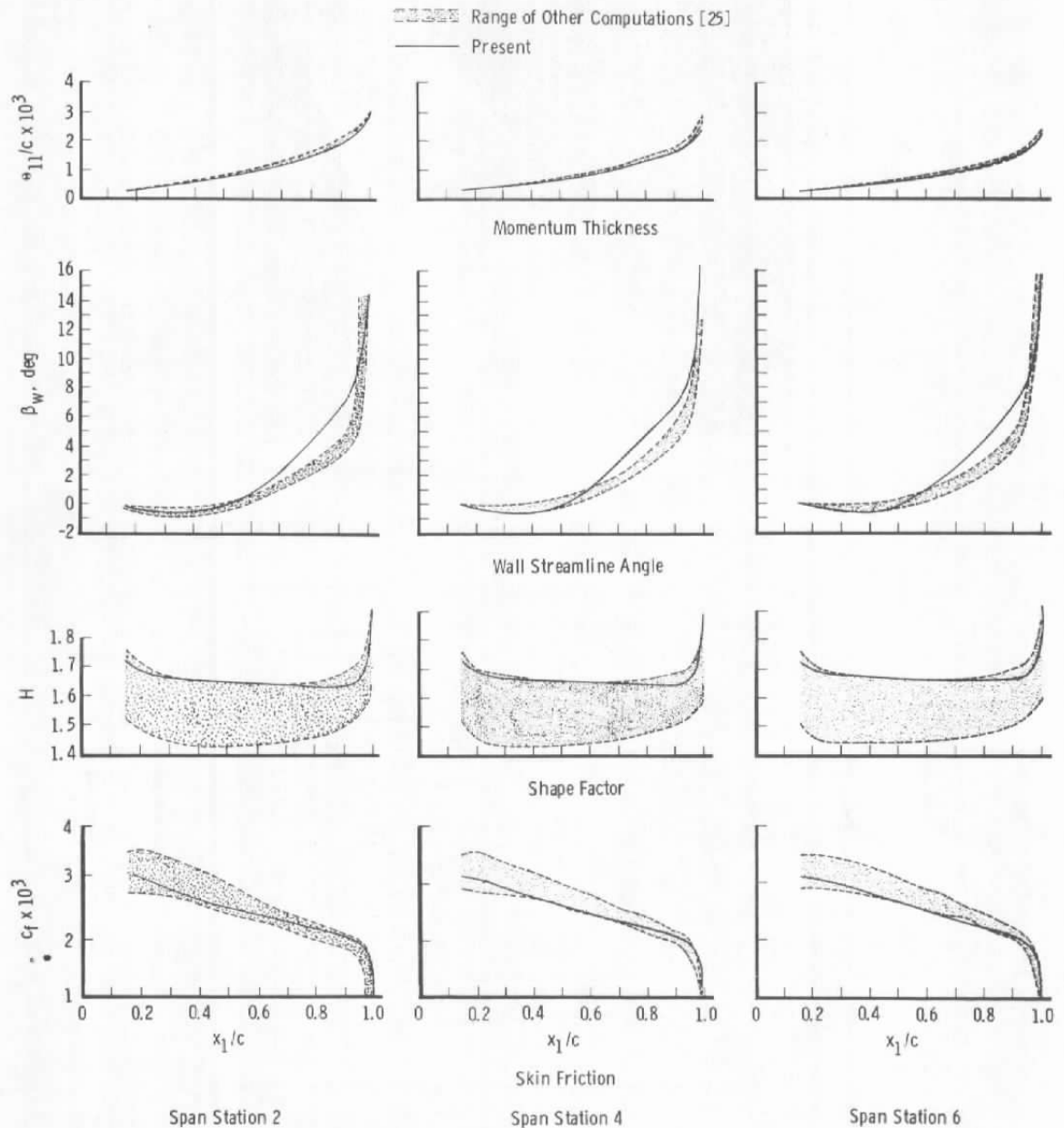
Figure 17. Calculated Boundary-Layer Parameters for the 1978 Stockholm Test Case [25] for Zero Angle of Attack.

79
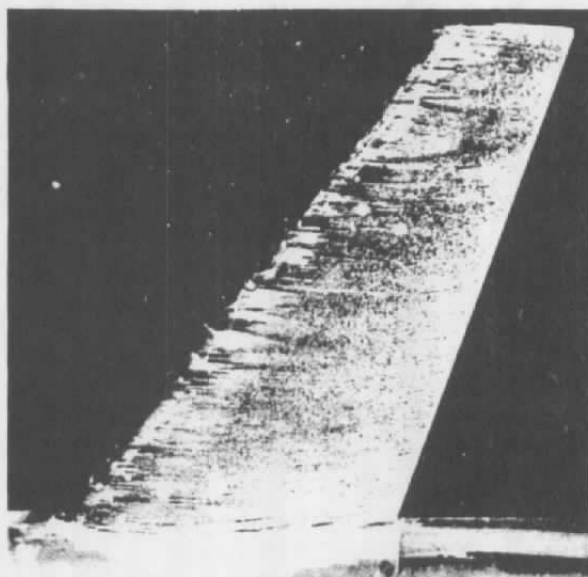
a.   Measured (Surface Flow Visualization)
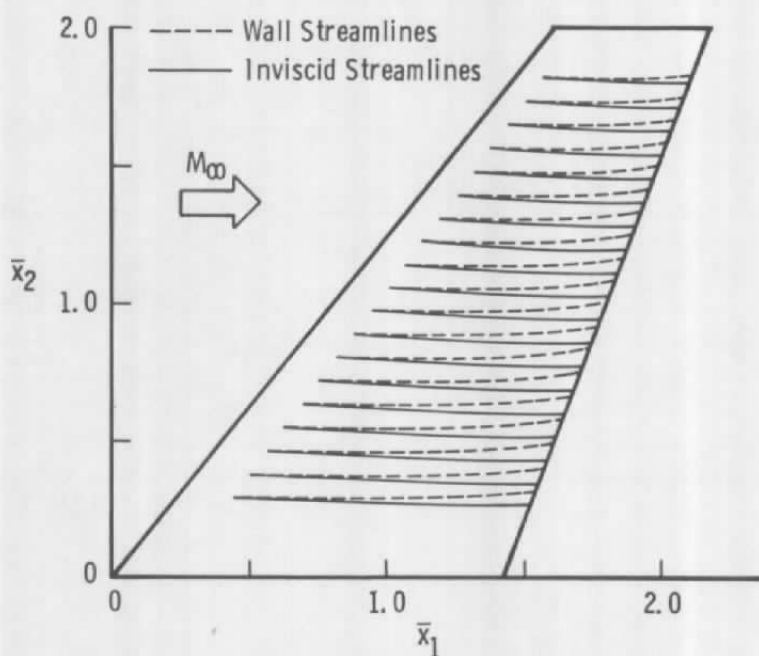


b.   Computed

Figure 18.   Computed and Measured Streamline Patterns for
the 1978 Stockholm Test Case [25] for
Zero Angle of Attack.

Although the general consensus from the results reported in [25] was that the flow was not separated (also implied by surface flow visualization), it is again suspected that separation is responsible for the observed program failure.

For this particular test case, the boundary conditions were not treated correctly according to the sign of the characteristics along both "side" boundaries; that is, $(i = 1 \rightarrow NI, j = 1)$ and $(i = 1 \rightarrow NI, j = NJ)$ (refer to Figure 6, page 54). The results presented in Figures 17 and 18 indicate that this erroneous treatment of boundary conditions seems to have had little effect on the computations for the zero angle-of-attack case. However, as noted above, the numerical procedure became unstable when attempting to compute the 8-deg angle-of-attack case; what effect (if any) the boundary conditions along the two "side" boundaries had on the computations for this test case is not known.

Chapter VI

SUMMARY, CONCLUSIONS, AND RECOMMENDATIONS

A method for computing three-dimensional, time-dependent, compressible, turbulent boundary layers in nonorthogonal curvilinear coordinates has been presented. The method solves the time-dependent momentum and mean-flow kinetic energy boundary-layer integral equations which provides the viscous portion of a viscous/inviscid interaction approach where identical surface grids for both the viscous and inviscid calculation methods can be used. A four-stage Runge-Kutta time-stepping scheme was used to numerically solve the system of equations using local time steps to accelerate convergence. Several space difference approximations were employed and it was found that a backward scheme gave the best results using no artificial smoothing. Calculated results using the present method were compared to experimental data and to results of other calculation methods; satisfactory agreement was obtained.

There are several areas where improvements could be incorporated which would in turn improve the overall outcome and performance of the present computational procedure. Firstly, incorporation of a more general method of computing surface metrics is needed in order to properly address three-dimensional geometries: for example, the

procedures of Smith and Gaffney [53], or Craidon [64].
The use of a more general cross-flow velocity profile
representation would make the present method more flexible
with respect to the classes of flows which could be
addressed. Although other models are available (e.g.,
Mager's cross-flow model [65]), none have sufficient flexi-
bility to allow a three-dimensional integral method to be
routinely applied to any flow field such that accurate
results can generally be expected. As discussed in
Appendix D, a more thorough treatment of the "cross-flow"
dissipation is needed. However, to properly handle this
term in the equations requires an accurate cross-flow
model which is valid for a wide variety of three-
dimensional boundary-layer flows.

All calculations presented herein were performed
using a CRAY-1S computer. Depending on the number of mesh
points and type of spatial differences used, solution
times ranged from 15 to 300 CPU seconds. This is somewhat
slow considering the relative simplicity of the geometries
involved. However, it is felt that performance of the
numerical procedure could be improved significantly by more
efficient coding and by incorporating a different numerical
scheme. For example, a two-stage R-K scheme operating at
a CFL of 0.9 was incorporated into the code and the

van den Berg and Elsenaar case [56] was recomputed. The solution was practically identical to that using the four-stage scheme with a 40% reduction in CPU time.

It is apparent that the major deficiency of the present method is its inability to compute some flow fields: in the present study, the van den Berg and Elsenaar case [56] (infinite swept wing) using the measured wall pressures and edge flow angles, and the 1978 Stockholm test case [25] (finite swept wing) at 8 deg angle of attack. This seems to be a significant hindrance when considering using this method as one part of a viscous-inviscid interaction approach. On the other hand, knowing that the method has failed for a particular case could possibly be interpreted as signaling whether or not separation has been encountered, although no information is generated pertaining to its location. As discussed by Cousteix and Houdeville [66], and Delery and Formery [62], it is apparent that an inverse formulation of the boundary-layer equations is required if separated flows are to be addressed, even for a time-dependent computational method.

BIBLIOGRAPHY

## BIBLIOGRAPHY

1. Prandtl, L., "Über Flüssigkeitsbewegung bei schr. kleiner Reibung," Proceedings of Third International Mathematical Congress, Heidelberg, 1904, pp. 484-491. Translated as NACA TM 452, 1928. See also Collected Works, Vol. II, pp. 575-584.

2. Lock, R. C., "A Review of Methods for Predicting Viscous Effects on Aerofoils and Wings at Transonic Speeds," AGARD-CPP-291, 1980.

3. Melnik, R. E., "Turbulent Interactions on Airfoils at Transonic Speeds--Recent Developments," AGARD-CPP-291, 1980.

4. Le Balleur, J. C., "Viscid-Inviscid Coupling Calculations for the Two- and Three-Dimensional Flows," Lecture Series 1982-04, von Karman Institute of Fluid Dynamics, March 29-April 2, 1982.

5. McLean, J. D., and Randall, J. L., "Computer Program to Calculate Three-Dimensional Boundary Layer Flows Over Wings with Wall Mass Transfer," NASA-CR-3123, 1978.

6. Jacocks, J. L., and Kneile, K. R., "Computation of Three-Dimensional Time-Dependent Flow Using the Euler Equations," AEDC-TR-80-49, Arnold Air Force Station, TN, October 1980.

7. Rizzi, A., and Eriksson, L. E., "Transfinite Mesh Generation and Damped Euler Equation Algorithm for Transonic Flow Around Wing-Body Configurations," AIAA Paper No. 81-0999, June 1981.

8. Schmidt, W., Jameson, A., and Whitfield, D., "Finite Volume Solutions to the Euler Equations in Transonic Flow," Journal of Aircraft, Vol. 20, No. 2, February 1983, pp. 127-133.

9. Whitfield, D., and Jameson, A., "Three-Dimensional Euler Equation Simulation of Propeller-Wing Interaction in Transonic Flow," AIAA Paper No. 83-0236, January 1983.

10. East, L. R., "Computation of Three-Dimensional Turbulent Boundary Layers," Euromech 60, Trondheim, 1975, AFA TN AE-1211.

11. Wesseling, P., and Lindhout, J. P. F., "A Calculation Method for Three-Dimensional Incompressible Turbulent Boundary Layers," AGARD Conference Proceedings, No. 73 on Turbulent Shear Flows, Paper 8, 1971.

12. Lindhout, J. P. F., Moek, G., de Boer, E., and van den Berg, B., "A Method for the Calculation of 3D Boundary Layers on Practical Wing Configurations," ASME Conference on Turbulent Boundary Layers, Niagara Falls, 1979.

13. Myring, D. F., "An Integral Prediction Method for Three-Dimensional Turbulent Boundary Layers in Incompressible Flow," RAE TR-70147, August 1970.

14. Smith, P. D., "An Integral Prediction Method for Three-Dimensional Compressible Turbulent Boundary Layers," RAE R&M No. 3739, December 1972.

15. Stock, H. W., "Integral Method for the Calculation of Three-Dimensional, Laminar and Turbulent Boundary Layers," NASA TM 75320, July 1978.

16. Cumpsty, N. A., and Head, M. R., "The Calculation of Three-Dimensional Turbulent Boundary Layers. Part 1: Flow over the Rear of an Infinite Swept Wing," The Aeronautical Quarterly, Vol. 18, 1967.

17. Cebeci, T., Kaups, K., and Ramsey, J. A., "A General Method for Calculating Three-Dimensional Compressible Laminar and Turbulent Boundary Layers on Arbitrary Wings," NASA CR-2777, 1977.

18. Tassa, A., Atta, E. H., and Lemmerman, L. A., "A New Three-Dimensional Boundary-Layer Calculation Method," AIAA Paper No. 82-0224, January 1982.

19. McLean, J. D., "Three-Dimensional Turbulent Boundary-Layer Calculations for Swept Wings," AIAA Paper No. 77-3, January 1977.

20. Cousteix, J., "Analyse théorique et moyens de prévision de la couche limite turbulente tri-dimensionelle," ONERA Publ. No. 157, 1974 (English Translation: ESA TT-238, January 1976).

21. Smith, P. D., "The Numerical Computation of Three-Dimensional Boundary Layers," Three-Dimensional Turbulent Boundary Layers, Editors H. H. Fernholz and E. Krause, Springer-Verlag, 1982, pp. 265-285.

22. Swafford, T. W., "Calculation of Skin Friction in Two-Dimensional, Transonic Turbulent Flow," AEDC-TR-79-12, Arnold Air Force Station, TN, April 1979.

23. White, F. M., Viscous Fluid Flow, McGraw-Hill Book Company, New York, 1974, pp. 516-518,532.

24. Whitfield, D. L., "Integral Solution of Compressible Turbulent Boundary Layers Using Improved Velocity Profiles," AEDC-TR-78-42, Arnold Air Force Station, TN, December 1978.

25. Humphreys, D. A., "Comparison of Boundary Layer Calculations for a Wing:  The May 1978 Stockholm Workshop Test Case," FFA TN AE-1522, January 1979.

26. Lindhout, J. P. F., van den Berg, B., and Elsenaar, A., "Comparison of Boundary Layer Calculations for the Root Section of a Wing--The September 1979 Amsterdam Workshop Test Case," NLR MP 80028 U, March 1981.

27. Wang, K. C., "On the Determination of the Zones of Influence and Dependence for Three-Dimensional Boundary Layer Equations," Journal of Fluid Mechanics, Vol. 48, Part 2, 1972.

28. Whitfield, D. L., Swafford, T. W., and Jacocks, J. L., "Calculation of Turbulent Boundary Layers with Separation and Viscous-Inviscid Interaction," AIAA Journal, Vol. 19, No. 10, October 1981, pp. 1315-1322.

29. Johnston, J. P., "Three-Dimensional Turbulent Boundary Layers," M.I.T. Gas Turbine Lab, Report 39, 1957.

30. Swafford, T. W., and Whitfield, D. L., "Numerical Solutions of Three-Dimensional, Time-Dependent, Compressible Turbulent Integral Boundary-Layer Equations in General Curvilinear Coordinates," AIAA Paper No. 83-1674, July 1983.

31. Nash, John R., and Patel, Virendru C., <u>Three-Dimensional Turbulent Boundary Layers</u>, SBC Technical Books, Atlanta, GA, 1972.

32. McDonald, Henry, and Shamroth, Stephen J., "An Analysis and Application of the Time-Dependent Turbulent Boundary-Layer Equations," <u>AIAA Journal</u>, Vol. 9, No. 8, August 1971, pp. 1553-1560.

33. Mager, A., "Three-Dimensional Laminar Boundary Layers," Section C of "Theory of Laminar Flows," <u>High Speed Aerodynamic Jet Propulsion</u>, Vol. 4, Editor F. K. Moore, Princeton University Press, Princeton, NJ, 1964, pp. 298-299.

34. Head, M. R., and Patel, V. C., "Improved Entrainment Method for Calculating Boundary-Layer Development," ARC 31043, 1969.

35. Whitfield, D. L., "Analytical Description of the Complete Two-Dimensional Turbulent Boundary-Layer Velocity Profile," AEDC-TR-77-79, Arnold Air Force Station, TN, September 1977 (also AIAA Paper No. 78-1158, July 1978).

36. Swafford, T. W., "Analytical Approximation of Two-Dimensional Separated Turbulent Boundary-Layer Velocity Profiles," <u>AIAA Journal</u>, Vol. 21, No. 6, June 1983, pp. 923-926.

37. Donegan, T. L., Private Communication, Calspan Field Services, Arnold Air Force Station, TN, August 1982.

38. Johnston, J. P., "Experimental Studies in Three-Dimensional Turbulent Boundary Layers," Report MD-34, Thermosciences Division, Dept. of Mech. Engr., Stanford University, Stanford, CA, July 1976.

39. Swafford, T. W., "Analytical Approximation of Two-Dimensional Separated Turbulent Boundary-Layer Velocity Profiles," AEDC-TR-79-99, Arnold Air Force Station, TN, October 1980.

40. Coles, D. E., "The Turbulent Boundary Layer in a Compressible Fluid," Rand R-403-PR(AD285651), Rand Corporation, Santa Monica, CA, September 1962.

41. Winter, K. G., and Gaudet, L., "Turbulent Boundary-Layer Studies at High Reynolds Numbers at Mach Numbers Between 0.2 and 2.8," ARC R&M No. 3712 (ARC33345), London, England, December 1970.

42. Whitfield, D. L., Swafford, T. W., and Donegan, T. L., "An Inverse Integral Computational Method for Compressible Turbulent Boundary Layers," _Recent Contributions to Fluid Mechanics_, Editor W. Haase, Springer-Verlag, 1982, pp. 294-302.

43. Thomas, J. L., "Viscous-Inviscid Interaction Using Euler and Inverse Boundary-Layer Equations," Ph.D. Dissertation, Mississippi State University, Mississippi State, MS, 1983.

44. Cebeci, T., and Smith, A. M. D., _Analysis of Turbulent Boundary Layers_, Academic Press, New York, 1974.

45. Ames, William F., _Numerical Methods for Partial Differential Equations_, Academic Press, New York, 1977.

46. Liskovets, O. A., "The Method of Lines" (English Translation), _Journal of Differential Equations_, Vol. 1, No. 1308, 1965.

47. Jameson, A., Schmidt, W., and Turkel, E., "Numerical Solutions of the Euler Equations by Finite Volume Methods Using Runge-Kutta Time-Stepping Schemes," AIAA Paper No. 81-1259, June 1981.

48. Lambert, J. D., _Computational Methods in Ordinary Differential Equations_, John Wiley and Sons, New York, 1979.

49. Mitchell, A. R., and Griffiths, D. F., _The Finite Difference Method in Partial Differential Equations_, John Wiley and Sons, New York, 1980.

50. Wilson, J. C., "Stability of Richtmyer Type Difference Schemes in Any Finite Number of Space Variables and Their Comparison with Multistep Strang Schemes," _Journal of Institute of Mathematics and Applications_, Vol. 10, 1972, pp. 238-257.

51. Vichnevetsky, R., and Bowles, J., "Fourier Analysis of Numerical Approximations of Hyperbolic Equations," SIAM _Studies in Applied Mathematics_, 1982.

52. Steger, Joseph L., and Warming, R. F., "Flux Vector Splitting of the Inviscid Gasdynamics Equations with Applications to Finite Difference Methods," NASA TM 78605, July 1979.

53. Smith, P. D., and Gaffney, P. L., "Approximation of the Surface Metric Tensor by Means of Bicubic Spline Interpolation," RAE-TR-72185, December 1972.

54. Cook, P. H., McDonald, M. A., and Firmin, M. C. P., "Aerofoil RAE 2822-Pressure Distributions, Boundary Layer and Wake Measurements," RAE, UK, AGARD WG 04, July 1977.

55. Winter, K. G., Rotta, J. C., and Smith, K. G., "Studies of the Turbulent Boundary Layer on a Waisted Body of Revolution in Subsonic and Supersonic Flow," ARC R&M No. 3633, August 1968.

56. van den Berg, B., and Elsenaar, A., "Measurements in a Three-Dimensional Incompressible Turbulent Boundary Layer in an Adverse Pressure Gradient Under Infinite Swept Wing Conditions," NLR TR 72092 U, 1972.

57. Bradshaw, P., and Terrell, M. G., "The Response of a Turbulent Boundary Layer on an Infinite Swept Wing to the Sudden Removal of Pressure Gradient," Aero Report 1305, National Physical Laboratory, London, England, 1969.

58. East, L. F., and Hoxey, R. P., "Low Speed Three-Dimensional Turbulent Boundary-Layer Data, Part 1," RAE Technical Report 69041 (ARC 31362), 1969.

59. Cebeci, T., "Calculation of Three-Dimensional Boundary Layers--I. Swept Infinite Cylinders and Small Cross Flow," AIAA Journal, Vol. 12, No. 6, June 1974, pp. 779-786.

60. Bradshaw, P., "Calculation of Three-Dimensional Turbulent Boundary Layers," Journal of Fluid Mechanics, Vol. 46, Part 3, 1971, pp. 417-445.

61. Cebeci, T., and Chang, K. C., "On the Turbulence Modeling Requirements of Three-Dimensional Boundary-Layer Flow," Recent Contributions to Fluid Mechanics, Editor W. Haase, Springer-Verlag, 1982, pp. 31-39.

62. Delery, J. M., and Formery, M. J., "A Finite Difference Method for Inverse Solutions of 3-D Turbulent Boundary-Layer Flow," AIAA Paper No. 83-0301, January 1983.

63. Bradshaw, P., Ferriss, D. H., and Atwell, N. P., "Calculation of Boundary Layer Development Using the Turbulent Energy Equation," *Journal of Fluid Mechanics*, Vol. 28, Part 3, 1967, pp. 593-616.

64. Craidon, Charlotte B., "A Computer Program for Fitting Smooth Surfaces to an Aircraft Configuration and Other Three-Dimensional Geometries," NASA TM X-3206, June 1975.

65. Mager, A., "Generalization of Boundary-Layer Momentum Integral Equations to Three-Dimensional Flows, Including Those of Rotating Systems," NACA Report 1067, 1952.

66. Cousteix, J., and Houdeville, R., "Singularities in Three-Dimensional Turbulent Boundary-Layer Calculations and Separation Phenomena," *AIAA Journal*, Vol. 19, No. 8, 1981, pp. 976-985.

APPENDICES

APPENDIX A

SURFACE METRIC COEFFICIENTS

Before boundary-layer computations can proceed, metrics associated with surface scale factors and curvatures must be determined. The following relationships for a general, nonorthogonal, curvilinear coordinate system embedded in the surface of a body (see Figure 1, page 8) are listed by Cebeci et al. [17] and are given here for completeness in slightly different form. As before, the subscript "i" takes on values of 1 and 2, and subscript 3 resulting from i + 1 when i = 2 is taken to be subscript 1.

$$h_i^2 = \left(\frac{\partial \overline{x}_1}{\partial x_i}\right)^2 + \left(\frac{\partial \overline{x}_2}{\partial x_i}\right)^2 + \left(\frac{\partial \overline{x}_3}{\partial x_i}\right)^2 \tag{A.1}$$

$$g \equiv h_1 h_2 \cos\lambda = \left(\frac{\partial \overline{x}_1}{\partial x_1}\right)\left(\frac{\partial \overline{x}_1}{\partial x_2}\right) + \left(\frac{\partial \overline{x}_2}{\partial x_1}\right)\left(\frac{\partial \overline{x}_2}{\partial x_2}\right) + \left(\frac{\partial \overline{x}_3}{\partial x_1}\right)\left(\frac{\partial \overline{x}_3}{\partial x_2}\right) \tag{A.2}$$

$$K_i = \frac{1}{h_1 h_2 \sin\lambda}\left[\frac{1}{h_i}\left(\frac{\partial g}{\partial x_i} - h_{i+1} \cos\lambda \frac{\partial h_i}{\partial x_i}\right) - \frac{\partial h_i}{\partial x_{i+1}}\right] \tag{A.3}$$

$$K_{i,i+1} = \frac{1}{\sin\lambda}\left[-K_i - \frac{1}{h_i}\frac{\partial\lambda}{\partial x_i} + \cos\lambda\left(K_{i+1} + \frac{1}{h_{i+1}}\frac{\partial\lambda}{\partial x_{i+1}}\right)\right] \tag{A.4}$$

$$\frac{\partial h_i}{\partial x_j} = \frac{1}{h_i}\Bigg[\left(\frac{\partial \overline{x}_1}{\partial x_i}\right)\left(\frac{\partial^2 \overline{x}_1}{\partial x_i \partial x_j}\right) + \left(\frac{\partial \overline{x}_2}{\partial x_i}\right)\left(\frac{\partial^2 \overline{x}_2}{\partial x_i \partial x_j}\right)$$

$$+ \left(\frac{\partial \overline{x}_3}{\partial x_i}\right)\left(\frac{\partial^2 \overline{x}_3}{\partial x_i \partial x_j}\right)\Bigg] \qquad (j = 1 \text{ or } 2) \qquad (A.5)$$

$$\frac{\partial g}{\partial x_i} = \left(\frac{\partial \overline{x}_1}{\partial x_i}\right)\left(\frac{\partial^2 \overline{x}_1}{\partial x_1 \partial x_2}\right) + \left(\frac{\partial \overline{x}_2}{\partial x_i}\right)\left(\frac{\partial^2 \overline{x}_2}{\partial x_1 \partial x_2}\right) + \left(\frac{\partial \overline{x}_3}{\partial x_i}\right)\left(\frac{\partial^2 \overline{x}_3}{\partial x_1 \partial x_2}\right)$$

$$+ \left(\frac{\partial \overline{x}_1}{\partial x_{i+1}}\right)\left(\frac{\partial^2 \overline{x}_1}{\partial x_i^2}\right) + \left(\frac{\partial \overline{x}_2}{\partial x_{i+1}}\right)\left(\frac{\partial^2 \overline{x}_2}{\partial x_i^2}\right) + \left(\frac{\partial \overline{x}_3}{\partial x_{i+1}}\right)\left(\frac{\partial^2 \overline{x}_3}{\partial x_i^2}\right) \qquad (A.6)$$

$$\frac{\partial \lambda}{\partial x_i} = \frac{1}{h_1 h_2 \sin\lambda}\left[\cos\lambda\left(h_1 \frac{\partial h_2}{\partial x_i} + h_2 \frac{\partial h_1}{\partial x_i}\right) - \frac{\partial g}{\partial x_i}\right] \qquad (A.7)$$

(It should be pointed out that $h_i$, $K_i$, and $K_{i,i+1}$ must be computed at each mesh point in the computation domain.)

## APPENDIX B

### DEFINITION OF STREAMLINE INTEGRAL LENGTHS

Using the sketch below, velocities in the non-orthogonal axis system are related to those in a streamline system by the following relations [13,14]:

$$u_1 = \frac{u_s \sin\xi - u_n \cos\xi}{\sin\lambda} \tag{B.1}$$

$$u_2 = \frac{u_s \sin\alpha + u_n \cos\alpha}{\sin\lambda} \tag{B.2}$$

At the boundary-layer edge, $\bar{u}_n \equiv 0$. Thus,

$$\bar{u}_1 = \bar{u}_s \frac{\sin\xi}{\sin\lambda} \tag{B.3}$$

$$\bar{u}_2 = \bar{u}_s \frac{\sin\alpha}{\sin\lambda} \tag{B.4}$$

where ($u_1$, $u_2$) are velocities resolved in the nonorthogonal system, and ($u_s$, $u_n$) are those in the streamline system (recall overbars denote values evaluated at the boundary-layer edge).
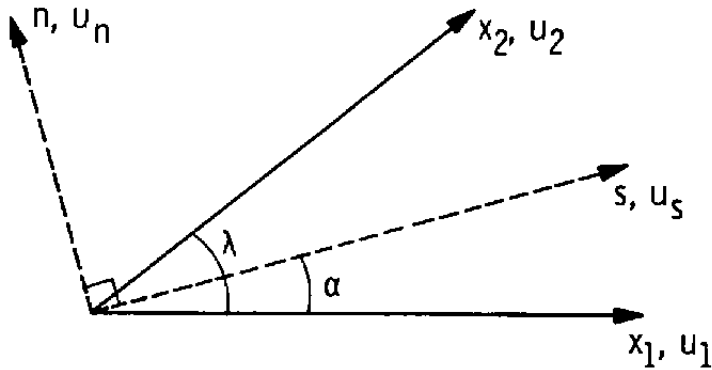
Sketch Showing Relationship Between Streamline
and Nonorthogonal Coordinates (Planform View)

Also, the resultant velocity is given by

$$q^2 = u_1^2 + u_2^2 + 2u_1u_2 \cos\lambda = u_s^2 + u_n^2 \tag{B.5}$$

and at the boundary-layer edge,

$$\overline{q}^2 = \overline{u}_1^2 + \overline{u}_2^2 + 2\overline{u}_1\overline{u}_2 \cos\lambda = \overline{u}_s^2 \tag{B.6}$$

Thus, integral lengths in the streamline coordinate system can be defined as [13,14]:

$$\overline{\rho}\,\overline{q}\,\Delta_1^* = \int_0^\infty (\overline{\rho}\,\overline{u}_s - \rho u_s)\,dx_3 \tag{B.7}$$

$$\overline{\rho}\,\overline{q}\,\Delta_2^* = -\int_0^\infty \rho u_n\,dx_3 \tag{B.8}$$

$$\overline{\rho}\,\overline{q}^2\,\Theta_{11} = \int_0^\infty \rho u_s(\overline{u}_s - u_s)\,dx_3 \tag{B.9}$$

$$\overline{\rho} \, \overline{q}^2 \, \Theta_{12} = \int_0^\infty \rho u_n \, (\overline{u}_s - u_s) \, dx_3 \qquad (B.10)$$

$$\overline{\rho} \, \overline{q}^2 \, \Theta_{21} = - \int_0^\infty \rho u_s u_n \, dx_3 \qquad (B.11)$$

$$\overline{\rho} \, \overline{q}^2 \, \Theta_{22} = - \int_0^\infty \rho u_n^2 \, dx_3 \qquad (B.12)$$

$$\overline{\rho} \, \overline{q}^3 \, E_{11} = \int_0^\infty \rho u_s \, (\overline{u}_s^2 - u_s^2) \, dx_3 \qquad (B.13)$$

$$\overline{\rho} \, \overline{q}^3 \, E_{12} = \int_0^\infty \rho u_n \, (\overline{u}_s^2 - u_s^2) \, dx_3 \qquad (B.14)$$

$$\overline{\rho} \, \overline{q}^3 \, E_{21} = - \int_0^\infty \rho u_s u_n^2 \, dx_3 \qquad (B.15)$$

$$\overline{\rho} \, \overline{q}^3 \, E_{22} = - \int_0^\infty \rho u_n^3 \, dx_3 \qquad (B.16)$$

$$\overline{q} \, \Delta_u^* = \int_0^\infty (\overline{u}_s - u_s) \, dx_3 \qquad (B.17)$$

$$\overline{q} \, \Delta_v^* = - \int_0^\infty u_n \, dx_3 \qquad (B.18)$$

## APPENDIX C

## STREAMWISE SHAPE FACTOR CORRELATIONS

Except for the correlation derived by Donegan [37] for $H_{\theta_\rho}$, all shape factor correlations used in the present study are listed in [24], [42], and [43], and are given here for completeness:

$$H = \bar{H} \, ( 1 + 0.113 \, M_e^2 ) + 0.29 \, M_e^2 \qquad\qquad (C.1)$$

$$(H_\theta\ast)_{M_e=0} = 1.48061 + 3.83781 e^{-2\bar{H}}$$

$$+ \, 0.33 - \frac{1}{8.5484} \, \tan^{-1}\left[\frac{10^{7-\bar{H}}-1}{1.23}\right]$$

$$- \, ( 0.33 - \frac{\pi}{17.1} ) \, \tanh^{1/2}$$

$$\left[\left(1.2874 \times 10^{-6}\right)\left(10^{7-\bar{H}}\right)^{1.45761}\right] \quad (C.2)$$

$$H_\theta\ast = \frac{(H_\theta\ast)_{M_e=0} + 0.028 \, M_e^2}{1 + 0.014 \, M_e^2} \qquad\qquad (C.3)$$

$$\frac{\Theta_{11}}{\Theta_u} = 1 - \frac{0.92 \, M_e^2}{7.09 + M_e^2} \, \tanh[1.49(\bar{H} - 0.9)] \qquad (C.4)$$

$$H_{\theta_\rho} = M_e^2 \, (0.185 \, \bar{H} + 0.150) \qquad\qquad (C.5)$$

$$\frac{c_f \, D_u^S}{2} = \left[ 0.01167 e^{-0.038\overline{H}^3} + \left( 9.0 \times 10^{-8} \right) e^{1.603\overline{H}} \right.$$

$$\left. + \, 0.0115 + \Delta CFD/1000 \right] / \left( 1 + 0.025 \, M_e^{1.4} \right) \quad (C.6)$$

where

$$\Delta CFD = m \overline{Re}_{\Theta_{11}}^n$$

$$m = 650\overline{H} - 743$$

$$n = -1.59\overline{H} + 1.45$$

$$\left. \right\} \quad \overline{H} \leq 1.6$$

$$\Delta CFD = m \, e^{n\overline{Re}_{\Theta_{11}}}$$

$$m = 3.25 \, e^{0.045\overline{H}^2}$$

$$n = \overline{H}/10000 - 0.0017$$

$$\left. \right\} \quad \overline{H} > 1.6$$

APPENDIX D

DISSIPATION INTEGRALS

The resolution of the dissipation integrals (appearing as the last term in the mean-flow kinetic energy integral equation, Eq. (2.20)) from quantities in nonorthogonal coordinates to those in the streamline coordinate system is given in this Appendix. These manipulations are performed such that correlations derived for two-dimensional turbulent boundary layers can be utilized for the general three-dimensional case.

From Eq. (2.20), the dissipation integrals are written as

$$D_{u_1} + D_{u_2} = \frac{1}{\rho \bar{q}^3} \int_0^\infty \left( u_1 \frac{\partial \tau_{x_1}}{\partial x_3} + u_2 \frac{\partial \tau_{x_2}}{\partial x_3} \right) dx_3 \qquad (D.1)$$

Integrating by parts and using the boundary conditions that

$$[\tau_{x_i}]_\infty = [u_1]_0 = [u_2]_0 = 0 \quad (i = 1 \text{ or } 2) \qquad (D.2)$$

Equation (D.1) becomes

$$D_{u_1} + D_{u_2} = - \frac{1}{\rho \bar{q}^3} \int_0^\infty \left( \tau_{x_1} \frac{\partial u_1}{\partial x_3} + \tau_{x_2} \frac{\partial u_2}{\partial x_3} \right) dx_3 \qquad (D.3)$$

Using the relations between velocities in nonorthogonal and streamline coordinates (see Eqs. (B.1) and (B.2) in Appendix B), Eq. (D.3) becomes

$$
D_{u_1} + D_{u_2} = \frac{-1}{\bar{\rho}\,\bar{q}^3\,\sin\lambda}\left[\sin\xi \int_0^\infty \tau_{x_1} \frac{\partial u_s}{\partial x_3}\,dx_3\right.
$$

$$
- \cos\xi \int_0^\infty \tau_{x_1} \frac{\partial u_n}{\partial x_3}\,dx_3
$$

$$
+ \sin\alpha \int_0^\infty \tau_{x_2} \frac{\partial u_s}{\partial x_3}\,dx_3
$$

$$
\left. + \cos\alpha \int_0^\infty \tau_{x_2} \frac{\partial u_n}{\partial x_3}\,dx_3\right] \tag{D.4}
$$

Substituting the outer portion (Eq. (2.31b)) of Johnston's cross-flow profile [29] into the above yields

$$
D_{u_1} + D_{u_2} = -\frac{1}{\bar{\rho}\,\bar{q}^3\,\sin\lambda}\left[(\sin\xi + A\cos\xi) \int_0^\infty \tau_{x_1} \frac{\partial u_s}{\partial x_3}\,dx_3\right.
$$

$$
\left. + (\sin\alpha - A\cos\alpha) \int_0^\infty \tau_{x_2} \frac{\partial u_s}{\partial x_3}\,dx_3\right] \tag{D.5}
$$

The total shear stress in the $x_1$ and $x_2$ directions can be resolved into streamwise components as

$$\tau_{x_1} = \frac{1}{\sin\lambda} ( \tau_s \sin\xi - \tau_n \cos\xi ) \qquad \text{(D.6a)}$$

$$\tau_{x_2} = \frac{1}{\sin\lambda} ( \tau_s \sin\alpha + \tau_n \cos\alpha ) \qquad \text{(D.6b)}$$

where $\tau_s$ is the streamwise component of the total shear stress and $\tau_n$ is normal to it. Substituting Eq. (D.6) into (D.5) gives

$$D_{u_1} + D_{u_2} = - \frac{1}{\sin^2\lambda} \frac{c_f}{2} D_u^s \left( t_1 + t_2 \frac{D_u^n}{D_u^s} \right) \qquad \text{(D.7)}$$

where

$$t_1 = \sin^2\xi + \sin^2\alpha + A(\sin\xi \cos\xi - \sin\alpha \cos\alpha) \qquad \text{(D.8a)}$$

$$t_2 = -\sin\xi \cos\xi + \sin\alpha \cos\alpha - A(\cos^2\xi + \cos^2\alpha) \qquad \text{(D.8b)}$$

$$D_u^s = \int_0^\infty \frac{\tau_s}{\tau_{s_w}} \frac{\partial\left(\frac{u_s}{\overline{q}}\right)}{\partial x_3} dx_3 \qquad \text{(D.8c)}$$

$$D_u^n = \int_0^\infty \tan\beta \frac{\tau_s}{\tau_{s_w}} \frac{\partial\left(\frac{u_s}{\overline{q}}\right)}{\partial x_3} dx_3 \qquad \text{(D.8d)}$$

and the relation

$$\tau_n = \tau_s \tan\beta \qquad \text{(D.9)}$$

has been used in Eq. (D.8d)

As discussed in Section 2.2.4, Eq. (D.7) is evaluated in the present study using a correlation for $c_f \, D_u^s/2$ [42,43] and assuming that

$$\frac{D_u^n}{D_u^s} \ll 1 \qquad\qquad (D.10)$$

In principle, the "crossflow" dissipation (Eq. (D.8d)) could be correlated in an analogous manner as was done for "streamwise" dissipation if $\tan\beta$ could be evaluated analytically for the general case. For example, the total shear stress components in streamline coordinates are given as[1]

$$\tau_s = \mu \frac{\partial u_s}{\partial x_3} - \rho \overline{u_s' u_3'} \qquad\qquad (D.11a)$$

$$\tau_n = \mu \frac{\partial u_n}{\partial x_3} - \rho \overline{u_n' u_3'} \qquad\qquad (D.11b)$$

---

[1]The overbars and primes denote time-averaged and fluctuating quantities, respectively; e.g.,

$$\overline{u_s' u_3'} = \frac{1}{2T} \int_{t-T}^{t+T} (u_s' u_3') \, dt$$

where the averaging period $T$ is much larger than the time scale of the fluctuations (see [31] and [44]).

The Reynolds stresses can be modeled using the eddy viscosity concept (e.g., see [59]) as

$$- \overline{\rho u_s' u_{x_3}'} \equiv \mu_{t_1} \frac{\partial u_s}{\partial x_3} \qquad (D.12a)$$

$$- \overline{\rho u_n' u_{x_3}'} \equiv \mu_{t_2} \frac{\partial u_n}{\partial x_3} \qquad (D.12b)$$

where $\mu_{t_1}$ and $\mu_{t_2}$ are the eddy viscosities, and $\mu$ is the molecular viscosity. Thus, Eqs. (D.11a,b) become

$$\tau_s = (\mu + \mu_{t_1}) \frac{\partial u_s}{\partial x_3} \qquad (D.13a)$$

$$\tau_n = (\mu + \mu_{t_2}) \frac{\partial u_n}{\partial x_3} \qquad (D.13b)$$

Therefore, $\tan\beta$ could be evaluated using

$$\tan\beta = \frac{\tau_n}{\tau_s} \qquad (D.14)$$

by using Johnston's cross-flow profile [29] for $u_n$ and by making appropriate assumptions concerning the evaluation of the eddy viscosities $\mu_{t_1}$ and $\mu_{t_2}$ (e.g., see [59]).

However, similar to the "streamwise" dissipation correlation [42,43], which is based upon a very general description of the streamwise velocity profile [28] and an eddy viscosity formulation ($\mu_{t_1}$) derived from two-dimensional boundary-layer analysis [44], a correlation of the "crossflow" dissipation would, in turn, be based upon the cross-flow velocity profile plus an additional eddy viscosity formulation ($\mu_{t_2}$). Therefore, in lieu of the lack of generalities of both the cross-flow profile representation and the eddy viscosity $\mu_{t_2}$, the contribution of $D_u^n$ was simply neglected in comparison with $D_u^s$. Obviously, more study is needed concerning the evaluation of $D_u^n$.

## APPENDIX E

## RELATIONS BETWEEN THE STREAMWISE INTEGRAL LENGTHS

For a given cross-flow velocity profile, certain relations exist between streamwise integral lengths which enable the 13 unknowns to be expressed in terms of five. These relations are given here for the Johnston cross-flow profile [29] only.

The 13 unknowns in streamline coordinates are $\Delta_1^*$, $\Delta_2^*$, $\Theta_{11}$, $\Theta_{12}$, $\Theta_{21}$, $\Theta_{22}$, $E_{11}$, $E_{12}$, $E_{21}$, $E_{22}$, $\Delta_u^*$, $\Delta_v^*$, and $\theta_\rho$ (see Appendix B for these definitions). As an example of how these integral lengths are interrelated, consider Eq. (B.12):

$$\bar{\rho}\, \bar{q}^2\, \Theta_{22} = - \int_0^\infty \rho u_n^2\, dx_3 \tag{E.1}$$

Thus, using only the outer portion of Johnston's cross-flow model [29,14],

$$\bar{\rho}\, \bar{q}^2\, \Theta_{22} = - A^2 \int_0^\infty (\, \rho \bar{u}_s^2 - 2\rho u_s \bar{u}_s + \rho u_s^2\,)\, dx_3$$

$$= - A^2 \int_0^\infty [\, \bar{u}_s\, (\bar{\rho}\, \bar{u}_s - \rho u_s\,) - \bar{u}_s^2(\bar{\rho}-\rho) - \rho u_s\, (\bar{u}_s - u_s\,)]\, dx_3$$

$$= - A^2\, [\, \bar{\rho}\, \bar{u}_s^2\, \Delta_1^* - \bar{\rho}\, \bar{u}_s^2\, \theta_\rho - \bar{\rho}\, \bar{u}_s^2\, \Theta_{11}\,]$$

or,

$$\Theta_{22} = A^2 ( \Theta_{11} + \theta_\rho - \Delta_1^* ) \qquad (E.2)$$

The remaining relationships can be derived in an analogous manner, and are summarized as follows:

$$\Delta_2^* = - A ( \Delta_1^* - \theta_\rho ) \qquad (E.3)$$

$$\Theta_{12} = A ( \Delta_1^* - \theta_\rho - \Theta_{11} ) \qquad (E.4)$$

$$\Theta_{21} = - A \Theta_{11} \qquad (E.5)$$

$$\Theta_{22} = A^2 ( \Theta_{11} + \theta_\rho - \Delta_1^* ) \qquad (E.6)$$

$$E_{21} = A^2 ( E_{11} - 2\Theta_{11} ) \qquad (E.7)$$

$$E_{12} = A ( \Delta_1^* + \Theta_{11} - E_{11} - \theta_\rho ) \qquad (E.8)$$

$$E_{22} = - A^3 ( \Delta_1^* - \theta_\rho + E_{11} - 3\Theta_{11} ) \qquad (E.9)$$

$$\Delta_v^* = - A \Delta_u^* \qquad (E.10)$$

It is computationally more efficient to use the shape factors as defined in Eq. (2.27) and rewrite Eqs. (E.3) to (E.10) as

$$\Theta_{21} = - A \Theta_{11} \qquad (E.11)$$

$$\Delta_2^* = \Theta_{21} ( H - H_{\theta_\rho} ) \qquad (E.12)$$

109

$$\Theta_{12} = \Theta_{21} - \Delta_2^* \tag{E.13}$$

$$\Theta_{22} = - A\, \Theta_{12} \tag{E.14}$$

$$E_{12} = \Theta_{12} + \Theta_{21}\,(H_{\theta^*} - 2) \tag{E.15}$$

$$E_{21} = - \Theta_{22} - A\, E_{12} \tag{E.16}$$

$$E_{22} = - A\,(E_{21} - \Theta_{22}) \tag{E.17}$$

$$\Delta_v^* = - A\, \Delta_u^* \tag{E.17}$$

APPENDIX F

RELATIONS BETWEEN INTEGRAL LENGTHS IN STREAMLINE
AND NONORTHOGONAL COORDINATE SYSTEMS

The derivation of the relationships between the integral thicknesses in the two coordinate systems is algebraically tedious but straightforward (as cited earlier, Smith [14] gives as an example the derivation of $\theta_{11}$ in terms of $\Theta_{11}$, $\Theta_{12}$, etc.). The complete list of the 12 relationships is as follows (recall that upper-case Greek letters denote integral lengths using velocities expressed in the streamline coordinate system; whereas, lower-case Greek letters represent those resolved in the nonorthogonal system):

$$\delta_1^* = \frac{1}{\sin\lambda} (\Delta_1^* \sin\xi - \Delta_2^* \cos\xi) \tag{F.1}$$

$$\delta_2^* = \frac{1}{\sin\lambda} (\Delta_1^* \sin\alpha + \Delta_2^* \cos\alpha) \tag{F.2}$$

$$\theta_{11} = \frac{1}{\sin^2\lambda} [\Theta_{11} \sin^2\xi - (\Theta_{12} + \Theta_{21})\sin\xi \cos\xi$$
$$+ \Theta_{22} \cos^2\xi] \tag{F.3}$$

$$\theta_{12} = \frac{1}{\sin^2\lambda} [\Theta_{11} \sin\alpha \sin\xi + \Theta_{12} \sin\xi \cos\alpha$$
$$- \Theta_{21} \cos\xi \sin\alpha - \Theta_{22} \cos\alpha \cos\xi] \tag{F.4}$$

$$\theta_{21} = \frac{1}{\sin^2\lambda} [\Theta_{11} \sin\alpha \sin\xi + \Theta_{21} \sin\xi \cos\alpha$$
$$- \Theta_{12} \cos\xi \sin\alpha - \Theta_{22} \cos\alpha \cos\xi] \tag{F.5}$$

$$\theta_{22} = \frac{1}{\sin^2\lambda} [\Theta_{11} \sin^2\alpha + (\Theta_{12} + \Theta_{21})\cos\alpha \sin\alpha$$

$$+ \Theta_{22} \cos^2\alpha] \qquad (F.6)$$

$$\varepsilon_{11} = \frac{1}{\sin^3\lambda} [E_{11} \sin^3\xi - (3E_{12} + 2\Delta_2^*)\sin^2\xi \cos\xi$$

$$+ 3E_{21} \sin\xi \cos^2\xi - E_{22} \cos^3\xi] \qquad (F.7)$$

$$\varepsilon_{12} = \frac{1}{\sin^3\lambda} [E_{11} \sin\alpha \sin^2\xi - 2(E_{12} + \Delta_2^*)\sin\alpha \sin\xi \cos\xi$$

$$+ E_{21} \sin\alpha \cos^2\xi + E_{12} \sin^2\xi \cos\alpha$$

$$- 2E_{21} \sin\xi \cos\xi \cos\alpha + E_{22} \cos^2\xi \cos\alpha] \qquad (F.8)$$

$$\varepsilon_{21} = \frac{1}{\sin^3\lambda} [E_{11} \sin\xi \sin^2\alpha + 2(E_{12} + \Delta_2^*)\sin\alpha \sin\xi \cos\alpha$$

$$+ E_{21} \sin\xi \cos^2\alpha - E_{12} \sin^2\alpha \cos\xi$$

$$- 2E_{21} \sin\alpha \cos\alpha \cos\xi - E_{22} \cos^2\alpha \cos\xi] \qquad (F.9)$$

$$\varepsilon_{22} = \frac{1}{\sin^3\lambda} [E_{11} \sin^3\alpha + (3E_{12} + 2\Delta_2^*)\sin^2\alpha \cos\alpha$$

$$+ 3E_{21} \sin\alpha \cos^2\alpha + E_{22} \cos^3\alpha] \qquad (F.10)$$

$$\delta_{u_1}^* = \frac{1}{\sin\lambda} (\Delta_u^* \sin\xi - \Delta_v^* \cos\xi) \qquad (F.11)$$

$$\delta_{u_2}^* = \frac{1}{\sin\lambda} (\Delta_u^* \sin\alpha + \Delta_v^* \cos\alpha) \qquad (F.12)$$

# APPENDIX G

# FORMULATION OF THE SYSTEM OF EQUATIONS
# FOR SOLUTION

The system of equations (Eq. (2.25)) can be written as

$$\frac{\partial \delta_1^*}{\partial t} - \frac{\bar{u}_1}{\bar{q}} \frac{\partial \theta_\rho}{\partial t} = b_1 \qquad \text{(G.1a)}$$

$$\frac{\partial}{\partial t}(\theta_{11} + \theta_{22}) = b_2 \qquad \text{(G.1b)}$$

$$\frac{\partial \delta_2^*}{\partial t} - \frac{\bar{u}_2}{\bar{q}} \frac{\partial \theta_\rho}{\partial t} = b_3 \qquad \text{(G.1c)}$$

where $b_1$, $b_2$, and $b_3$ are defined by referring to Eq. (2.25). Consider Eq. (G1.a) first. Using Eq. (F.1) from Appendix F and the definition of $H_{\theta_\rho}$, Eq. (G.1a) becomes

$$\frac{\partial}{\partial t}\left[\frac{1}{\sin\lambda}(\Delta_1^* \sin\xi - \Delta_2^* \cos\xi)\right] - \frac{\bar{u}_1}{\bar{q}} \frac{\partial}{\partial t}(H_{\theta_\rho} \theta_{11}) = b_1 \qquad \text{(G.2)}$$

Using Eq. (E.3) from Appendix E and various shape factor definitions, some algebraic manipulation gives

$$\left[ \frac{\sin\xi}{\sin\lambda} H + \frac{\cos\xi}{\sin\lambda} AH - \frac{\cos\xi}{\sin\lambda} AH_{\theta_\rho} - \frac{\bar{u}_1}{q} H_{\theta_\rho} \right] \frac{\partial \Theta_{11}}{\partial t}$$

$$- \left[ \frac{\cos\xi}{\sin\lambda} A\Theta_{11} + \frac{\bar{u}_1}{q} \Theta_{11} \right] \frac{\partial H_{\theta_\rho}}{\partial t}$$

$$+ \Theta_{11} \left[ \frac{\sin\xi}{\sin\lambda} + \frac{\cos\xi}{\sin\lambda} A \right] \frac{\partial H}{\partial t}$$

$$+ \left[ \frac{\cos\xi}{\sin\lambda} ( H - H_{\theta_\rho} ) \Theta_{11} \right] \frac{\partial A}{\partial t} = b_1 \qquad (G.3)$$

Recall from Section 2.5 that

$$H = H(\bar{H}, M_e) \qquad (G.4a)$$

$$H_{\theta_\rho} = H_{\theta_\rho}(\bar{H}, M_e) \qquad (G.4b)$$

such that

$$\frac{\partial H}{\partial t} = \frac{\partial H}{\partial \bar{H}} \frac{\partial \bar{H}}{\partial t} + \frac{\partial H}{\partial M_e} \frac{\partial M_e}{\partial t} \qquad (G.5a)$$

$$\frac{\partial H_{\theta_\rho}}{\partial t} = \frac{\partial H_{\theta_\rho}}{\partial \bar{H}} \frac{\partial \bar{H}}{\partial t} + \frac{\partial H_{\theta_\rho}}{\partial M_e} \frac{\partial M_e}{\partial t} \qquad (G.5b)$$

For the case of steady edge conditions, $\partial M_e/\partial t = 0$. Thus, using the shape factor correlations given in Appendix C, Eqs. (G.5a,b) become

$$\frac{\partial H}{\partial t} = (1 + 0.113 \ M_e^2) \ \frac{\partial \overline{H}}{\partial t} \qquad\qquad (G.6a)$$

$$\frac{\partial H_{\theta_\rho}}{\partial t} = (0.185 \ M_e^2) \ \frac{\partial \overline{H}}{\partial t} \qquad\qquad (G.6b)$$

Substituting Eqs. (G.6a,b) into Eq. (G.3) results in

$$\left[ \frac{\sin\xi}{\sin\lambda} \ H + \frac{\cos\xi}{\sin\lambda} \ (H-H_{\theta_\rho}) \ A - \frac{\overline{u}_1}{q} \ H_{\theta_\rho} \right] \frac{\partial \Theta_{11}}{\partial t}$$

$$+ \left[ \frac{\cos\xi}{\sin\lambda} \ A\Theta_{11}(1-0.072 \ M_e^2) + \frac{\sin\xi}{\sin\lambda} \ \Theta_{11}(1+0.113 \ M_e^2) \right.$$

$$\left. - \ 0.185 \ M_e^2 \ \frac{\overline{u}_1}{q} \ \Theta_{11} \right] \frac{\partial \overline{H}}{\partial t} + \left[ \frac{\cos\xi}{\sin\lambda} \ (H-H_{\theta_\rho}) \ \Theta_{11} \right] \frac{\partial A}{\partial t} = b_1 \qquad (G.7)$$

Analogous results can be obtained for Eqs. (G.1b,c).
After these operations have been performed, the final form
of the equations can be written as

$$\begin{bmatrix} a_{11} & a_{12} & a_{13} \\ a_{21} & a_{22} & a_{23} \\ a_{31} & a_{32} & a_{33} \end{bmatrix} \frac{\partial}{\partial t} \begin{bmatrix} \Theta_{11} \\ \overline{H} \\ A \end{bmatrix} = \begin{bmatrix} b_1 \\ b_2 \\ b_3 \end{bmatrix} \qquad (G.8)$$

where

$$a_{11} = \frac{\sin\xi}{\sin\lambda} H + \frac{\cos\xi}{\sin\lambda} A(H-H_{\theta_\rho}) - \frac{\overline{u}_1}{\overline{q}} H_{\theta_\rho} \qquad (G.9)$$

$$a_{12} = \frac{\cos\xi}{\sin\lambda} A\Theta_{11}(1-0.072\,M_e^2) + \frac{\sin\xi}{\sin\lambda} \Theta_{11}(1+0.113\,M_e^2)$$

$$- 0.185\,M_e^2\,\frac{\overline{u}_1}{\overline{q}}\,\Theta_{11} \qquad (G.10)$$

$$a_{13} = \frac{\cos\xi}{\sin\lambda} (H-H_{\theta_\rho})\Theta_{11} \qquad (G.11)$$

$$a_{21} = \frac{1}{\sin^2\lambda} [\sin^2\xi + \sin^2\alpha$$

$$+ A(H-H_{\theta_\rho}-2)(\cos\alpha\,\sin\alpha - \cos\xi\,\sin\xi)$$

$$- A^2(H-H_{\theta_\rho}-1)(\cos^2\xi + \cos^2\alpha) ] \qquad (G.12)$$

$$a_{22} = \frac{1}{\sin^2\lambda} [A\Theta_{11}(\cos\alpha\,\sin\alpha - \cos\xi\,\sin\xi)$$

$$- A^2\Theta_{11}(\cos^2\xi + \cos^2\alpha) ] (1-0.072\,M_e^2) \qquad (G.13)$$

$$a_{23} = \frac{1}{\sin^2\lambda} [\Theta_{11}(H-H_{\theta_\rho}-2)(\cos\alpha\,\sin\alpha - \cos\xi\,\sin\xi)$$

$$- 2A\Theta_{11}(H-H_{\theta_\rho}-1)(\cos^2\xi + \cos^2\alpha) ] \qquad (G.14)$$

$$a_{31} = \frac{\sin\alpha}{\sin\lambda} H - \frac{\cos\alpha}{\sin\lambda} A(H-H_{\theta_\rho}) - \frac{\overline{u}_2}{\overline{q}} H_{\theta_\rho} \qquad (G.15)$$

$$a_{32} = \frac{\sin\alpha}{\sin\lambda} \Theta_{11}(1+0.113\,M_e^2) - \frac{\cos\alpha}{\sin\lambda} A\Theta_{11}(1-0.072\,M_e^2)$$

$$- 0.185\,M_e^2\,\frac{\overline{u}_2}{\overline{q}}\,\Theta_{11} \qquad (G.16)$$

$$a_{33} = -\frac{\cos\alpha}{\sin\lambda}(H - H_{\theta_\rho})\theta_{11} \tag{G.17}$$

$$b_1 = -\bar{q}\left\{\frac{1}{h_1 h_2 \sin\lambda\ \bar\rho\ \bar{q}^2}\left[\frac{\partial}{\partial x_1}(h_2\ \sin\lambda\ \bar\rho\ \bar{q}^2\ \theta_{11})\right.\right.$$

$$\left.+\frac{\partial}{\partial x_2}(h_1\ \sin\lambda\ \bar\rho\ \bar{q}^2\ \theta_{12})\right]+\frac{\delta_1^*}{h_1\bar{q}}\frac{\partial\bar{u}_1}{\partial x_1}+\frac{\delta_2^*}{h_2\bar{q}}\frac{\partial\bar{u}_1}{\partial x_2}$$

$$-K_1\cot\lambda\left(\frac{\bar{u}_1}{\bar{q}}\delta_1^*+\theta_{11}\right)+K_2\csc\lambda\left(\frac{\bar{u}_2}{\bar{q}}\delta_2^*+\theta_{22}\right)$$

$$\left.+K_{12}\left(\frac{\bar{u}_1}{\bar{q}}\delta_2^*+\theta_{12}\right)-\frac{1}{2}c_{f_{x_1}}\right\} \tag{G.18}$$

$$b_3 = -\bar{q}\left\{\frac{1}{h_1 h_2 \sin\lambda\ \bar\rho\ \bar{q}^2}\left[\frac{\partial}{\partial x_1}(h_2\ \sin\lambda\ \bar\rho\ \bar{q}^2\ \theta_{21})\right.\right.$$

$$\left.+\frac{\partial}{\partial x_2}(h_1\ \sin\lambda\ \bar\rho\ \bar{q}^2\ \theta_{22})\right]+\frac{\delta_1^*}{h_1\bar{q}}\frac{\partial\bar{u}_2}{\partial x_1}+\frac{\delta_2^*}{h_2\bar{q}}\frac{\partial\bar{u}_2}{\partial x_2}$$

$$-K_2\cot\lambda\left(\frac{\bar{u}_2}{\bar{q}}\delta_2^*+\theta_{22}\right)+K_1\csc\lambda\left(\frac{\bar{u}_1}{\bar{q}}\delta_1^*+\theta_{11}\right)$$

$$\left.+K_{21}\left(\frac{\bar{u}_2}{\bar{q}}\delta_1^*+\theta_{21}\right)-\frac{1}{2}c_{f_{x_2}}\right\} \tag{G.19}$$

117

$$b_2 = -2\overline{q}\Bigg\{ \frac{1}{2\overline{\rho}\,\overline{q}^3\,h_1 h_2\,\sin\lambda} \Bigg\{ \frac{\partial}{\partial x_1}\left[ h_2\,\sin\lambda\,\overline{\rho}\,\overline{q}^3\,(\varepsilon_{11} + \varepsilon_{21})\right]$$

$$+ \frac{\partial}{\partial x_2}\left[ h_1\,\sin\lambda\,\overline{\rho}\,\overline{q}^3\,(\varepsilon_{12} + \varepsilon_{22})\right]\Bigg\}$$

$$+ \frac{\overline{u}_1}{h_1\overline{q}^2}\,(\delta_1^* - \delta_{u_1}^*)\,\frac{\partial \overline{u}_1}{\partial x_1} + \frac{1}{h_1\overline{q}^2}\,(\overline{u}_2\,\delta_1^* - \overline{u}_1\delta_{u_2}^*)\,\frac{\partial \overline{u}_2}{\partial x_1}$$

$$+ \frac{1}{h_2\overline{q}^2}\,(\overline{u}_1\,\delta_2^* - \overline{u}_2\,\delta_{u_1}^*)\,\frac{\partial \overline{u}_1}{\partial x_2} + \frac{\overline{u}_2}{h_2\overline{q}^2}\,(\delta_2^* - \delta_{u_2}^*)\,\frac{\partial \overline{u}_2}{\partial x_2}$$

$$- K_1\,\cot\lambda\left[\varepsilon_{11} + \frac{\overline{u}_1^2}{\overline{q}^2}\,(\delta_1^* - \delta_{u_1}^*)\right]$$

$$- K_2\,\cot\lambda\left[\varepsilon_{22} + \frac{\overline{u}_2^2}{\overline{q}^2}\,(\delta_2^* - \delta_{u_2}^*)\right]$$

$$+ K_1\,\csc\lambda\left[\varepsilon_{12} + \frac{\overline{u}_1^2}{\overline{q}^2}\,(\delta_2^* - \delta_{u_2}^*)\right]$$

$$+ K_2\,\csc\lambda\left[\varepsilon_{21} + \frac{\overline{u}_2^2}{\overline{q}^2}\,(\delta_1^* - \delta_{u_1}^*)\right]$$

$$+ K_{12}\left[\varepsilon_{12} + \frac{\overline{u}_1}{\overline{q}^2}\,(\overline{u}_1\,\delta_2^* - \overline{u}_2\,\delta_{u_1}^*)\right]$$

$$+ K_{21}\left[\varepsilon_{21} + \frac{\overline{u}_2}{\overline{q}^2}\,(\overline{u}_2\,\delta_1^* - \overline{u}_1\,\delta_{u_2}^*)\right]$$

$$+ (D_{u_1} + D_{u_2})\Bigg\} - \frac{\overline{u}_1}{\overline{q}}\,b_1 - \frac{\overline{u}_2}{\overline{q}}\,b_3 \qquad\qquad \text{(G.20)}$$

(Note that $b_2$ and $b_3$ are listed above in reverse order. This is for computational convenience because $b_2$ is defined in terms of $b_1$ and $b_3$).

APPENDIX H

LINEAR STABILITY ANALYSIS OF THE MODEL PROBLEM
USING FOUR-STAGE RUNGE-KUTTA WITH VARIOUS
SPACE DIFFERENCE APPROXIMATIONS

First-Order Backward

Recall from Eq. (3.13), the model equation can be written using first-order backward differences as

$$\frac{du_i}{dt} = -\frac{a}{\Delta x} \nabla (u_i^n) = f(t, u_i^n) \qquad \text{(H.1a)}$$

where

$$\nabla (u_i^n) = u_i^n - u_{i-1}^n \qquad \text{(H.1b)}$$

Substitution of Eq. (H.1b) into Eqs. (3.3b-e) results in

$$k_1 = -\frac{a}{\Delta x} \nabla (u_i^n) \qquad \text{(H.2a)}$$

$$k_2 = k_1 + \frac{a^2 \Delta t}{2(\Delta x)^2} \nabla^2 (u_i^n) \qquad \text{(H.2b)}$$

$$k_3 = k_2 - \frac{a^3 (\Delta t)^2}{4(\Delta x)^3} \nabla^3 (u_i^n) \qquad \text{(H.2c)}$$

$$k_4 = -k_1 + 2k_3 + \frac{a^4 (\Delta t)^3}{4(\Delta x)^4} \nabla^4 (u_i^n) \qquad \text{(H.2d)}$$

where

$$\nabla^2 (u_i^n) = u_i^n - 2u_{i-1}^n + u_{i-2}^n \qquad \text{(H.3a)}$$

$$\nabla^3 (u_i^n) = u_i^n - 3u_{i-1}^n + 3u_{i-2}^n - u_{i-3}^n \qquad \text{(H.3b)}$$

$$\nabla^4 (u_i^n) = u_i^n - 4u_{i-1}^n + 6u_{i-2}^n - 4u_{i-3}^n + u_{i-4}^n \qquad \text{(H.3c)}$$

By letting the solution at time-level n be represented by

$$u_i^n = e^{\kappa \gamma (i\Delta x)} = e^{\kappa i \phi} \qquad \text{(H.4)}$$

where

$$\phi = \gamma \Delta x \quad (\gamma = \text{constant})$$

$$\kappa = \sqrt{-1}$$

and use the definition $e^{\pm \kappa \phi} = \cos\phi \pm \kappa \sin\phi$, successive substitutions result in the R-K scheme being expressed as

$$\frac{u_i^{n+1}}{u_i^n} = R(CFL, \phi) + \kappa I(CFL, \phi) \qquad \text{(H.5a)}$$

where

$$R(CFL, \phi) = 1 - (CFL)(1-\cos\phi) + \frac{1}{2}(CFL)^2(1-2\cos\phi + \cos 2\phi)$$

$$- \frac{1}{6}(CFL)^3(1-3\cos\phi + 3\cos 2\phi - \cos 3\phi)$$

$$+ \frac{1}{24}(CFL)^4(1-4\cos\phi + 6\cos 2\phi - 4\cos 3\phi + \cos 4\phi) \qquad \text{(H.5b)}$$

$$I(CFL,\phi) = -(CFL)\sin\phi + \frac{1}{2}(CFL)^2(2\sin\phi - \sin2\phi)$$

$$-\frac{1}{6}(CFL)^3(3\sin\phi - 3\sin2\phi + \sin3\phi)$$

$$+\frac{1}{24}(CFL)^4(4\sin\phi - 6\sin2\phi + 4\sin3\phi - \sin4\phi) \qquad \text{(H.5c)}$$

and

$$CFL = a\frac{\Delta t}{\Delta x} \qquad \text{(H.5d)}$$

Thus, the amplification factor $|G|$ is

$$|G| = \left|\frac{u_i^{n+1}}{u_i^n}\right| = [R^2(CFL,\phi) + I^2(CFL,\phi)]^{1/2} \qquad \text{(H.6)}$$

which must be less than one for the solution to remain bounded as $n \to \infty$.

Similar expressions can be obtained for $R(CFL,\phi)$ and $I(CFL,\phi)$ for second-order central and second-order backward spatial differences, as follows.

Second-Order Central

$$R(CFL,\phi) = 1 - \frac{1}{2}(CFL)^2 \sin^2\phi + \frac{1}{24}(CFL)^4 \sin^4\phi \qquad \text{(H.7a)}$$

$$I(CFL,\phi) = (CFL)\sin\phi - \frac{1}{6}(CFL)^3 \sin^3\phi \qquad \text{(H.7b)}$$

## Second-Order Backward

$$R(CFL, \phi) = 1 - (CFL) \left( \frac{3}{2} - 2\cos\phi + \frac{1}{2} \cos2\phi \right)$$

$$+ (CFL)^2 \left( \frac{9}{8} - 3\cos\phi + \frac{11}{4} \cos2\phi - \cos3\phi + \frac{1}{8} \cos4\phi \right)$$

$$- (CFL)^3 \left( \frac{9}{16} - \frac{9}{4} \cos\phi + \frac{57}{16} \cos2\phi - \frac{17}{6} \cos3\phi \right.$$

$$+ \frac{19}{16} \cos4\phi - \frac{1}{4} \cos5\phi + \frac{1}{48} \cos6\phi \left. \right)$$

$$+ (CFL)^4 \left( \frac{27}{128} - \frac{9}{8} \cos\phi + \frac{81}{32} \cos2\phi - \frac{25}{8} \cos3\phi \right.$$

$$+ \frac{443}{192} \cos4\phi - \frac{25}{24} \cos5\phi + \frac{9}{32} \cos6\phi - \frac{1}{24} \cos7\phi$$

$$+ \frac{1}{384} \cos8\phi \left. \right) \qquad \text{(H.8a)}$$

$$I(CFL, \phi) = - (CFL)\left( 2\sin\phi - \frac{1}{2} \sin2\phi \right)$$

$$+ (CFL)^2 \left( 3\sin\phi - \frac{11}{4} \sin2\phi + \sin3\phi - \frac{1}{8} \sin4\phi \right)$$

$$- (CFL)^3 \left( \frac{9}{4} \sin\phi - \frac{57}{16} \sin2\phi + \frac{17}{6} \sin3\phi - \frac{19}{16} \sin4\phi \right.$$

$$+ \frac{1}{4} \sin5\phi - \frac{1}{48} \sin6\phi \left. \right)$$

$$+ (CFL)^4 \left( \frac{9}{8} \sin\phi - \frac{81}{32} \sin2\phi + \frac{25}{8} \sin3\phi - \frac{443}{192} \sin4\phi \right.$$

$$+ \frac{25}{24} \sin5\phi - \frac{9}{32} \sin6\phi + \frac{1}{24} \sin7\phi - \frac{1}{384} \sin8\phi \left. \right) \qquad \text{(H.8b)}$$

## NOMENCLATURE

<u>Symbol</u>

| | |
|---|---|
| $a,b$ | Constants used in model equation, Eqs. (3.1) and (3.4) |
| $a_{ij}$ | Elements of $\hat{A}$--see Appendix G |
| $A$ | Parameter used in Johnston's cross-flow velocity profile, Eq. (2.31b) |
| $\hat{A}$ | Coefficient matrix of the system of equations to be solved, Eq. (2.41)--see Appendix G |
| $\underset{\sim}{b}$ | Vector defined by Eq. (2.41)--see Appendix G |
| $b_1, b_2, b_3$ | Components of $\underset{\sim}{b}$ |
| $c$ | Airfoil chord |
| $\underset{\sim}{c}$ | Vector used in Eq. (3.9) |
| $c_f$ | Skin friction coefficient using streamwise component of wall shear stress |
| $c_{f_{x_i}}$ | Skin friction coefficient using shear stress component in $x_i$-direction, Eq. (2.12) |
| CFL | $a\,\Delta t/\Delta x$, Eq. (3.17) |
| $c_p$ | Static pressure coefficient |
| $\Delta$CFD | Parameter used in Appendix C |
| $D_x, D_{x_1}, D_{x_2}$ | Spatial difference operators, Eqs. (3.2) and (3.5)--see Appendix H |
| $D_{u_1}, D_{u_2}$ | Dissipation integrals expressed in the nonorthogonal coordinate system--see Eq. (D.1) |
| $D_u^s, D_u^n$ | Dissipation integrals, Eqs. (H.8c) and (H.8d), respectively |

Symbol

| | |
|---|---|
| $f(t, u_i^n)$ | Defined by Eq. (3.2) |
| $F_c$ | Compressibility factor, Eq. (2.34d) |
| $g$ | Variable used in computing metric coefficients--see Appendix A |
| $g(u_{ij}^n)$ | Defined by Eq. (3.5) |
| $|G|$ | Amplification factor, Eq. (3.16)--see Appendix H |
| $h_1, h_2$ | Surface metric coefficients, Eq. (A.1)--see Appendix A |
| $H$ | Streamwise shape factor, Eq. (2.27b) |
| $\bar{H}$ | "Incompressible" shape factor, Eq. (2.27a) |
| $H_{\theta}*$ | Streamwise shape factor, Eq. (2.27d) |
| $H_{\theta \rho}$ | Streamwise shape factor, Eq. (2.27c) |
| $(\bar{H}_t)_{rms}$ | Convergence parameter, Eq. (3.19) |
| $i, j$ | Parameters corresponding to $x_1, x_2$-directions, respectively |
| $I$ | Imaginary part of $|G|$, Eq. (3.16)--see Appendix H |
| $k$ | Velocity gradient |
| $k_1, k_2, k_3, k_4$ | Defined in Eq. (3.3) or (3.6) |
| $K_1, K_2, K_{12}, K_{21}$ | Surface curvatures, Eqs. (A.3) and A.4)--see Appendix A |
| $\ell_i$ | Defined by Eq. (2.21) |
| $L$ | Defined by Eq. (2.22); also denotes body length |
| $L_1, L_2, L_3, L_4$ | Used in writing Eq. (2.6)--see Eq. (2.13) |
| $m, n$ | Used as parameters in Appendix C |

Symbol

| | |
|---|---|
| $M, M_{ij}$ | Coefficient matrices for $\partial \underset{\sim}{U}/\partial x_1$ and $\partial \underset{\sim}{U}_{ij}/\partial x_1$ vectors, respectively, Eqs. (3.7) and (3.9) |
| $N, N_{ij}$ | Coefficient matrices for $\partial \underset{\sim}{U}/\partial x_2$ and $\partial \underset{\sim}{U}_{ij}/\partial x_2$ vectors, respectively, Eqs. (3.7) and (3.9) |
| NI, NJ | Maximum values of i and j, respectively |
| p | Static pressure |
| q | Magnitude of total velocity |
| $\underset{\sim}{r}$ | Position vector--see Figure 1 |
| $r_w$ | Local body radius |
| R | Real part of $|G|$, Eq. (3.16)--see Appendix H |
| $Re_{length}$ | Reynolds number based on some character-istic length; e.g., $Re_{\theta_{11}}$ |
| t | Time |
| $t_1, t_2$ | Defined by Eqs. (D.8a,b) |
| $\Delta t$ | Time-step increment |
| $T_{\ell_i}$ | Defined in Eq. (2.24) (i = 1 or 2) |
| $T_L$ | Defined in Eq. (2.24) |
| $u_i$ | Velocity in $x_i$-direction; also denotes general dependent variable in model equation--see Chapter III |
| $u_{ij}$ | Any component of the vector of dependent variables at the (i,j) mesh point |
| $u_{e_c}, u_{e_s}$ | Chordwise and spanwise velocity components, respectively, used as inputs for Cumpsty and Head Test Case--see Section 5.3 |
| $u_s, u_n$ | Velocity components in streamline coordi-nate system |

### Symbol

| | |
|---|---|
| $\underset{\sim}{U}$ | Vector of dependent variables $= (\Theta_{11}, \bar{H}, A)^T$ --see Eq. (2.41) |
| $\underset{\sim}{U}_{ij}$ | Vector of dependent variables at $(i,j)$ mesh point--see Eq. (3.9) |
| $x_c$ | Chordwise coordinate--see Figures 8 and 9 |
| $x_i$ | General curvilinear coordinate $(i = 1,2,3)$--see Figure 1 |
| $\bar{x}_i$ | Cartesian coordinate $(i = 1,2,3)$--see Figure 1 |
| $\Delta x$ | Either $\Delta x_1$ or $\Delta x_2$ |

### Greek Symbol

| | |
|---|---|
| $\alpha$ | Angle measured positive from $x_1$-axis to local resultant edge velocity vector |
| $\alpha_o$ | Sweep angle |
| $\beta$ | $\tan^{-1}(u_n/u_s)$ |
| $\beta_w$ | Angle between resultant wall shear stress vector and resultant edge velocity vector |
| $\gamma$ | Ratio of specific heats, taken as 1.4; also used as an arbitrary constant in Appendix H |
| $\delta_i^*$ | Displacement thickness defined using velocities in nonorthogonal coordinate system, Eq. (2.10a) |
| $\delta_{u_i}^*$ | Displacement thickness defined using velocities in nonorthogonal coordinate system, Eq. (2.10d) |
| $\nabla$ | Finite-difference operator--see Appendix H |
| $\Delta_i^*, \Delta_u^*, \Delta_v^*$ | Displacement thickness defined using velocities in streamline coordinate system, Eqs. (B.7), (B.8), (B.17), (B.18) |

## Greek Symbol

| | |
|---|---|
| $\epsilon_{ij}$ | Energy thickness defined using velocities in nonorthogonal coordinate system, Eq. (2.10c) |
| $E_{ij}$ | Energy thickness defined using velocities in streamline coordinate system, Eqs. (B.13)→(B.16) |
| $\theta_{ij}$ | Momentum thickness defined using velocities in nonorthogonal coordinate systems, Eq. (2.10b) |
| $\theta_\rho$ | Density thickness, Eq. (2.10e) |
| $\Theta_{ij}, \Theta_u$ | Momentum thickness defined using velocities in streamline coordinate system, Eqs. (B.9)→(B.12), (2.27a) |
| $\kappa$ | $\sqrt{-1}$ |
| $\lambda$ | Angle between $x_1$ and $x_2$ axes, measured positive from the $x_1$ to $x_2$ coordinate axis |
| $\mu$ | Molecular viscosity |
| $\mu_{t_i}$ | Eddy viscosity, Eqs. (D.12a,b) |
| $\xi$ | $\lambda - \alpha$ |
| $\rho$ | Density |
| $\rho_{ij}(M), \rho_{ij}(N)$ | Spectral radii of M and N matrices, respectively, at (i,j) mesh point |
| $\tau_{x_i}$ | Total shear stress (molecular plus turbulent) in $x_i$-direction |
| $\theta$ | Wave number |
| $\omega$ | Smoothing factor, Eq. (3.20) |

## Subscripts

| | |
|---|---|
| edge | Denotes boundary-layer edge value |
| i or i,j | Denotes quantity evaluated at the (i) or (i,j) mesh point; also denotes parameters corresponding to $x_i$- or $x_j$-direction |
| s,n | Denotes quantity resolved in the stream-line coordinate system |
| w,o | Denotes quantity evaluated at the body surface |
| $x_i$ | Denotes quantity in the $x_i$-direction |
| $\infty$ | Denotes free-stream condition |

## Superscripts

| | |
|---|---|
| $(\overline{\phantom{x}})$ | Denotes boundary-layer edge value; also denotes "incompressible" quantity |
| n | Denotes quantity using velocity normal to streamwise direction |
| s | Denotes quantity using streamwise velocity |